Development of Novel Structured Catalysts and Testing for Dehydrogenation of Methylcyclohexane

A Thesis submitted to the University of Manchester for the degree of

Doctor of Philosophy

in the Faculty of Engineering and Physical Sciences

2014

by

Chandni Rallan

under the supervision of

Dr.Arthur Garforth

School of Chemical Engineering and Analytical Science

Table of Contents

List of Tables

List of Figures

Nomenclature

T	Temperature (°C)
W/F	Reactor space time (g s mol^{-1})
P	Pressure (bar)
k_s	Intrinsic thermal conductivity
k_w	Intrinsic thermal conductivity of washcoat
ξ	Monolithic void fractions
$\Delta H°_r$	Heat of reaction (kJ mol^{-1})
r	Rate of dehydrogenation of MCH
R	Gas constant
θ_T	Fraction of active sites covered by toluene
k_f	Rate constant for rate determining step in fouling reaction (s^{-1})
K_6	Equilibrium constant for fouling precursor
K_3	Equilibrium rate constant for toluene
$\Delta G°$	Gibbs free energy (kJ mol^{-1})
θ	Diffraction angle (radian)
λ	X-ray wavelength (nm)
X_e	Equilibrium Conversion
X_{obs}	Observed conversion
S_T	Selectivity to toluene
E_{act}	Activation energy (kJ mol^{-1})
T_m	Mean bed temperature (°C)
T_w	Wall temperature of reactor (°C)
T_r	Reaction temperature (°C)
K_e	Equilibrium rate constant (bar^3)
P_T	Total pressure of system (bar)
p_i	Partial pressure of component i (bar)
F_T	Total molar flowrate of feed (mol h^{-1})
F_i	Flowrate of component i (mol h^{-1})
y_i	Mole fraction of component i

Abstract

Hydrogen storage for stationary and mobile applications is an expanding research topic. Using liquid organic hydrides for hydrogen storage is one of the most promising alternatives as it provides simple and safe handling. Liquid organic hydrides are largely compatible with current transport infrastructure, whereas alternatives such as liquid and gaseous hydrogen and metal hydrides would require a completely new infrastructure. An attractive storage system is the so-called MTH system (Methylcyclohexane, Toluene and Hydrogen).

The dehydrogenation of methylcyclohexane is a highly endothermic reaction. To improve the reaction kinetics, this research was to develop a structured catalyst with a conductive metal support (Fecralloy) which could hold an adherent catalytic washcoat (γ - Al_2O_3). The active phase was impregnated onto this support and the developed catalyst was tested for the dehydrogenation of methylcyclohexane.

The catalyst preparation involved three key steps which were support oxidation, loading of an adherent washcoat and finally impregnation of the active phase. The oxidation and washcoat stages required significant optimisation. The optimum oxidation conditions were found to be 950 °C for 10 h. The washcoating procedure was optimised by modifying a one-step hybrid washcoating method suggested in patent literature. Characterization techniques including SEM, XRD and EDX were used to study each step of catalyst preparation. In addition the technique of STEM was used to study platinum dispersion on the catalytic washcoat.

Finally the catalytic activity of the developed catalyst was compared with an in-house pelleted catalyst based on the material used to prepare the structured catalyst and commercially available platinum on γ - Al_2O_3. Three key factors: activity, selectivity and stability were evaluated. The activity and selectivity were studied at varied operating conditions of T = 340 °C - 400 °C, W/F = 7345 - 14690 g s mol^{-1}, H_2/MCH molar ratio = 0 - 9 and P = 1.013 bar. The dehydrogenation reaction of methylcyclohexane was found to be very selective to toluene (above 99%). Compounds, which are considered coke precursors, were identified, to attempt to explain the mechanism of catalyst deactivation. By-product distribution was monitored and possible reaction pathways were postulated.

To gauge the stability of the catalyst, long term life tests were also performed on the structured catalyst at 400 °C and W/F = 14690 g s mol^{-1} for approximately 400 h. The stability study investigated the different types of deactivation mechanisms. The catalyst evaluation study helped identify the effect of the alloy support, the alumina washcoat and platinum dispersion on the selectivity of the catalyst.

Declaration

No portion of the work referred to in the thesis has been submitted in support of an application for another degree or qualification of this or any other university or other institute of learning.

Chandni Rallan

Copyright Statement

Copyright and the ownership of intellectual property rights:

1. Copyright in text of this thesis rests with the Author. Copies (by any process) either in full, or of extracts, may be made only in accordance with instructions given by the Author and lodged in the John Rylands University Library of Manchester. Details may be obtained from the Librarian. This page must form part of any such copies made. Further copies (by any process) of copies made in accordance with such instructions may not be made without the permission (in writing) of the Author

2. The ownership of any intellectual property rights, which may be described in this thesis, is vested in The University of Manchester, subject to any prior agreement to the contrary, and may not be made available for use by third parties without the written permission of the University, which will prescribe the terms and conditions of any such agreement.

3. Further information on the conditions under which disclosures and exploitation may take place is available from the Head of School of Chemical Engineering and Analytical Science (CEAS).

Acknowledgements

The journey to get to the end has been long, tough and grueling but it would not have been possible without the help and support I received.

I would like to thank my supervisor Dr.Arthur Garforth for his patience, help, guidance and supervision over the last few years. I have been very lucky to have a wonderful research group to work with, and I would like to thank the other research members of the Catalysis research group for their valuable inputs, especially Dr.Aaron Akah. I am very grateful to Dr.Patrick Hill for his help with the SEM and EDX characterization and all the other technical staff in SCEAS.

I would like to thank my wonderful family especially my much better half, for always being there.

1 Introduction and Research Background

1.1 Introduction

The last few decades have seen a great rise in population and with it increased industrial growth. This has resulted in rapid depletion of fossil fuels; increased air pollution which many scientists argue has resulted in the current global climate change. Growing concerns about these factors as well as availability of secure energy supply has led to great interest in the hydrogen fuel economy. Hydrogen is a safe and clean energy carrier and has the potential to alleviate the current pollution problems currently faced today. The hydrogen fuel economy is a long term goal for many nations. It has a lot of environmental as well as economic benefits. However the future of this economy is dependent on the development of a suitable technology that is both safe and economically viable for the storage and transport of hydrogen.

Currently hydrogen is stored and transported through pressurised tanks, or by storing and transporting hydrogen in its liquefied state (Grünenfelder and Schucan, 1989). However these are both energy intensive processes and hence the efficiency is highly reduced. There is current on-going research on the adsorption of hydrogen onto metal hydrides, cryogenic storage with hydrogen adsorbing materials and also storage in organic liquid hydrides.

Comparison of the different storage systems based on the efficiency with respect to cost and energy suggests, the most suitable method for storage of hydrogen and its transportation is the usage of organic chemical hydrides (Edwards et al., 2008). The various organic metal hydrides from which hydrogen can be generated are decalin, methylcyclohexane and cyclohexane (Taube et al., 1983). The system maintains a closed carbon circle, resulting in reduced toxic emissions. Usage of hydrogen storage in liquid organic hydrides is based on the concept on reversible catalytic hydrogenation and dehydrogenation reactions.

1.2 Liquid Organic Hydride cycles

The most favourable cycles which are currently studied are the methylcyclohexane-toulene-hydrogen (MTH) cycle, cyclohexane-benzene-hydrogen (CBH) cycle and decaline-napthalene-hydrogen (DNH) cycle. Figure 1.1 is a schematic representation of the different cycles and Table 1.1 describes the gravimetric storage densities of the different cycles (Satyapal et al., 2007).

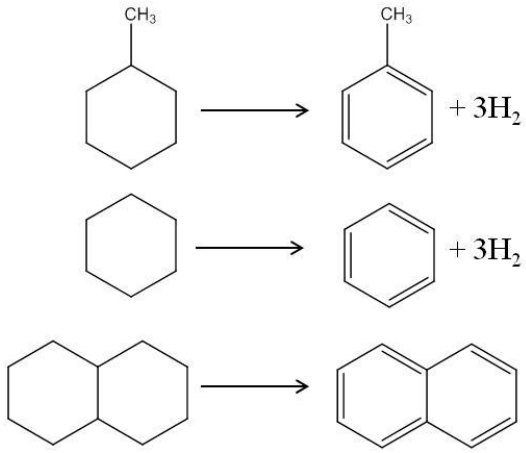

Figure 1.1 Dehydrogenation of the difference liquid organic hydride cycles (Okada et al., 2006).

Reaction	Gravimetric Content (wt%)	Volumetric Content (kg H_2/m^3)
$C_7H_8+3H_2 \leftrightarrow C_7H_{14}$	6.1	47
$C_6H_6+3H_2 \leftrightarrow C_6H_{12}$	7.1	55.5
$C_{10}H_8+5H_2 \leftrightarrow C_{10}H_{18}$	7.2	64.9

Table 1.1 Storage densities of the different organic liquid hydrides (Okada et al.,2006).

Despite the higher storage content of the CBH cycle and DNH cycles, researchers prefer the MTH cycle. The CBH cycle contains benzene which is carcinogenic and naphthalene which is produced in the solid state. The CBH and DNH cycles, both result in products which do not comply with the standards prescribed by the DOE.

1.3 Methylcyclohexane-Toluene-Hydrogen Cycle

The MTH cycle is applicable to stationary as well as mobile systems, such as fuel cell power stations and hydrogen powered vehicles. The main principle of the system is the storage of surplus electricity in a feasible manner. The electricity is used for electrolysis of water to generate hydrogen which further is used to hydrogenate toluene to produce methylcyclohexane. This liquid organic hydride has properties similar to gasoline and is storable under atmospheric conditions (Taube et al., 1985). Methylcyclohexane is dehydrogenated to produce hydrogen which is used as the fuel and the toluene produced is further re-hydrogenated. Hydrogen fuel results only in emission of N_2, NO_x and water vapour thus proving to be a clean source and eliminating the production of harmful toxic gases. This cycle is schematically described in Figure 1.2.

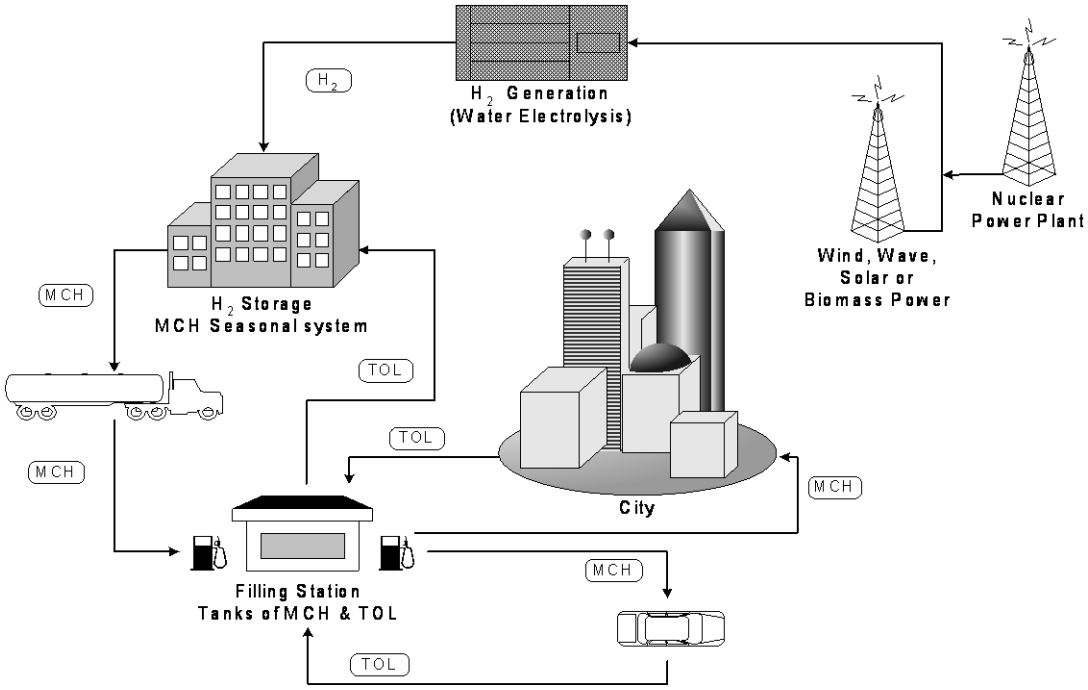

Figure 1.2 Schematic Adaptation of the MTH cycle redrawn from (Tsakiris, 2007).

The MTH cycle could be used for both stationary and/or mobile applications. In stationary applications, methylcyclohexane could be used in a combined heat-power (CHP) system to supply heat or power to the buildings. In mobile applications (cars, buses, lorries, etc.) the vehicles would be filled with methylcyclohexane at the filling station. On board, a dehydrogenation (catalytic reaction) and power generation (fuel cell) system will use the

methylcyclohexane as fuel. The produced toluene would be condensed and collected, as a liquid in a tank situated in the vehicle. The toluene tank would be emptied at a filling station whilst the methylcyclohexane tank was being refilled. The toluene would then be transported by road and/or sea tanker to the central hydrogenation plant, where it would be re-hydrogenated to methylcyclohexane.

1.4 Research objectives

One of the main factors that hinders the application of hydrogen storage in liquid organic hydrides is the amount of energy required to extract the hydrogen from the liquid organic carrier. In order to overcome this barrier, the aim of the research was to develop a suitable structured support which would be conductive in nature and thus improve the kinetics of the reaction. Two primary research objectives were set for the research. The first objective was to develop a suitable structured catalyst with an adherent catalytic washcoat, by optimising and modifying each step of catalytic preparation. The second research objective was to test the developed catalyst for MCH dehydrogenation and compare the results with a conventional pelleted catalyst and study the various effects of the developed catalyst on the selectivity and efficiency of the reaction. The optimum catalyst should have the following characteristics: high dehydrogenation activity, high product selectivity towards aromatics and low deactivation rate.

1.5 Thesis outline

This research thesis consists of eight chapters and three appendices. Chapter one gives a brief introduction to the hydrogen fuel economy and describes the primary objectives of this research. Chapter two introduces the current development and usage of structured catalytic reactors. Chapter three reviews the past literature on MCH dehydrogenation on platinum catalysts and the deactivation mechanisms. Further a review on the different reactions taking place on the different platinum crystal sites has been detailed in the chapter. Chapter four describes the methodology and characterization involved in each step of preparation of the novel structured catalyst, in addition a review of past work done by previous authors has been detailed for each step of preparation. Chapter five details the experimental set-up used for

testing the structured catalyst and additionally details the reactor design specifications. Chapter six discussed the reaction selectivity and by-product distribution for the structured catalyst and the results have been compared with conventional pelleted catalysts. Chapter seven focuses on the reaction kinetic parameters and deals with the catalyst deactivation mechanism. Chapter eight exemplifies the research conclusions and the future work.

2 Review on Structured Catalytic Reactors and Metallic Substrates

2.1 Introduction

Conventional fixed bed reactors have obvious disadvantages such as large pressure drop and limited mass transfer capabilities. In addition given the nature of fixed beds, precision in scale-up, modeling and design of conventional reactors is limited. Another limiting factor in design of fixed bed reactors is the particle diameter, which needs to be small to enable improved selectivity and activity, but results in large pressure drop. To enable the elimination of these set-backs arising from the usage of conventional fixed reactors, a lot of research in the last few decades has been focused on structured catalysts. The structured catalysts can be classified into three main categories:

- Monolithic catalysts
- Membrane catalysts
- Arranged catalysts

The classification and properties of these different catalysts has been described in Table 2.1. *Monolithic catalysts* are also honeycomb structures, since the first catalysts that were made had a honeycomb structure. They are usually metallic or ceramic and consist of many narrow parallel straight or zig-zag channels. The active catalyst phase is either incorporated into the monolithic structure or deposited on the walls of the channels.

When the catalytic material is present on the walls of the monolithic passages, radial mass transfer occurs by diffusion through these permeable walls. Such catalysts are called *membrane catalysts*.

Arranged catalysts are particulate catalysts that are arranged in varied geometric configurations in order to improve the radial heat and mass transfer characteristics of the process. Non-particulate catalysts, for example packing used in distillation columns which consist of particulate catalyst embedded between structured catalytic materials. However the pressure drop in arranged catalysts is a lot higher when compared to monolithic catalysts.

Design / Type	Monolithic catalysts, membrane catalysts and arranged catalysts
Support Material	Ceramics and metal
Mode of Operation	Stationary application (eg: treatment of industrial flue gases); Non-stationary applications (eg : mobile emission catalysts)

Table 2.1 Classification of Structured catalysts (A. Moulijn and Cybulski, 2005).

Research over the last two decades has seen a growing interest in these structured catalysts especially monolithic catalysts. The metallic substrates used to make the monolithic catalysts have been used to make supports of different geometries such as foams, rods and tubes, to name a few. Depending on the nature and properties of the reaction which the support is to be used for, a suitable geometry is chosen. The following sections, reviews the work done by various authors in the catalytic testing of these metallic substrates.

2.2 Monolithic Reactors

Using a metallic substrate to support a catalytic coating is highly beneficial due to its improved properties of thermal conductivity. Heck et al in their review described extensively the use of monoliths for gas-phase catalytic reactions (Heck et al., 2001). In their review they suggested it was possible to use a metallic substrate with a catalytic coating either applied onto the surface of the substrate by a washcoating method or grown in-situ. As the reactants enter the each and of the channels, they interact with the catalyst on the walls as described in Figure 2.1. Monoliths have an open frontal area which resulted in a lowering of pressure drop and decreased resistance to flow. Monoliths have been extensively used as automobile car exhaust systems for NOx abatement (Avila et al., 2005). However the application in petrochemical and petroleum industry is still limited. The application of monolithic reactors is currently found in (Heck et al., 2001) :

- Three way catalysts
- Diesel catalysts
- Ozone abatement in aircrafts
- Natural gas engines
- Ozone destruction on automobile radiators
- Selective reduction of NOx
- Destruction of VOCs
- Catalytic combustion
- Hydrogen generation for fuel cell
- Steam reforming of hydrocarbons
- Water-gas shift catalysts
- Preferential oxidation of CO

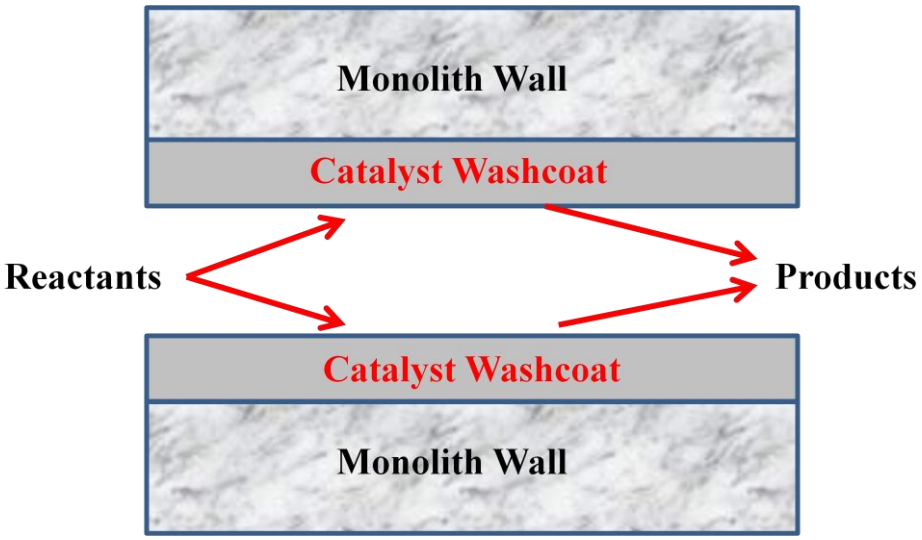

Figure 2.1 Reaction in an idealized monolith channel (Heck et al., 2001).

Nijhuis et al in their work suggested that the monolithic reactors are highly beneficial for processes where improved mass transfer was required due to their open frontal area (Nijhuis et al., 2001). In their paper they compared the properties of monolithic reactor and packed bed reactor which has been summarized in Table 2.2. Despite the improved benefits of using a monolithic catalyst there are many steps involved in preparing the catalyst.

Factor	Monolithic Reactor	Packed bed reactor
Pressure drop	Low	High
Catalyst Efficiency	High, Thin and active layer	Low, large particle required to reduce pressure dorp
Catalyst Separation	Easy	Easy
Catalyst Loading	Open structure for washcoated systems	Dense tightly packed bed
Catalyst Preparation	Complex, not much background literature	Easy
Catalyst replacement	Difficult, shutdown required monoliths have to be carefully stacked	Difficult-Shutdown required
Experince/knowledge	Gas-phase extensive, liquid and multiphase very limited	Extensive

Table 2.2 Comparison of Monolithic and packed bed reactors (Nijhuis et al., 2001).

De Deugd et al and more recently Holmen et al used washcoated monoliths for Fisher-Tropsch synthesis for the conversion of syngas (De Deugd et al., 2003, Holmen et al., 2013). In their research they showed by using monolithic reactors, they were able to remove the mass transfer limitations that are usually faced during Fisher-Tropsch synthesis. They compared the activity with conventional pelleted fixed bed reactors, and found both catalysts to depict a similar activity and selectivity.

Groppi and Tronconi in their work described the major challenges that hinder the application of monolithic catalysts to chemical synthesis (Groppi and Tronconi, 1996). They found the main factor limiting the application of monolithic catalysts was the high cost of the metallic substrates. In addition the loading, packaging, sealing and unloading of monolithic catalysts was a lot more complex compared to conventional pelleted catalysts and required to be optimized. Groppi and Tronconi further suggested that monolithic catalysts due to their heat conductive properties provided an even heat distribution across the bed which cannot be found with conventional pelleted catalysts. In addition the researchers developed a correlation (*Equation 2.1*) to describe the axial heat conductivity of monolith structures :

$$k_{e,a} = k_s\,(1-\varepsilon) \qquad (2.1)$$

where, k_s was the intrinsic thermal conductivity of the support material and ε was the open frontal area of the monolithic support. Groppi and Tronconi modified the correlation to accommodate washcoated monoliths (Groppi and Tronconi, 2005). Equation 2.2 describes the updated correlation,

$$k_{e,r} = k_s \left((1-\sqrt{\varepsilon+\xi}) + \frac{\sqrt{\varepsilon+\xi}-\sqrt{\varepsilon}}{(1-\sqrt{\varepsilon+\xi})+\frac{k_w}{k_s}\sqrt{\varepsilon+\xi}} + \frac{\sqrt{\varepsilon}}{(1-\sqrt{\varepsilon+\xi})+\frac{k_w}{k_s}(\sqrt{\varepsilon+\xi}-\sqrt{\varepsilon})+\frac{k_w}{k_s}\sqrt{\varepsilon}} \right)^{-1} \qquad (2.2)$$

where, ε and ξ were used to describe the monolithic volume fractions of voids and washcoat respectively, k_s was the intrinsic thermal conductivity of the support and k_w the intrinsic thermal conductivity of the washcoat (Groppi and Tronconi, 2005). Thus from the equation it is possible to interpret that the adoption of highly conductive materials greatly improves the radial heat transfer properties of the catalyst. The correlation also shows that the increased void fractions adversely affected the radial heat transfer properties of the monolithic catalysts.

Despite the improved benefits of the monolithic catalysts, these catalysts provide poor radial heat transfer across the reactor bed thus proving un-feasible for application in non-adiabatic fixed bed reactors. Thus metallic substrates of foam or tubes could be used for reactions where improved heat transfer across the bed was required. This has been detailed in the following sections.

2.3 Metallic Foam reactors

Recent developments in metallic substrates, have led to the production of metallic substrates with different geometries. The last few years have seen a growing interest in metallic foams. These foams when compared to monoliths describe voids which are much smaller in nature thus enabling better heat transfer across the reaction bed. Löfberg et al developed washcoated metallic foams and tested the prepared catalysts for the dehydrogenation of methylcyclohexane which is a highly endothermic reaction (Löfberg et al., 2011). They compared the activity of the catalyst with pelleted catalysts. At similar W/F,

Löfberg et al were able to achieve similar catalytic activity for both the catalysts in addition to reducing the temperature drop to 13 °C from 30 °C (pelleted catalysts).

Cristiani et al developed metallic foam reactors and tested it for the highly endothermic reaction, steam reforming of methane (Cristiani et al., 2012). The metallic foams were impregnated with a $Ni/MgAl_2O_4$ washcoat prior to testing for steam reforming of methane. The group was able to achieve the thermodynamic equilibrium of methane at high reaction temperatures of 450 °C.

Gräf et al in their recent paper, tested metallic foams with a Ni/Al_2O_3 catalyst supported on the foam, for the highly exothermic reaction of hydrogenation of benzene (Gräf et al., 2014). The supported catalyst was prepared by applying a γ - Al_2O_3 washcoat onto metallic foams and impregnating the washcoat support with a nickel salt. Gräf et al in their work found that by using the metallic foams they were able to reduce the formation of hot spots across the bed when compared to packed bed reactors. In addition, they also suggested that there was radial and axial heat conduction across the bed.

2.4 Metallic substrates with novel geometry

The last few years have seen a growing interest in structured reactors especially metallic substrates to be used as metallic supports. The geometry of the substrate largely depended on the application and type of reactor system to be used. Recently, Lefevere et al in their work utilized three dimensional fiber deposition (3DFD) to manufacture different types of metallic catalyst supports (Lefevere et al., 2013). They used 3DFD technology to manufacture supports of different geometries to study the effect of the geometry on the heat and mass transfer properties of methanol to olefins conversion. They found the metallic substrate containing zig-zag channels in the direction of the flow (1.1 x 1.1 mm) and the smaller straight channels in the two radial directions, to result in the highest yield of light olefins for the methanol to olefin conversion due to the improved mass transfer capabilities of the narrow channels.

Jodlowski et al, used metallic wires to make a wire gauze reactor which was tested for the combustion of methane (Jodłowski et al., 2013). The metallic substrate used in their research had a diameter of 0.16 mm and was used to make stacked wire gauze mesh reactors.

The current study has focused on the usage of metallic substrates in the form of rods, and after loading a suitable catalytic washcoat onto the coated rods were packed into a fixed reactor and tested for dehydrogenation of methylcyclohexane. Review of the past literature suggests limited usage of the metallic substrate with this geometry.

3 Review on MCH dehydrogenation and surface reactions on Platinum

3.1 Introduction

Work since the 1960s has shown that the most suitable catalyst to be used for the dehydrogenation of methylcyclohexane reaction is platinum on a support such as alumina. John.H Sinfelt carried out several studies on the kinetic study of MCH over a platinum catalyst. In 1960, Sinfelt et al were the first to report the rate kinetics of the system under study (Sinfelt et al., 1960). The measure of the dehydrogenation activity of platinum was determined, which is a very important parameter in the characterization of the bi-functional platinum-alumina system. The rate of dehydrogenation of MCH was nearly a zero order reaction with respect to methylcyclohexane and was zero order with respect to hydrogen (Sinfelt et al., 1960).

3.2 Dehydrogenation of Methylcyclohexane

In addition to providing hydrogen for the hydrogen fuel economy, the dehydrogenation of methylcyclohexane to form toluene is an important reforming reaction for petroleum naphtha fractions. Product selectivity is very crucial for applicability to industrial reactions. Transition metals and their oxides are active catalysts for the catalytic dehydrogenation of saturated six-membered ring hydrocarbons for the formation of aromatics (Richardson, 1989). Supported metal catalysts, such as platinum or palladium combined with an additional metal such as rhenium, gold or ruthenium on alumina and/or silica, are particularly active and have been extensively studied and investigated over the dehydrogenation of methylcyclohexanene.

The dehydrogenation reaction of methylcyclohexane, is a highly endothermic ($\Delta H_r° = 205$ kJ mol^{-1}) reaction, but fast reaction that is favoured at high temperatures and low pressures. Monometallic and bimetallic catalysts with aluminium or zeolite supports have

been reported in the literature. However, it was found the metal loaded zeolite supports demonstrated a lower selectivity to the formation of toluene (Sinfelt et al., 1960). Researchers have shown that platinum supported on an alumina support was found to have a much higher selectivity towards the formation of toluene and hence are the best catalysts for the dehydrogenation of methylcyclohexane.

3.2.1 Dehydrogenation of Methylcyclohexane over Pt/Al_2O_3

The application of platinum catalysts for dehydrogenation was initially recognised by Zelinski in 1911. Kariya and co-workers believe the good dehydrogenation capability of the catalyst could be attributed to the hydrogen spill-over and hydrogen recombination reactions (Kariya et al., 2002). The dehydrogenation of MCH over Pt/Al_2O_3 has attracted many research groups over the past decades.

Sinfelt et al have investigated the kinetics of MCH dehydrogenation over Pt/Al_2O_3 catalysts under the following conditions; temperature range of 315 °C - 372 °C, MCH partial pressure of 0.07 - 2.2 atmospheres, and hydrogen partial pressure of 1.1 - 4.1 atmospheres (Sinfelt et al., 1960). Sinfelt and co-workers found the reaction to be nearly zero order with respect to methylcyclohexane and hydrogen over the range of conditions studied. The near zero order of the reaction with respect to MCH suggested that the active catalyst sites were highly covered with adsorbed MCH molecules. The presence of toluene on the other hand had a small retarding effect on the dehydrogenation rate. Therefore Sinfelt et al suggested that the rate determining step of MCH dehydrogenation was toluene desorption.

Based on the observations Sinfelt et al derived a rate expression for MCH dehydrogenation over Pt/Al_2O_3. The rate expression derived by the group is shown in Equation 3.1. The equation does not include the inhibition effect of toluene that was observed by Sinfelt and co-workers later on. The temperature dependencies of parameters *k* and *b* are given by Equations 3.2 and 3.3 respectively (Sinfelt et al., 1960).

$$r = \frac{k' b p_m}{1 + b p_m} \tag{3.1}$$

Where, *k'* is a rate constant, p_m is the methyl cyclohexane partial pressure, *b* is a parameter which is a function of temperature.

$$k' = 4.2 \times 10^{11} \exp\left(\frac{-33{,}000}{RT}\right) s^{-1} \tag{3.2}$$

$$b = 2.1 \times 10^{-10} \exp\left(\frac{30{,}000}{RT}\right) atm^{-1} \tag{3.3}$$

The conversion of methyl cyclohexane takes place through several steps. The mechanism proposed by Sinfelt et al suggested that the active catalyst sites are covered with adsorbed toluene and that the reaction rate is the rate of desorption of toluene from the surface (Sinfelt et al., 1960). A simple kinetic scheme was proposed in order to account for the observed kinetics.

$$M_{(g)} \xrightarrow{k_1} T_a \xrightarrow{k_2} T_{(g)} \tag{3.4}$$

where M and T represent methylcyclohexane and toluene in the gas phase, and T_a represents adsorbed toluene. It was postulated that adsorption equilibrium was not established and that the individual steps were effectively irreversible. Step 1 represented the adsorption of methylcyclohexane with subsequent reaction to form toluene on the surface, while step 2 represented the desorption of toluene from the surface. The first step was not simple but as mentioned earlier a combination of steps involving partially dehydrogenated hydrocarbon molecules or radicals is taking part. The parameters k_1 and k_2 were rate constants for steps 1 and 2 respectively. The following equation is a steady-state expression for the net rate of formation of adsorbed toluene, assuming that coverage of the active sites by components other than toluene is negligible, according to Sinfelt and his co-workers (Sinfelt et al., 1960):

$$\frac{dT_a}{dt} = k_1 p_M (1 - \theta_T) - k_2 \theta_T \tag{3.5}$$

where θ_T represents the fraction of the active sites covered by toluene. The rate of formation of the product toluene is given by:

$$r = k_2 \theta_T \tag{3.6}$$

Solving Equation 3.5 for θ_T and substituting in Equation 3.6 the rate expression is obtained:

$$r = \frac{k_2\left(\frac{k_1}{k_2}\right)p_M}{1+\left(\frac{k_1}{k_2}\right)p_M} \qquad (3.7)$$

Wolf and Petersen studied the dehydrogenation of methylcyclohexane in the temperature range of 350 °C - 400 °C and MCH and hydrogen partial pressure of 0 - 800 torr respectively (Wolf and Petersen, 1977). They found the reaction to be first order with respect to MCH and H_2.

Jossens and Petersen presented similar observations to those of Sinfelt and co-workers (Jossens and Petersen, 1982). They found the rate of MCH dehydrogenation to be nearly zero order when the concentrations of MCH were below 6 x 10^{-7} gmol cm^3. At higher concentrations the reaction order decreased and eventually approached zero. They also found an increase in temperature led to an increase in toluene inhibition whilst an increase in hydrogen partial pressure decreased the toluene inhibition.

Jothimurugesan et al proposed a single site mechanism to account for the methylcyclohexane dehydrogenation on Pt/Al_2O_3 (Jothimurugesan et al., 1985). Their study showed that toluene inhibited the reaction by competing for the active dehydrogenation-hydrogenation sites. They further suggested that dehydrogenation took place in two major reaction steps. The first step which was the rate controlling step, accounted for the reaction of MCH with an active site to form an adsorbed toluene molecule. The second step involved desorption of the toluene molecule from the active site. Toluene inhibition has been reported by many researchers such as, Sinfelt et al, Jossens and Petersen and Jothimurugesan et al (Jossens and Petersen, 1982, Jothimurugesan et al., 1985, Sinfelt et al., 1960).

Van Trimpont et al also researched the competitive adsorption between MCH, toluene and n-heptane on Pt/Al_2O_3 catalyst (Van Trimpont et al., 1986). Their assessment of competitive adsorption revealed that MCH did not compete with MCH for platinum sites, which contradicted the work of the previously mentioned authors.

3.2.2 Deactivation of Pt/Al_2O_3 for dehydrogenation of MCH

Catalyst deactivation occurs through different deactivation mechanisms such as fouling, sintering, poisoning and sintering. Developing a catalyst that has high stability requires deep understanding of the deactivation phenomena. Various groups, Wolf and Petersen, Jossens and Petersen, Pacheco and Petersen, Alhumaidan et al have investigated the deactivation kinetics of reforming catalysts during MCH dehydrogenation (Alhumaidan et al., 2010, Jossens and Petersen, 1982, Pacheco and Petersen, 1984a, Wolf and Petersen, 1977).

Wolf and Petersen studied the deactivation mechanism and poisoning in MCH dehydrogenation over Pt/Al_2O_3 (Wolf and Petersen, 1977). In their research they found that the increase in hydrogen pressure stabilized the catalyst by decreasing the formation of coke. In addition, Wolf and Petersen suggested that during the deactivation process two types of poison structures were formed, reversible poisons that could be removed by a stream of hydrogen and irreversible poison structures that cannot. The relative amount of poison structures formed depends on the hydrogen partial pressures and time-on-stream. Wolf and Petersen suggested that catalyst deactivation through poisoning occurred through three different mechanisms, parallel, series and triangular self-poisoning as illustrated in Figure 3.1.

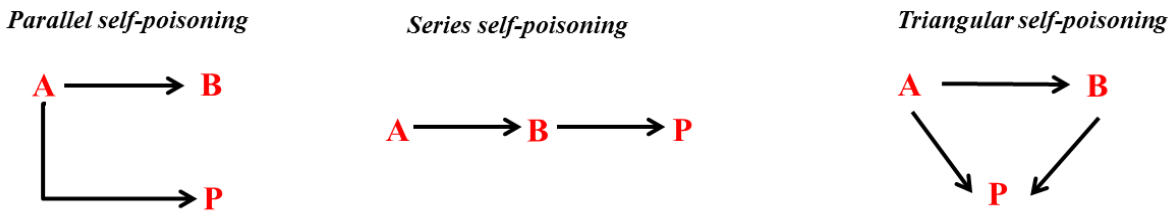

Figure 3.1 Self-poisoning mechanisms.

In parallel self-poisoning the poison comes from the reactant whilst the precursor is produced from the product in series self-poisoning. For the dehydrogenation of methylcyclohexane, deactivation was predominantly caused through parallel and series poisoning. Based on their findings, Wolf and Petersen reported a two phase deactivation for dehydrogenation of methylcyclohexane. The initial phase of deactivation was characterized

by a rapid rate of deactivation caused by parallel self-poisoning. The second phase of deactivation was caused by uniform self-poisoning, which was a combination of parallel and series poisoning mechanisms.

Jossens and Petersen in their work proposed a deactivation mechanism which was in agreement with the work of Wolf and Petersen (Jossens and Petersen, 1982). Jossens and Petersen observed a two phase deactivation mechanism. They found the initial phase of deactivation to be rapid with low activation energy (33 kJ mol^{-1}) in addition to the deactivation being reversible in a stream of hydrogen. The rate of reaction for the initial phase was nearly zero order with respect to MCH and toluene partial pressures. However the second phase of deactivation was characterized by a slower rate of deactivation, high activation energy (163 kJ mol^{-1}) and partially reversible deactivation in a stream of hydrogen.

Pacheco and Petersen proposed a deactivation model which was an empirical Rideal-Eley type fouling mechanism for dehydrogenation of MCH (Pacheco and Petersen, 1984a). The fouling mechanism was initiated with the sequential adsorption of MCH onto a group of active metal sites which were in the form a sextet (six active metal sites). This further resulted in a loss of 11 hydrogen atoms from the MCH ring through a number of reversible dissociative adsorption steps which caused the formation of a multiply bound surface carbon skeleton. The carbon skeletal structure formed, reacts with the toluene in the gas phase in a Rideal-Eley manner to result in the formation of fouled sextet. The rate determining step in this fouling mechanism was the reaction between toluene and the multiply bound carbon skeleton. The apparent activation energy for the fouling reaction was found to be 305 kJ mol^{-1}.

Pacheco and Petersen proposed a hyperbolic deactivation function (k) to describe the six-site fouling mechanism (*Equation 3.8*). In Equation 3.8, k_f is the rate constant for the rate determining step in the fouling reaction, K_6 is the equilibrium constant for the fouling precursor and K_3 is the adsorption equilibrium constant for toluene. The hyperbolic deactivation function suggests that the fouling mechanism is directly proportional to the MCH partial pressure and inversely related to hydrogen partial pressure. The deactivation function also suggests inhibition of fouling by toluene. This deactivation rate proposed by Pacheco and Petersen fitted the deactivation data well at high level of catalytic activity. However as the catalyst activity declined with time the experimental data curve deviated

from the predicted model. This behaviour suggested that the fouling model could not be based on a single reaction order but on a variable one to represent the wider range of catalytic activity. The variable reaction order would include the different competing parallel fouling reactions. The dominant fouling reaction mechanism would change with activity and time-on-stream.

$$k = \frac{30\, k_f\, K_6\, [MCH]}{K_3^{\,6}\, [TOL][H2]^{1/2}} \qquad (3.8)$$

Pacheco and Petersen modified their research on the sextet fouling mechanism and suggested a fouling model that was based on a multiplet fouling mechanism (Pacheco and Petersen, 1984b). This was done in order to fit the fouling data below 40% activity. The modified model suggested that initially fouling took place on the sextets and as these sextets got exhausted, the fouling took place on smaller multiplets. Pacheco and Petersen thus implied that the initial phase of deactivation occurred mainly on the six site multiplet until the surface on it was depleted and the deactivation then proceeded over a five site mutliplet and the process continued until it reached a two site multiplet. The fouling reaction preferred the highest order multiplets due to their lower fouling activation energy.

Chai and Kawakami suggested a different mechanism for the deactivation of methylcyclohexane over Pt/Al_2O_3 (Chai and Kawakami, 1991). In their research they showed that the rate controlling step for the dehydrogenation of MCH was methylcyclohexene to methylcyclohexadiene. Chai and Kawakami further suggested that the methylcyclohexadiene that was formed was adsorbed in a different way to form coke precursor. The polymerization of "n" adsorbed precursors was the rate controlling step for the deactivation mechanism. According to Chai and Kawakami, the parameter n could be interpreted in different ways such as the number of active sites involved in coke formation, number of adsorbed coke precursors or the order of deactivation reaction. Chai and Kawakami suggested the value of "n" was between 2.6 and 2.8 for a Pt/Al_2O_3 catalyst.

In agreement with Chai and Kawakami, De la Banda and Melo also suggested that the precursor to coke formation was the partially dehydrogenated products and not toluene (De La Banda and Melo, 1986). Their observations were in agreement with Jossens and Petersen who also suggested that the precursors to coke formation were the unsaturated olefins.

3.2.3 Regeneration of Pt/Al_2O_3 catalysts

A reforming catalyst tends to undergo deactivation through coke deposition. The deactivation process is accelerated if platinum sinters or there are hot spots in the reactor bed. The regeneration of platinum is initiated with a heat treatment in air to burn off the coke. This treatment converts the platinum crystallites into precursors that allow the initial activity to be restored after reduction. The temperature during regeneration must be suitably controlled, as a spike in temperature could lead to reduction in surface area or increase in platinum crystallites to size that can no longer be re-dispersed.

Several researchers have investigated the role of coking in catalyst deactivation during dehydrogenation of napthalenes. Davis et al reported two types of carbonaceous deposits, reversible deposits which had a one dimensional structure and irreversible deposits with a three dimensional graphitic structure (Davis et al., 1984). Ngomo and Susu work was in agreement with that of Davis et al and classified the coke deposition associated with naphthalene dehydrogenation into three categories which are primary, secondary and tertiary deposits (Ngomo and Susu, 2001). The primary coke that is formed can be regenerated in a stream of air. The secondary coke that is formed can be removed by hydrogen. However the tertiary coke that is formed can neither be oxidized or reduced and causes irreversible deactivation. This form of coke was found to have low H/C ratios with graphitic structures.

Coughlin et al studied the regeneration of Pt/Al_2O_3 in a hydrogen stream (Coughlin et al., 1984). They found that immediately after regeneration the selectivity towards aromatics increased. However, with exposure to MCH the toluene selectivity gradually decreased over time. In addition Couglin et al in their research found that the regeneration in a stream of hydrogen resulted in reactivation of the dehydrogenation sites and decreased activity of the hydrogenolysis sites. As the exposure to MCH was started, there was a gradual decrease in activity of the dehydrogenation sites and increase in activity of the hydrogenolysis sites. Thus Coughlin et al in their work showed that the catalyst was able to regain its catalyst activity through a suitable regeneration method. Doolittle et al in their work reported similar observations to that of Coughlin et al (Doolittle et al., 1987). They found the aromatics yield to increase after the Pt/Al_2O_3 catalyst was subjected to regeneration in a hydrogen stream.

3.3 Platinum single crystal site reactions

Platinum is a very versatile heterogeneous metal catalyst. There are different reactions that take place on the different sites of the platinum crystals (Somorajai, 1994). The different reactions catalyzed on the platinum surface are:

- Hydrogenation
- Dehydrogenation
- Hydrogenolysis
- Isomerization
- Dehydrocyclization

Previous researchers have found that the selectivity towards the different reactions depends on the atomic structure of the catalyst surface (Rioux et al., 2008, Somorjai, 1977). The Platinum crystal surface has flat, stepped and kinked sites. The different sites show different selectivity to the different hydrocarbon reactions (Somorjai, 1994). The high rate hydrogenation and dehydrogenation reactions tend to take place on the flat sites. The activity of aromatization reactions are highly increased by the presence of the stepped and kinked platinum surfaces. Isomerization reactions tend to take place on the flat sites and the presence of surface irregularities have shown to increase the isomerization activity by a small extent. The hydrogenolysis (C-C bond incision reaction) reaction rates markedly increased with the when kink sites were present in high concentration. In order to obtain the desired selectivity and activity of the catalyst it is essential to prepare the catalyst in order to obtain the appropriate structure.

3.3.1 Single crystal surfaces

Microscopy techniques such as scanning tunnelling microscopy (STM) and low energy electron diffraction (LEED) have led to advances in understanding the morphology of single crystals at the atomic scale. Using these techniques Somorjai was able to construct an atomic scale model of the surface structure as shown in Figure 3.2 (Somorjai, 1994). The model constructed indicates that the surface of the crystal is heterogeneous at the atomic scale. The figure describes the presence of step, kink and terrace atoms. Atoms in terrace sites

are surrounded by the largest neighbours, followed by atoms in step sites which have fewer neighbours and atoms in kink sites have even fewer neighbours.

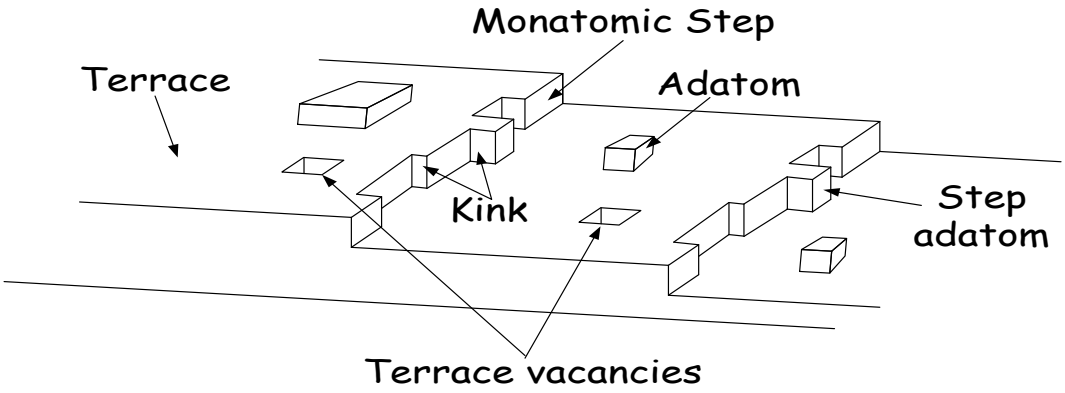

Figure 3.2 Atomic model of a heterogeneous solid surface describing the surface morphology (Somorjai, 1994).

Surfaces were found to consist of a mixture of flat regions, called terraces, and imperfections, which were called steps, kinks and adatoms. Steps and kinks are also called line defects and adatoms, which are atomic vacancies, are called point defects. The local distribution of atoms around each of these individual surface sites is different and therefore one should imagine their electronic properties to differ and be distinguishable. Hence, each surface site demonstrates its own characteristic surface chemistry and physical property.

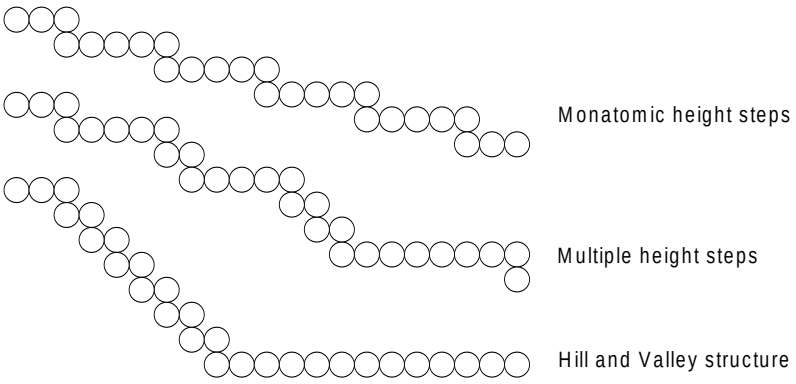

Figure 3.3 Main structural arrangements of surface morphology. (a) Monatomic height steps, (b) Multiple height steps, (c) Hill and Valley structure, (Blakely and Somorjai, 1977).

Blakely and Somorjai in their research on LEED studies on platinum surfaces showed that the surfaces consisted of three structural arrangements as illustrated in Figure 3.3 (Blakely and Somorjai, 1977). Blakely and Somorjai showed that, there were one-atom high steps separated by terraces, known as monatomic height step-terrace configurations and were produced when the plane was stable with respect to surroundings planes. They also showed that, there were multiple height steps separated by terraces of varying width and the third structural type was the hill-valley configuration, which consisted of large planes that could form a surface of hills with valleys in between them.

3.3.2 Surface reactions on Platinum single crystal surface

Somorjai and his co-workers for over two decades extensively studied the mechanism of heterogeneous catalysis of hydrocarbon reactions on platinum single crystal surfaces (Blakely and Somorjai, 1976, Blakely and Somorjai, 1977, Somorjai, 1994, Somorjai and Blakely, 1975). A few important findings emerged from their LEED and AES studies on both low and high Miller index platinum planes which has been summarized in Table 3.1.

Structure Sensitive		**Structure Insensitive**	
Hydrogenolysis	Methylcyclopentane	Ring Opening	Cyclopropane
Isomerization	Isobutane Hexane	Hydrogenation	Benzene
			Ethylene
Cyclization	Hexane Heptane	Dehydrogenation	Cyclohexane

Table 3.1 Structure Sensitive and Structure Insensitive Catalytic Reactions.

The four stepped platinum surfaces and Pt(111) crystal face, which were studied by Somorjai and his team, depicted different behaviour during the chemisorption of hydrocarbons (studied over n-heptane, toluene, benzene, ethylene and cyclohexane chemisorption). It was found that they were essentially four competing processes that took place during the chemisorption of hydrocarbons on the platinum sites, which were,

- the nucleation and growth of ordered carbonaceous surface structures,
- the dehydrogenation of the organic molecules (breaking of C-H bonds),
- the decomposition (hydrogenolysis reaction) of the organic molecules (breaking of C-H and C-C bonds),
- the rearrangement of the substrate (faceting).

On the lower miller index Pt(111) plane, the surface was inactive at temperatures less than 200 °C. However at elevated temperatures (> 500 °C), the surface acted as a site for thermal decomposition process, and could potentially lead to the formation of a disordered graphitic layer (Baron et al., 1974).

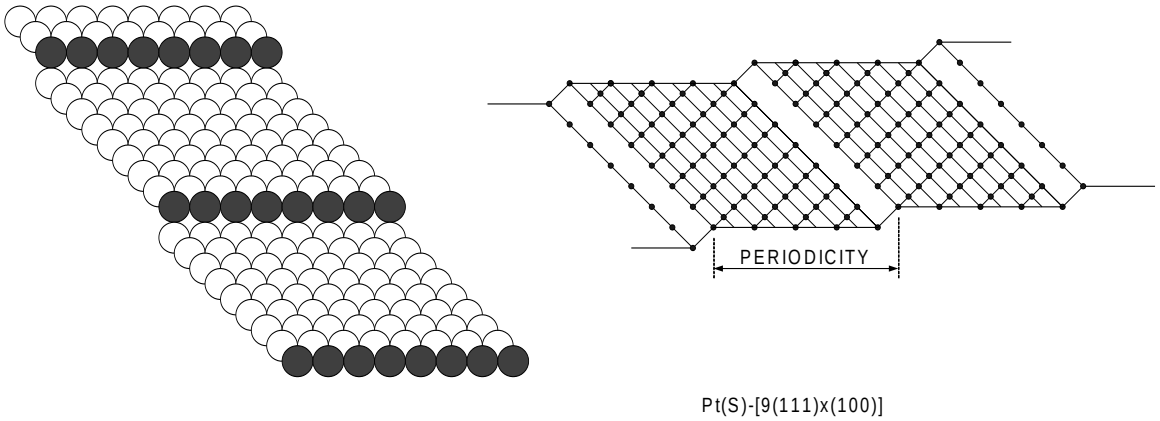

Figure 3.4 3D and 2D schematic of Pt(S)-[9(111)x(100)] crystal face (Baron et al., 1974).

On the Pt(S)-[9(111)x(100)] crystal face of platinum (*Figure 3.4*), the presence of atomic steps increased the rate of dehydrogenation which further resulted in the nucleation of ordered carbonaceous structures. At low hydrogen partial pressures, dehydrogenation was found to be rapid and a disordered carbonaceous deposit was formed on the wide terrace structures. At increased hydrogen partial pressure the rate of dehydrogenation decreased whilst the mobility of adsorbed species increased simultaneously. At this stage, the rate of nucleation and growth of ordered carbonaceous deposit successfully competed with the dehydrogenation process. Therefore, in the presence of high partial pressures of hydrogen, the formation of ordered carbonaceous structures predominate (Baron et al., 1974).

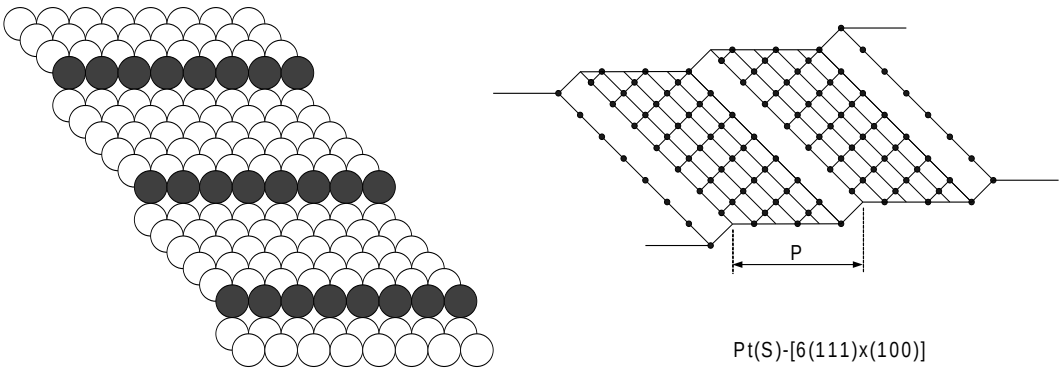

Figure 3.5 3D and 2D schematic of Pt(S)-[6(111)x(100)] crystal face (Baron et al., 1974).

Figure 3.5 describes the Pt(S)-[6(111)x(100)] crystal face of platinum site, which had a decreased terrace width which resulted in an increase in the step density. This increased the formation of an ordered carbonaceous overlayer as the rate of the C-C bond breaking reaction was much slower than the formation of the carbonaceous overlayer (Baron et al., 1974, Zaera et al., 1986).

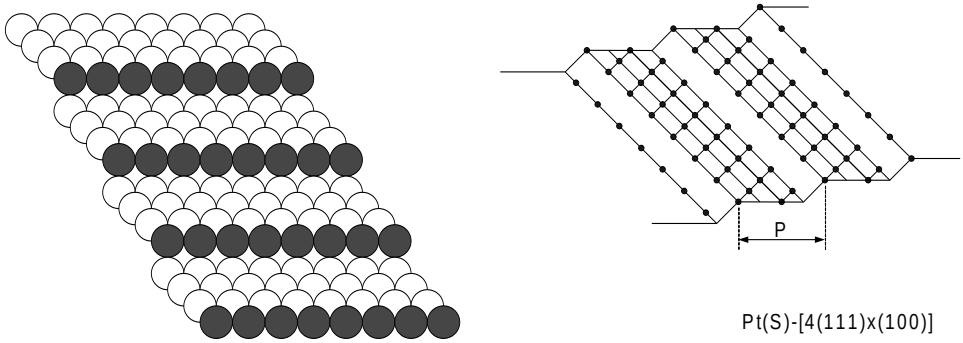

Figure 3.6 3D and 2D schematic of Pt(S)-[4(111)x(100)] crystal face (Baron et al., 1974).

It was found the Pt(S)-[4(111)x(100)] crystal face of platinum (*Figure 3.6*), behaved differently when compared to the Pt(S)-[9(111)x(100)] and Pt(S)-[6(111)x(100)] faces. The surface was no longer stable in the presence of chemisorbed hydrocarbons. Rearrangement (faceting) of the substrate was faster than dehydrogenation and nucleation and growth of ordered carbonaceous deposits. The new surfaces seemed to be stabilized by the presence of carbon and hydrogen (Baron et al., 1974, Zaera et al., 1986).

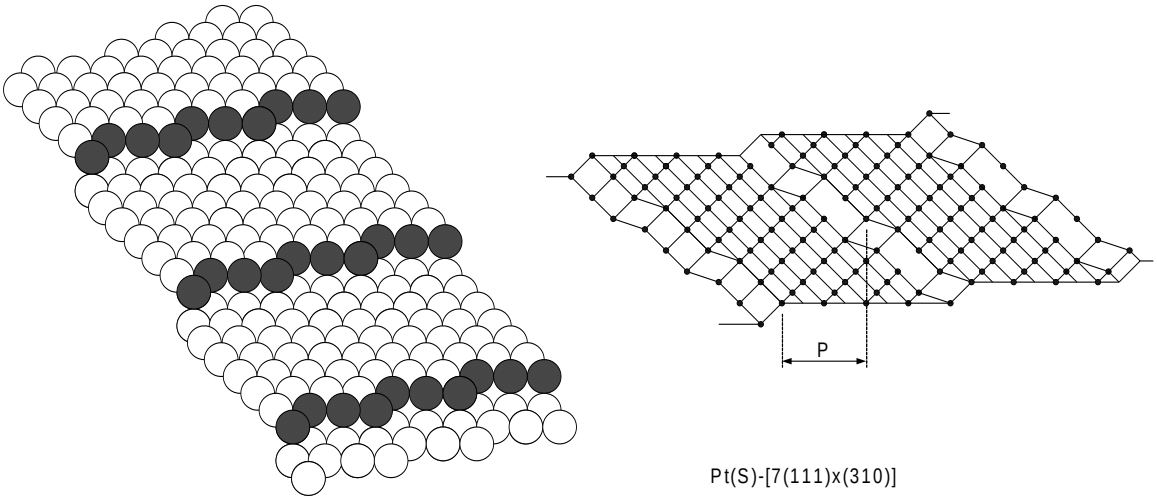

Figure 3.7 3D and 2D schematic of Pt(S)-[7(111)x(310)] crystal face.

Figure 3.7 describes the Pt(S)-[7(111)x(310)] platinum crystal surface which was found to be highly kinked. The rate of hydrocarbon decomposition was the most rapid compared to the other three processes. This resulted in the formation of disordered carbonaceous layers. Excess of hydrogen did not appear to have any significant impact on the ability of this surface to decompose organic molecules. More strongly adsorbed species, such as sulfur, could block the kink sites and slow down the decomposition of hydrocarbons, enabling the formation of ordered layers (Baron et al., 1974).

There is therefore evidence that chemisorbed molecules interact much stronger with the stepped (and kinked) platinum surfaces than with low Miller index planes of platinum. The reason for this increased chemical activity of the stepped surfaces can be attributed to the different atomic structures at the steps. An adsorbed molecule at the step has more nearest neighbour metal atoms compared to a molecule at a flat (low index plane, terrace) surface. Therefore, there is availability of metal atom orbitals at the stepped surface for adsorption and reaction. Somorjai and his team, in their investigation on dehydrogenation and hydrogenolysis reactions of cyclohexane and cyclohexene on stepped platinum surfaces, identified two surface sites on platinum crystal surface that differ in the number of nearest neighbour platinum atoms (Blakely and Somorjai, 1976, Blakely and Somorjai, 1977). The first site, monatomic steps (low index plane steps) were found to be responsible mainly for the breaking of C-H bond (dehydrogenation reaction), while the second site, kinked steps (high index plane steps), were responsible for the breaking of both C-C (hydrogenolysis

reaction) and C-H bonds. Therefore, the active sites for breaking mainly C-H and C-C bonds were the stepped and kinked sites.

The high activation energy across a step site is shown in Figure 3.8, which describes a one-dimensional potential energy profile in the direction of a surface step. An atom/molecule in general chemisorbs more strongly and stays longer at a step site than on the atomically flat terrace. This is often leads to C-H and/or C-C breaking bonds and nucleation of adsorbed overlayers (carbonaceous deposits).

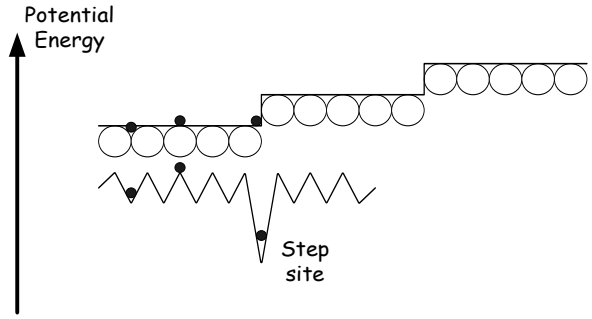

Figure 3.8 One-dimensional energy profile in the direction of a surface step. Note, the larger activation energy barrier for diffusion from step to terrace sites when compared to diffusion on terraces (Attard and Barnes, 1998).

3.3.3 Carbonaceous deposit on platinum single crystal surface

As mentioned previously, during hydrocarbon reactions, the metal surface is covered with a carbonaceous deposit (overlayer). The amount of this deposit could be very small corresponding to very minute coverage but it could potentially be large resulting in coverage of all the active sites. The coverage varies with temperature and the molecular weight of the saturated hydrocarbon reactant molecule. Certain surface reactions take place in the presence of, and possibly with the participation of, such deposits.

The carbonaceous overlayer, that is formed may be ordered or disordered, depending on the platinum surface structure, the nature of the reactant and the hydrogen-hydrocarbon ratio in the experiment. A number of reactions are very sensitive to the presence of ordering on the layer (Blakely et al, 1976). Cyclohexane dehydrogenation to benzene is poisoned

unless the overlayer is ordered, and n-heptane dehydrocyclization to toluene takes place only in the presence of an ordered overlayer (Herz et al., 1981). Other reactions, such as hydrogenolysis of cyclohexane happen even in the presence of a disordered overlayer (Blakely and Somorjai, 1976). Therefore, two different types of carbon deposit can be distinguished on the platinum crystal surface. Ordered overlayer (active carbon), which does not appear to block the chemical activity of the transition metal. Disordered overlayer (graphitic carbon), which poisons the activity of the active metal surface. This type of carbon, although eliminates the reaction rate, it may not necessarily be undesirable. It could play an important role in accelerating the desorption of the reaction products maintaining the active sites clean and accessible for the next incident reactant molecule. A schematic representation of both, ordered and disordered, carbonaceous overlayers on platinum single crystal surfaces as suggested by Somorjai and Blakely is illustrated in Figure 3.9 below :

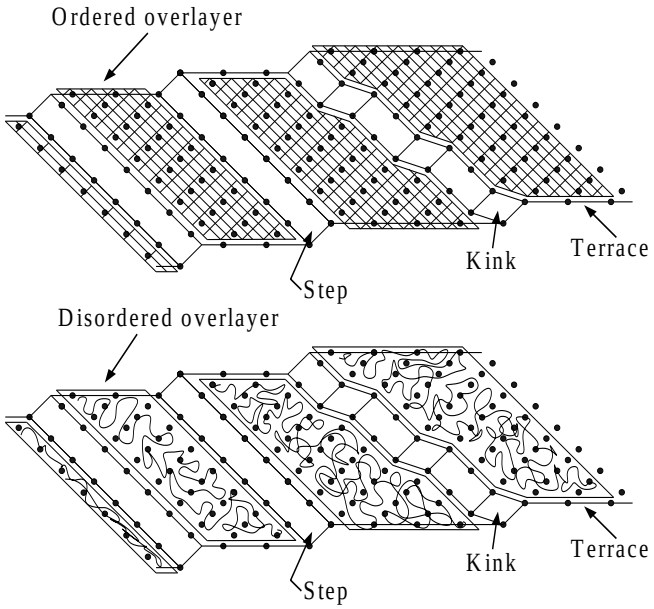

Figure 3.9 Model of active platinum catalyst surface with a full carbonaceous overlayer showing exposed catalytic sites (Somorjai and Blakely, 1975).

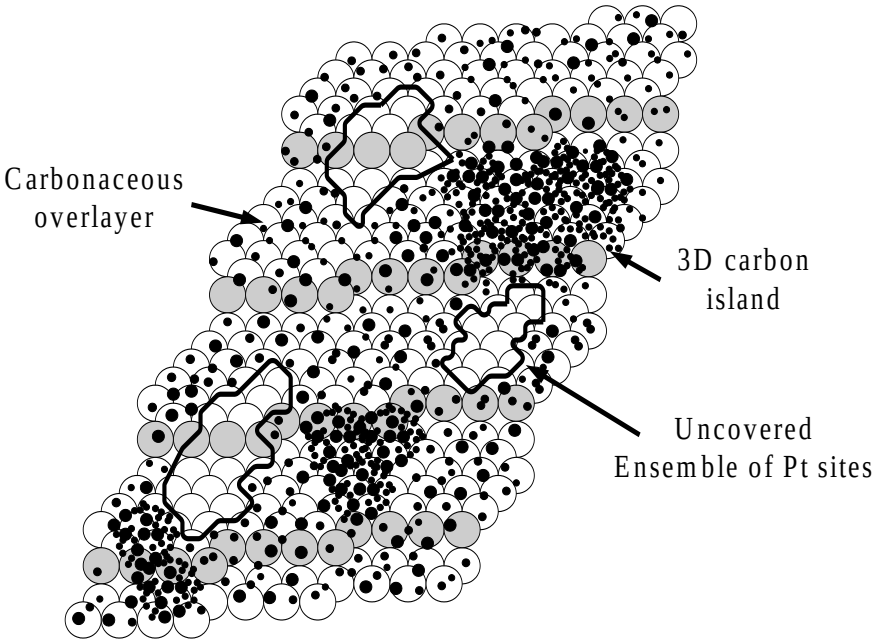

Figure 3.10 Model for the surface composition of platinum reforming catalysts.

Henn et al studied the adsorption of cyclohexane on clean and bismuth-covered Pt(111) crystal planes using thermal desorption spectroscopy (TDS), deuterium labelling, auger electron spectroscopy (AES) and X-ray photoelectron spectroscopy (XPS) (Henn et al., 1989). Their analysis of quantitative XPS data and the effect of bismuth poisoning on the chemisorption of cyclohexane showed that an ensemble of about five platinum atoms is necessary to chemisorb cyclohexane, while an ensemble of at least eight free platinum atoms (in addition of the five required for chemisorption) was required for the dehydrogenation reaction.

Previous work therefore suggests that during steady-state hydrocarbon reactions, the platinum surface was always covered with one, in some cases more, monolayers of strongly adsorbed carbonaceous deposit. Although carbon deposition tends to reduce the reactivity of the metal surface, this was not always the case, since it can provide sites for hydrogen transport with reacting surface species. Davis et al in their work suggested, the presence of carbonaceous deposit enhanced the exchange of hydrogen with reacting species and assisted the release of product molecules (Davis et al, 1982). Somorjai suggested that as long as the composition was $C_nH_{1.5n}$ and the reaction temperature was below 450 K, the organic deposit could be removed readily by heating in a stream of hydrogen (Somorjai, 1994). If the composition converts to $C_{2n}H_n$ then an irreversible adsorbed deposit would be formed, which cannot not be removed in the presence of excess hydrogen.

Although the platinum surface area was covered with carbonaceous deposit, Davis et al in their carbon monoxide adsorption-desorption studies revealed that a small amount of uncovered platinum surface sites was always present (Davis et al., 1984). Using the scanning tunnelling electron microscopy (STEM) studies were carried out at high hydrocarbon and hydrogen pressures. The results indicated that CH_2, C_2H and CH fragments of the carbonaceous deposit were mobile on the surface (they move around by surface diffusion in the presence of co-adsorbed reactant molecules (Baker et al., 1979, Davis et al., 1984, Somorjai and Zaera, 1982). Their mobility makes the active metal sites on the surface available to the reactant molecules forming uncovered metal islands. The coverage of these islands was found to be 2 - 25% of the total surface area. The uncovered metal islands seemed to exist in the form of groups or ensembles that contained several adjacent surface atoms (*Figure 3.10*). By increasing the reaction temperature, the concentration of these sites decreased. The existence of these exposed uncovered ensembles was found to enable hydrocarbon reactions to take place in the presence of carbonaceous deposits.

4 Characterisation and Preparation of Structured Catalysts

4.1 Introduction

Dehydrogenation of MCH is a highly endothermic reaction with a standard heat of reaction and a standard Gibbs free energy (25 °C,1 atm) of ($\Delta H°$) = 204.76 kJ mol^{-1} and ($\Delta G°$) = 95.02 kJ mol^{-1}, respectively (Table 4.1). One way to improve reaction kinetics is to elevate the operating temperature e.g. T > 300 °C.

$\Delta G°$(kJ mol^{-1})	**Feasibility**
$\Delta G° < -41.84$	Very High Equilibrium Conversion
$-41.84 < \Delta G° < 0$	Fairly High Equilibrium Conversion
$0 < \Delta G° < 41.84$	Low Equilibrium Conversion
$\Delta G° > 41.84$	Very Low Equilibrium Conversion

Table 4.1 Criteria for thermodynamic feasibility (Richardson, 1989).

Modification of the catalyst to give the following characteristics would also assist:

- High dehydrogenation activity
- High selectivity towards the formation of aromatics
- Low deactivation rate
- Improved heat transfer characteristics

Research in the 1950s led to a catalyst containing platinum dispersed on the pores of a high surface area alumina support (Maatman, 1959). In the last few decades, the alumina support used has been in the form of pellets. Despite the improved selectivity and deactivation rate of these catalysts, the efficiency of the reaction still appeared to be reduced due to the poor heat transfer characteristics of the support.

The research in this thesis, attempts to overcome this by, loading the alumina on to a metallic support such as Fecralloy, which is conductive and can limit the temperature drop across the reaction bed. The metallic alloy used was in the form of rods, diameter of 0.5mm, supplied by Goodfellows and the composition as provided by the supplier is listed in Table 4.2. Prior to being supplied the rods were annealed at 1100 °C by the manufacturers.

Element	Weight %
Fe	72.8
Cr	22
Al	5
Y	0.1
Si	0.1

Table 4.2 Elemental Composition of Fecralloy as supplied.

This chapter details the methodology involved in the preparation and characterisation of a novel structured catalyst. In addition previous research carried out on each step of the preparation has been reviewed.

4.2 Catalyst Characterisation Techniques

During each step of the catalyst preparation, the morphology along with the chemical composition was modified. After each preparation step, the altered surface of the rods was characterised by:

- Environmental Scanning Electron Microscope (ESEM)
- X-Ray Analysis (EDX)
- X-Ray Diffraction (XRD)
- Scanning Transmission Electron Microscopy (STEM)

4.2.1 Environmental Scanning Electron Microscope

The varied surface morphology of the oxidised alloy samples was analysed using an Environmental Scanning Electron Microscope *(Quanta 200 FEI)*. Each rod sample was examined using the ESEM under high vacuum conditions and coated with gold by the method of physical vapour deposition to enable improved image quality. All samples were analysed at an accelerated voltage of 30.0 kV at magnifications ranging from 50 times to 25,000 times the original size.

4.2.2 X-Ray Analysis

The Energy Dispersive X-Ray Spectrometer, (*EDAX Genesis),* was used to perform an elemental analysis on the surface of the oxidised samples to obtain an indication of the varied surface composition. EDX analysis when performed on powdered samples is a simple procedure with multiple spot analyses being carried out. However, given the geometry of the support, EDX analysis on the Fecralloy rods was non-trivial. The analysis could not be done on the curved surface of the rod as it would result in an error in the elemental composition. This is because; it would not be possible to confirm if the EDX relative signals were from the underlying alloy substrate or the thin oxide layer.

To avoid this ambiguity, prior to analysis, samples were embedded vertically in an electro-conductive DEMOTEC 70 (*Agar Scientific*) resin, which comprised of two material components, based on modified methyl methacrylate (liquid) and conductive carbon (powder). The resin was prepared as per manufacturer's instructions by mixing equal parts of the powder and liquid by weight in a mixing beaker. The rods were cut into strips of 2 cm and fitted onto a PTFE embedding mould, prior to the mixture being poured in. The DEMOTEC 70 resin cured and set within 30 minutes at room temperature (typically 15 °C). Following which, the cured resin was cautiously cut with a low speed saw, to avoid any damage to the embedded samples. The resin was then polished to a smooth finish using a Silicon Carbide plate (*Agar Scientific*) followed by a final polish using diamond paste (*Kemet diamond compound*). The prepared resin was mounted on the ESEM, and EDX analysis was performed on different multiple spots across the oxide layer grown.

Using a Back Scattering Electron Detector, a line scan was done across the oxide layer around the surface of the rod to estimate the thickness of the oxide layer. This technique ensured analysis was done on a flat surface rather than a curved surface, and further increased the interaction volume during analysis, thus reducing the error ($\pm$ 0.01%) and ambiguity in the results. Samples were analysed at an accelerated voltage of 20.0 kV under high vacuum conditions with a beam point size of 1 µm.

4.2.3 X-Ray Diffraction

Using the *Philips X'Pert PRO*, X-Ray Diffraction (XRD) experiments were performed on the samples in the 2θ range of 30 ° - 50 ° and a scanning speed of 0.009 °/min. Slit widths of ¼ ° and ½ ° were used for all the experiments. *X'Pert Data* viewer programme was used to analyse the results obtained from the scan. XRD data confirmed the presence of transition aluminas and further described the alumina phase change that took place with increasing time and temperature.

The XRD peak width (breadth of the peak *B*) is inversely related to the crystallite size of a given phase of the oxide layer as expressed in the Scherrer equation (Bartholomew and Farrauto, 2006);

$$B = \frac{K\lambda}{d\cos\theta} \tag{4.1}$$

where, K is a constant which is ~ 1, λ is X-ray wavelength, d is the crystallite size, θ is the diffraction angle. Using Braggs law, the inter-planar distances were calculated from the XRD data using the equation (Richardson, 1989):

$$n\lambda = 2d\sin\theta \tag{4.2}$$

where, n is an integer equal to 1, λ is X-ray wavelength, d is the inter-planar distance, θ is the diffraction angle.

Given the thin layer of the oxide formed; it was not possible to do a qualitative and quantitative phase analysis based on the crystallite size. However by calculating the inter-planar distances and comparing the results with data in the literature, it was possible to obtain a qualitative phase analysis. This has been detailed further on in the chapter.

4.2.4 Scanning Transmission Electron Microscopy

Using the probe side aberration corrected *FEI Titan G2* fitted with an *X-FEG* electron source, it was possible to study the platinum dispersion on the alumina coating applied on the Fecralloy rods. The alumina coating was removed off the Fecralloy rods by gently crushing the rods. The coating removed was gently crushed using a mortar and pestle with a few drops of ethanol (*Analytical Reagent, Sigma Aldrich*). The prepared suspension, was pipetted downwards on a carbon grid, once the ethanol had evaporated the samples were imaged on the STEM at an accelerated voltage of 200 kV under high vacuum conditions. Different particles were analysed in order to obtain an average size of platinum and also to understand the platinum dispersion on the alumina coating.

4.3 Preparation of Structured Catalyst

The last few years have seen a growing interest towards structured reactors. However the usage of these reactors requires the shaping of a suitable catalytic phase. Different combinations of treatment and coating methods have been proposed by researchers. The preparation of the catalyst requires four key steps which have been summarised in Figure 4.1. A detailed analysis of the key parameters involved in every step of the preparation has been done in order to obtain the most suitable preparation method.

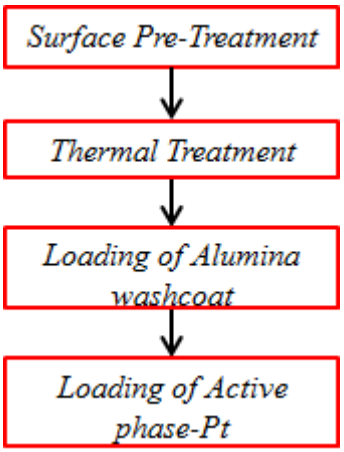

Figure 4.1 Steps in preparation of structured catalyst.

4.3.1 Surface Pre-Treatment

The Fecralloy rods were cut into lengths of 50 cm and sandpapered (*Emery cloth medium grade*) to remove any oxide layer which might have formed during the annealing process at the manufacturing site. In addition, previous work suggested that an increase in surface texture enhances the growth of an alumina layer (Zhang et al., 2009).

Following the mechanical surface roughening, a three step chemical treatment described by Wu et al was carried out to remove any silicon deposits which might have occurred during sandpapering and organic or water based contaminants from despatching (Wu et al., 2001). The rods were first subjected to a caustic wash in 0.1M KOH (*Fisher Scientific*) for 10 minutes followed by an acid wash in 0.1M HNO_3 (*Sigma-Aldrich*) for the same time. The final step was ultrasonification in acetone (*Fisher Scientific*) for 30 minutes followed by de-ionised water in an ultrasonic bath and dried in an oven at 100 °C for 15 minutes. ESEM images revealed the difference in surface morphology before and after roughening with sandpaper (Figure 4.2).

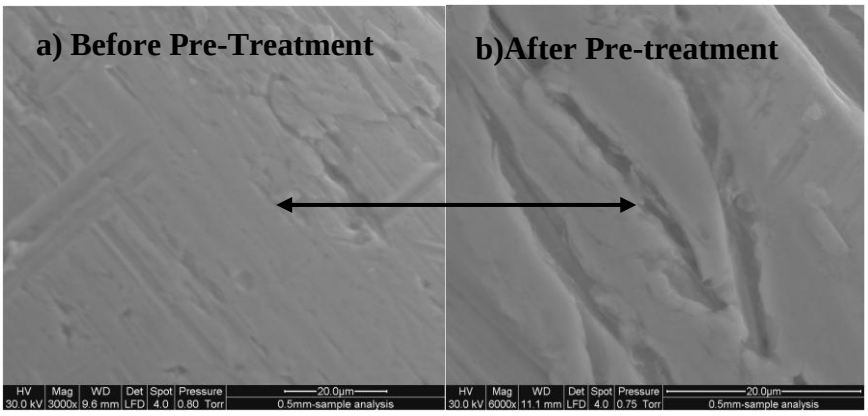

Figure 4.2 ESEM characterisation of rod surface before and after Pre-treatment.

4.3.2 Thermal Oxidation

Fecralloy prior to being loaded with an alumina washcoat was thermally oxidised to obtain a uniform γ - Al_2O_3 substructure layer. In order to obtain the desired layer, it was

essential to do a detailed thermal oxidation study. The following sections details previous research and a comparison with the work carried out by the author.

4.3.2.1 Thermal Oxidation - Literature review

Previous authors have shown that the alloy can be used as a good catalyst support. Alumina scales can be grown at temperatures as high as 1300 °C, depending on the type of layer required (Blachère et al., 2003). These surfaces provide good oxidation resistance and protect the alloy from degradation when the alloy is to be used as a catalyst support at high temperatures. Different phases of alumina are formed at different temperatures of oxidation. The phase transformation that takes place is a very slow process. Figure 4.3 describes the various phases that are formed at the different temperatures of oxidation. The phase changes from boehmite to alpha occur with the loss of hydroxyl groups, which results in the formation of the η -, γ -, δ - phases at the different stages of oxidation as illustrated in Figure 4.3. Alumina formed at lower temperatures (η - ,γ - ,δ -) are based on the cubic close packing of oxygen ions. Alumina formed at higher temperatures (θ -, α -) are anhydrous in nature with a low surface area and hence are less suitable as catalytic supports.

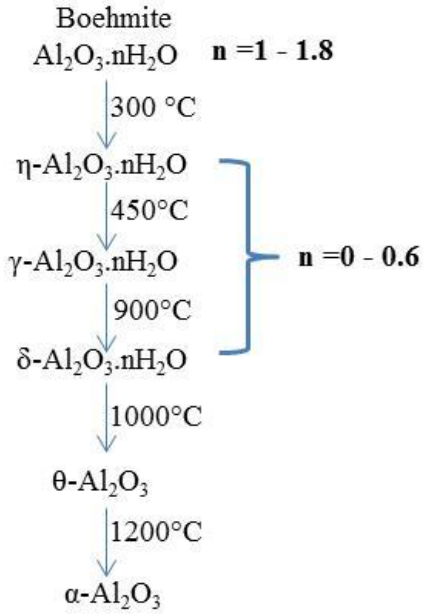

Figure 4.3 Different phases of alumina formed at different stages of oxidation (Richardson, 1989).

Liu et al in their work suggested that, in the presence of water vapour γ - Al_2O_3 did not transform to α - Al_2O_3 (Liu et al., 2008). Their work also showed that the presence of water vapour during the high temperature oxidation resulted in the formation of a more stable γ - Al_2O_3 layer. This could be attributed to the tendency of the γ - Al_2O_3 to adsorb water at high temperatures (Buscail et al., 1997). In addition, it was found that the resulting layer was thermodynamically and kinetically more stable.

Work done by numerous authors has suggested that during the different stages of oxidation different phases of alumina grow on the surface of the alloy depending on the time and temperature of oxidation as summarised in Table 4.3. The authors have proven that different phases of alumina exhibit different growth mechanisms. Lee et al in their research showed that the alumina scale was formed due to the outward diffusion of aluminium, which was prevalent even at temperatures of 1200 °C (Lee et al., 1998). Lee et al further suggested the outward diffusion of the cations created a vacancy influx at the oxide/metal interface, which when present in excess resulted in increased growth stress and spallation. Badini and Laurella in their work showed that the different growth mechanisms could be attributed to the different rates of diffusion that aluminium and oxygen exhibit at varied oxidation temperatures (Badini and Laurella, 2001). It was found that at temperatures of 900 °C, the outward diffusion of aluminium was predominant which resulted in the growth of an alumina scale which had a whisker like morphology. However, when the temperature was increased to 1200 °C, alumina grown on the surface had a flat scale. Badini and Laurella attributed the growth of the flat scale to the inward diffusion of oxygen which became more prevalent at higher temperatures. They described the formation and growth of the oxide layer by the parabolic rate equation

$$x^2 = K_p t \tag{4.3}$$

where, x was the layer thickness, K_p the parabolic rate constant and t the oxidation time.

The growth mechanism described by Badini and Laurella was further confirmed by Berthome et al (Berthome et al., 2005). The various researchers in their work suggested that the transient aluminas were formed by an outward diffusion of aluminium whilst the flat scale α - Al_2O_3 was formed due to an inward diffusion of oxygen.

Author	Thermal Oxidation		Alumina Phase
	Time	Temperature (°C)	
Lee et al., 1998	2 h	1200 °C	α - Al_2O_3
Badini and Laurella, 2001	30 days	900 °C	α - Al_2O_3,,underlying transient alumina scales present
Blachère et al., 2003	14 h	1200 °C	α - Al_2O_3
Berthome et al., 2005	5 h	850 °C - 925 °C	Transient aluminas
El Kadiri et al., 2005	110 h	900 °C	γ - Al_2O_3
Chapman and Watton, 1981	24 h	900 °C	γ - Al_2O_3
Buscail et al., 1997	2 h	1000 °C	Transient aluminas
Valentini et al., 2001	10 h	900 °C	α - Al_2O_3
Samad et al., 2011	1 h	930 °C	α - Al_2O_3

Table 4.3 Previous research done on oxidation of Fecralloy.

Thermal oxidation results in a weight change which could be attributed to the formation of an oxide layer. The weight change associated with the formation of transient oxides is higher than the weight change associated with the formation of a more stable alpha layer (El Kadiri et al., 2005). In Figure 4.4, the early stages of oxidation have been illustrated, during which the needle like morphology can be seen growing on the surface and was mainly γ - Al_2O_3.

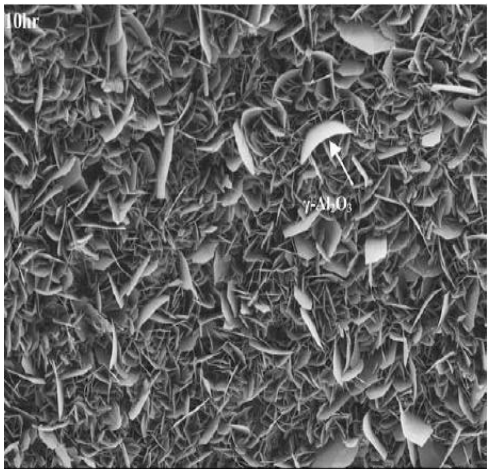

Figure 4.4 Oxide Surface after 10 h at 900 °C (El Kadiri et al. 2005).

Research by Clemendot et al showed that the addition of reactive elements such as yttrium, by the manufacturers, improved the adhesion of the oxide layers which are formed on the metal supports (Clemendot et al., 1993). This increased the hot oxidation resistance of these alloys and was attributed to the stable oxides that yttrium forms. To support this finding, heats of formation for the key components of the rods are shown in Table 4.4 with yttrium far exceeding all other elements. In addition, work by Blachere et al and, Nychya and Clark, showed that the addition of yttrium to Fecralloy resulted in the growth of an oxide layer which had a columnar morphology (Blachère et al., 2003, Nychka, 2005). This columnar morphology limited the mobility of the aluminium cations and thus limited the outward diffusion of aluminium to the surface. Therefore, the depletion of aluminium from the alloy was limited and which resulted in decreased lateral stresses and spallation of the oxide layer.

Oxide	**ΔH_f (kJ/mol)**
Fe_2O_3	825
Cr_2O_3	1140
Al_2O_3	1676
Y_2O_3	1905

Table 4.4 Heats of formation of potential oxides formed during oxidation of Fecralloy.

Based on the review of the work done by previous researchers on the oxidation of Fecralloy, an experimental study was carried out in order to obtain the most suitable oxidation conditions of time and temperature in addition to studying the effect the different oxidation parameters had on the Fecralloy.

4.3.2.2 Experimental study of the thermal oxidation of Fecralloy rods

Small samples of the Fecralloy rods were initially oxidised in a TGA, at varied operating parameters of temperature and time. This enabled the author to obtain the optimum conditions to scale-up the thermal oxidation of the Fecralloy rods in order to obtain the required alumina morphology.

Small scale oxidation study

To investigate the oxidation of Fecralloy rods, samples were isothermally oxidised and the weight change of the samples analysed using the *TA Instruments, Q5000-IR*, TGA. Six samples of Fecralloy rods; each weighing 50 mg (± 1%) were placed in ceramic pans. Each sample was oxidised, in air (constant flowrate 50 ml/min) at a ramp rate of 10 °C/min and isothermally oxidised at temperatures between 800 °C - 1200 °C and various sampling times of 0.5 h - 16 h. Following which, the effect of the oxidation parameters, time and temperature, on the Fecralloy rods was investigated using the characterisation techniques of ESEM, EDX and XRD.

Effect of Oxidation Temperature on Fecralloy rods

A comparison of the surface structure when oxidised isothermally for 16 h at different temperatures in the range of 800 °C - 1200 °C has been shown in Figure 4.5. The surface appeared to be smooth when oxidised at 800 °C (*Figure 4.5(a)*). ESEM images revealed a morphology which was very similar to the rod surface prior to any oxidation treatment (*Figure 4.2*(b)). At 900 °C short alumina oxide platelets appeared to be forming on the surface which at 1000 °C seemed to have transformed into a dense growth of platelets. However a further increase in temperature resulted in sintering of the oxide later (1100 °C) and a complete phase transformation occurred at 1200 °C as shown in Figure 4.5(e). At 1200 °C (*Figure 4.5(e)*) there appeared to be a wrinkling effect taking place on the surface of the rods. Chapman and Watton in their research showed that increased time of exposure or very high temperature oxidation resulted in sintering of the oxide scale which would render the alloy unsuitable to be used catalytically (Chapman and Watton, 1981). The research in their patent also suggested, that the most suitable morphology on the alloy surface, when used as a catalytic support was the growth of randomly oriented whiskers. High temperature oxidation of the Fecralloy rods carried out by the author resulted in spallation of the oxide layer as can be seen from the ESEM image Figure 4.6.

Mennicke et al in their research found, exposure to high temperature oxidation for very long periods resulted in a depletion of the Al reservoir (Mennicke et al., 1998). This depletion further resulted in breakaway oxidation of Fe and Cr resulting in a thick mixed oxide layer and also increased strain in the oxide layer. Lateral growth strains further caused

an increase of compressive stress in the oxide layer, resulting in fragments of the layer being ejected from the surface.

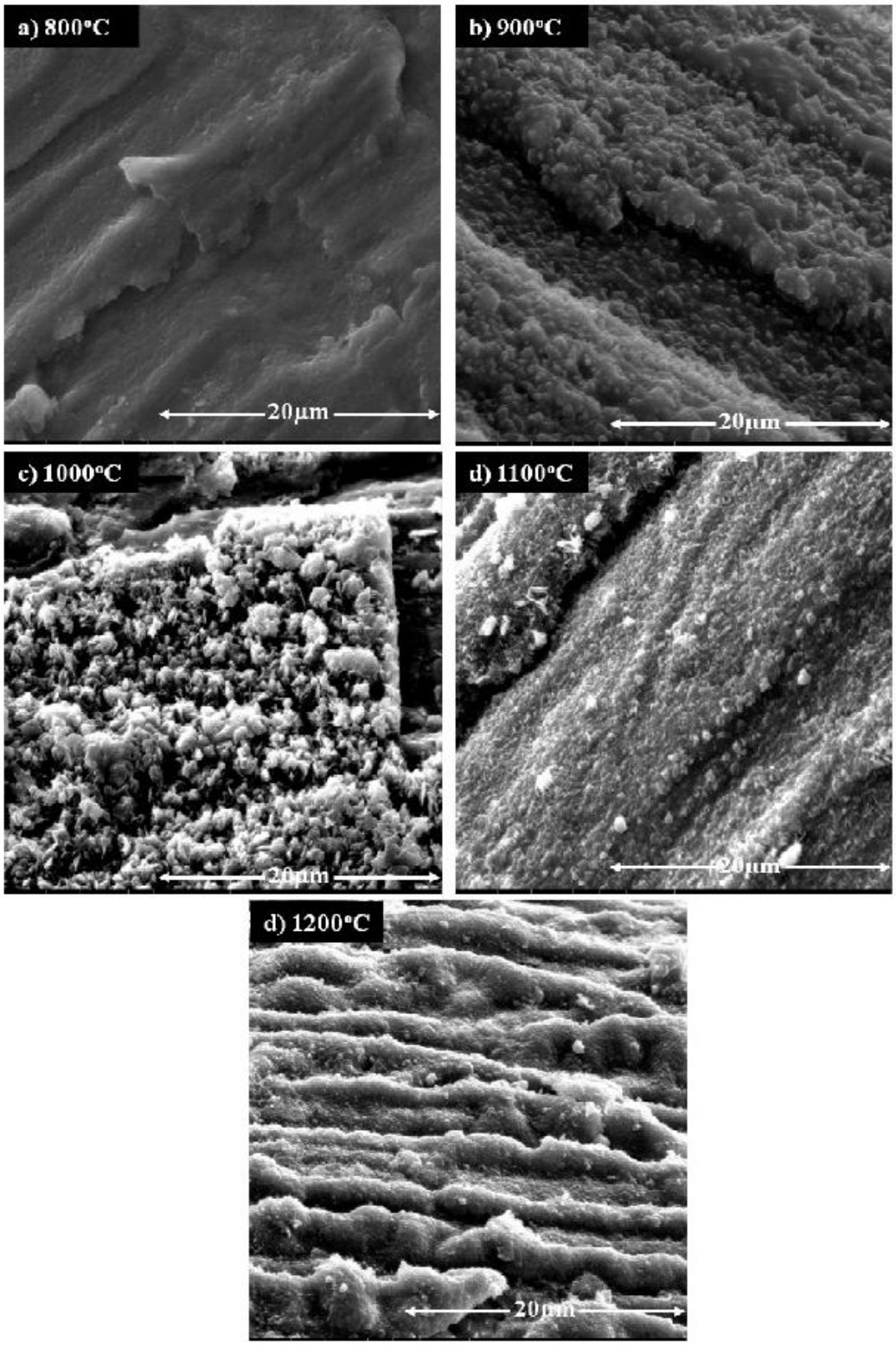

Figure 4.5 Varied morphology when isothermally oxidised at 800 °C - 1200 °C for 16 h.

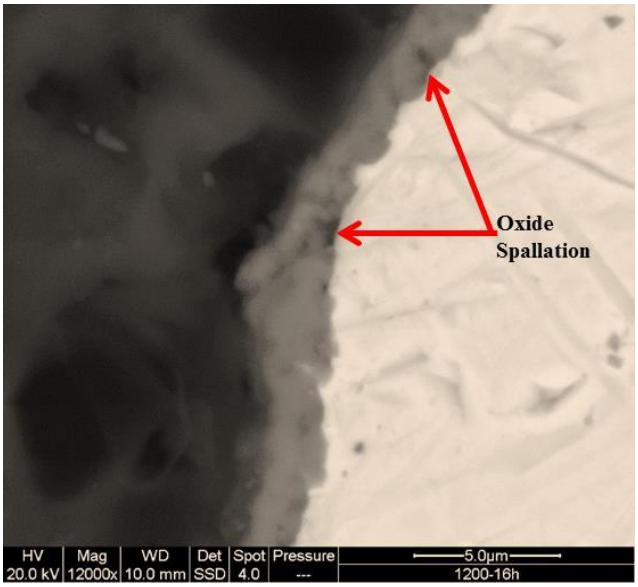

Figure 4.6 Cross-section of Fecralloy rod oxidised at 1200 °C for 16 h.

The data obtained from the EDX characterisation on the surface of the rods when isothermally oxidised for 16 h at temperatures between 800 °C - 1200 °C has been shown in Table 4.5. The Al content increased with increase in temperature resulting in an increase of the Al/Fe ratio. By embedding the samples in an electro-conductive resin, it was possible to do a line scan analysis across the cross-section of the oxide layer using the back scattering electron detector. This gave a better understanding of the nature of the oxide layer grown on the Fecralloy rods Figure 4.7.

	Weight%				
T	**O**	**Al**	**Cr**	**Fe**	**Al/Fe**
800 °C	4.3	18.7	27.3	49.8	0.4
900 °C	23.6	74.5	0.6	1.2	60.1
1200 °C	11.9	85.7	1.3	1.2	73.0

Table 4.5 EDX characterisation of Fecralloy when oxidised for 16 h at 800 °C - 1200 °C.

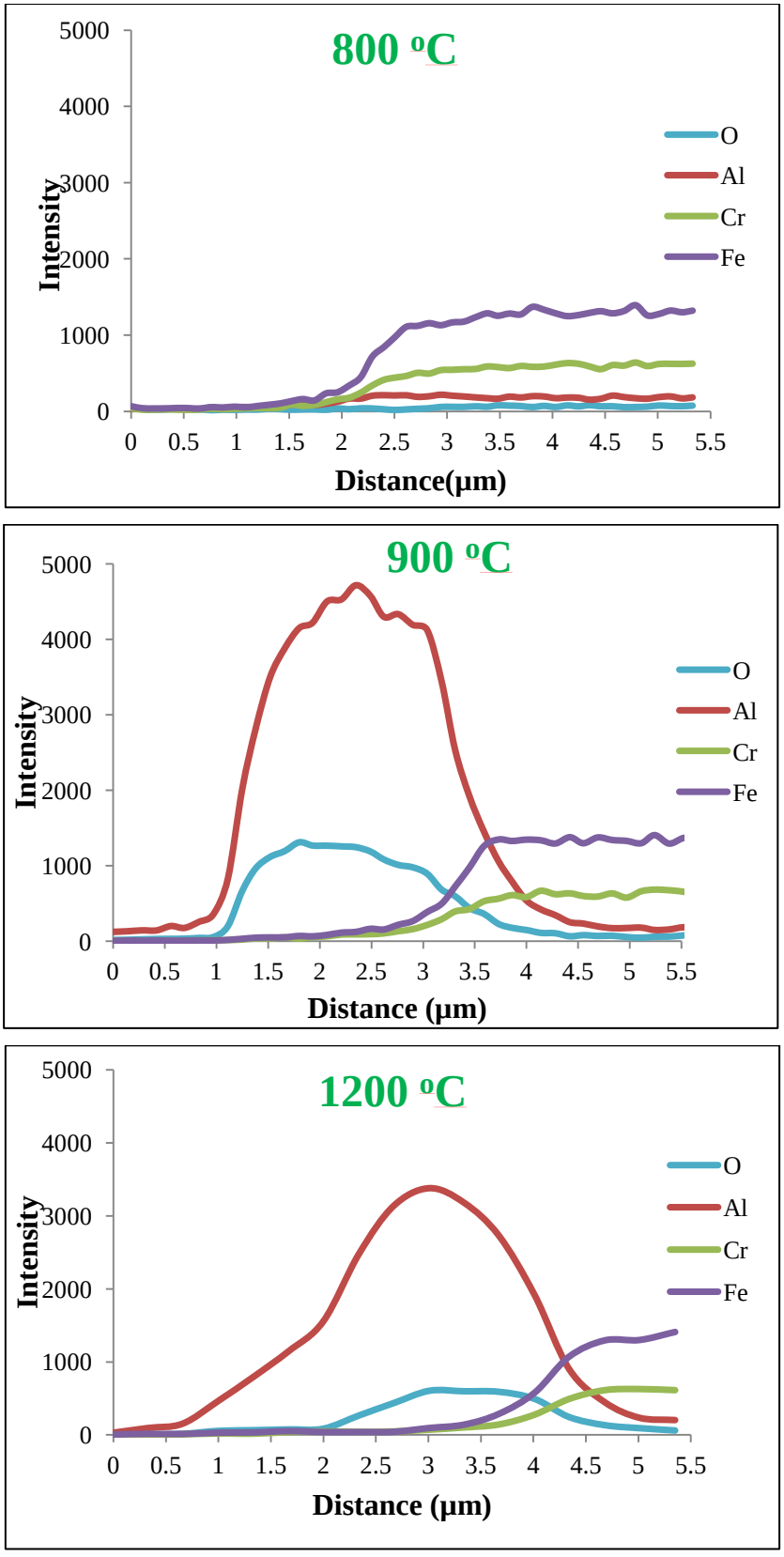

Figure 4.7 Line scan analysis of cross-section of Fecralloy rod oxidised for 16 h at 800 °C - 1200 °C.

The line scan analysis of samples heated in air at 800 °C indicated that the oxidation process of the Fecralloy rods was very slow thus suggesting the temperature of oxidation was too low. Thermal oxidation at 900 °C and 1200 °C resulted in an oxide layer of thickness 2 µm and 3 µm respectively. Figure 4.7 illustrates a clear difference in the intensity of the O signals. The apparent difference in the oxygen content (at 900 °C and 1200 °C) can be attributed to the formation of an anhydrous α - Al_2O_3 layer at 1200 °C i.e. a complete phase transformation.

A thorough investigation of the varied elemental composition at different points on the alloy and oxide scale was done and has been summarised in Figure 4.8. The graphs describe the change in elemental concentration of the oxide layer, the alloy/scale interface and at approximately 3 µm below the scale substrate. The graphs confirm that the alumina scale growing on the alloy rods was by an Al outward diffusion mechanism. In addition it can also be inferred, that the Al was preferentially oxidised when compared to the Fe and Cr with increasing temperature.

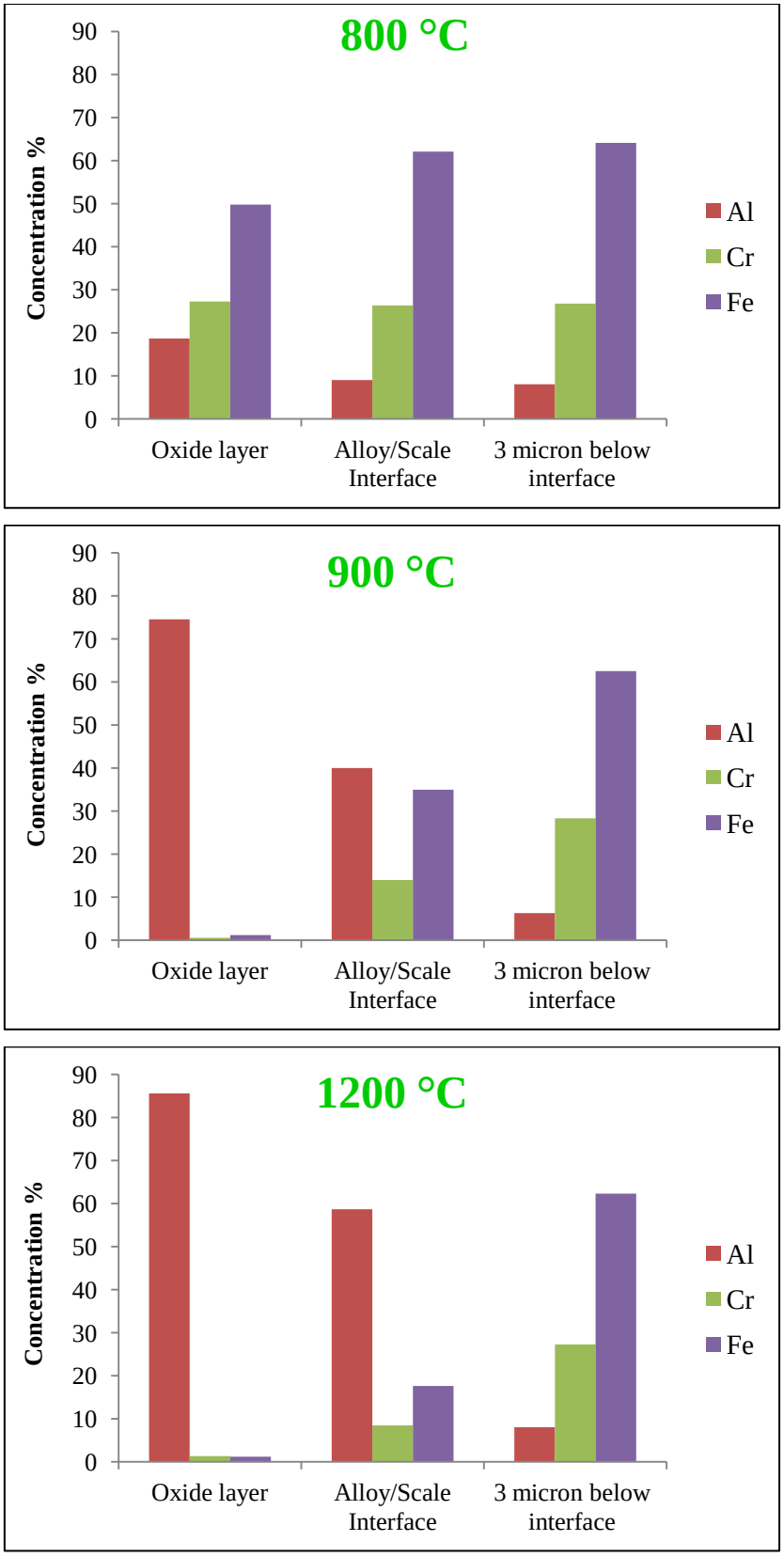

Figure 4.8 Changing concentration of Al, Cr and Fe across the Fecralloy rods when oxidized at 800 °C - 1200 °C for 16 h.

Figure 4.9 shows the increasing intensity of Al_2O_3 peaks when samples were oxidised isothermally for 16 h between 800 °C - 1200 °C. With increasing temperature the peaks appeared to be getting sharper indicating a phase transformation and the formation of lower surface area θ - and α - Al_2O_3. The increasing intensity of the alumina peaks was an indication of the oxide layer growing thicker with increasing temperature. Using Braggs law (*Equation 4.2*), the inter-planar distances were calculated and compared to the work done by Jedlinski to obtain a qualitative phase analysis which has been shown further in the chapter in Table 4.8 (Jedliński et al., 2009).

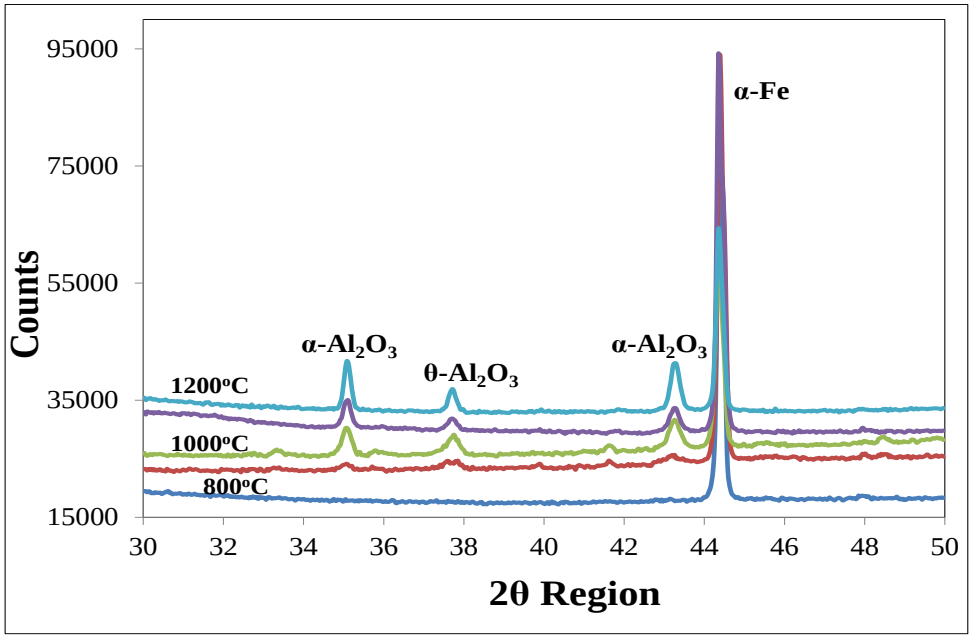

Figure 4.9 XRD peaks of Fecralloy oxidized for 16 h at temperatures between 800 °C - 1200 °C.

Characterisation results of the Fecralloy samples post thermal oxidation, revealed the most suitable temperature of oxidation was between 900 °C - 1000 °C.

Effect of Oxidation Time on Fecralloy rods

Following the temperature study, an oxidation time optimization study was carried out using the TGA. Samples were isothermally oxidised at 1000 °C for varying time periods between 0.5 h - 16 h, and the varied morphology is shown in Figure 4.10.

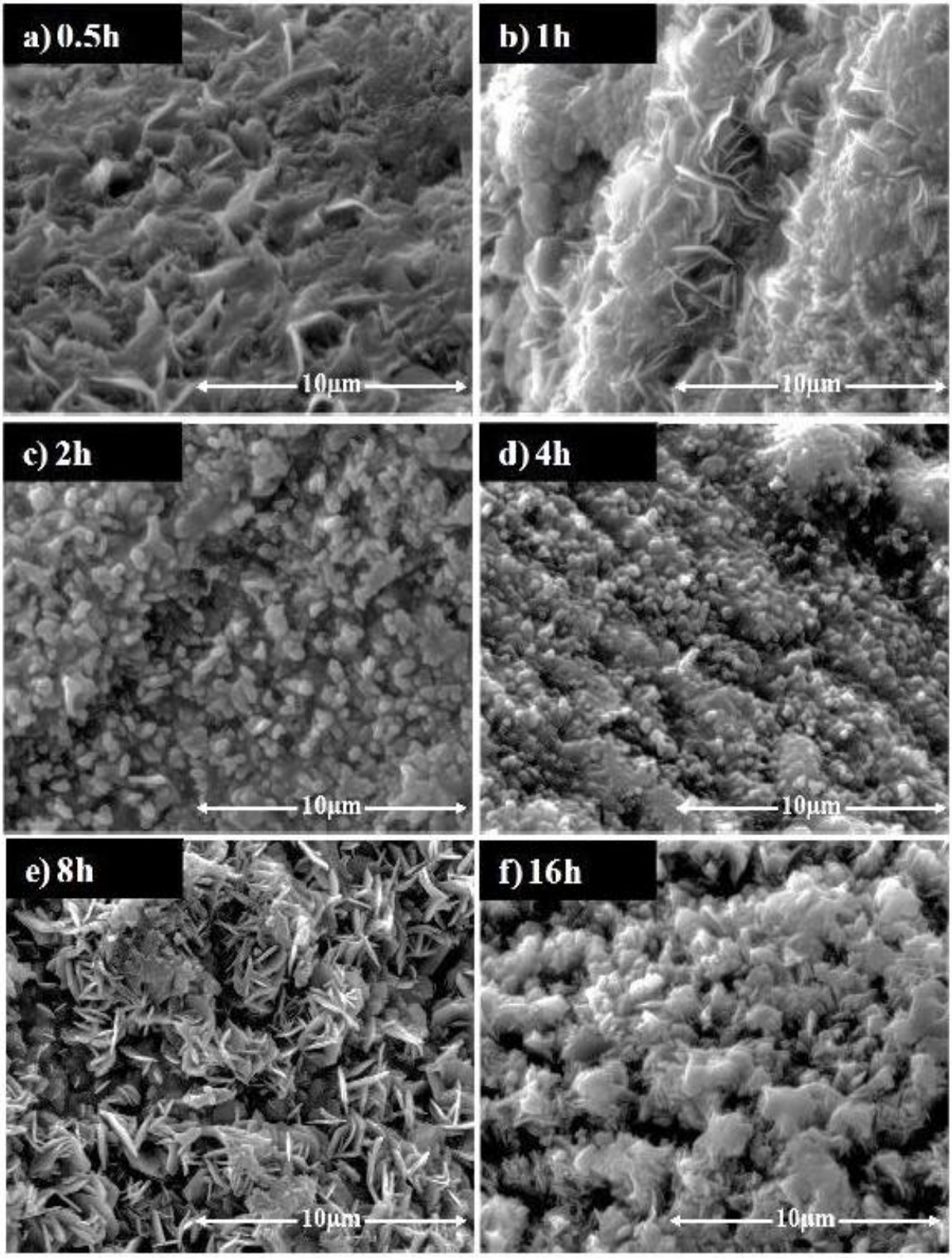

Figure 4.10 Varied morphology when isothermally oxidized at 1000 °C for 0.5 h - 16 h.

During the initial stages of oxidation, it is known that, Fe and Cr ions tend to get preferentially oxidised due to their increased concentration and lower heats of formation as shown in Table 4.2. However, Al has a higher affinity for O when compared to Fe and Cr ions, thus with the passage of time and increased outward diffusion of Al, the Al gets preferentially oxidised resulting in an alumina layer (Airiskallio et al., 2010). The Cr_2O_3 that is initially formed has been reported as acting as nucleation centres for the Al_2O_3 (Asteman and Spiegel, 2008).

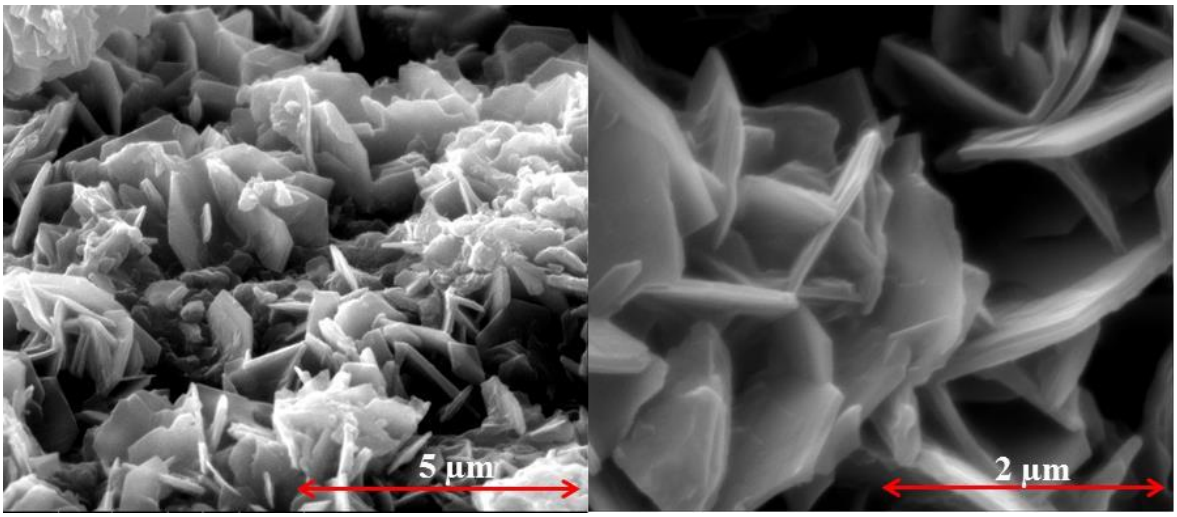

Figure 4.11-ESEM images describing the whisker like morphology growing on the Fecralloy after oxidation at 1000 °C for 8 h

Isothermal oxidation at 1000 °C resulted in a growth of platelets formed across the surface. Although a platelet-like morphology was seen forming on the surface, as early as 0.5 h (*Figure 4.10(a)*), they were short and flat during the initial stages of thermal oxidation, which would not be suitable when the washcoat layer was to be applied. With increasing time these platelets transformed into α - Al_2O_3 nodules which form nucleation centres for further densification and growth of new platelets as depicted in Figure 4.10(c & d). Finally by 16 h these platelets sintered producing a more condensed phase. The alloy surface shown in Figure 4.10(e) has long randomly oriented whiskers formed on the alloy surface after 8 h of isothermal oxidation at 1000 °C. ESEM analysis at a higher magnification described the morphology in greater detail as illustrated in Figure 4.11. Previous authors have described this morphology to be that of transient aluminas. (Badini and Laurella, 2001, Kadiri et al., 2005). ESEM analysis of a cross section of the Fecralloy rod oxidised for 8 h at 1000 °C (*Figure 4.12*) revealed a well attached uniformly grown oxide layer.

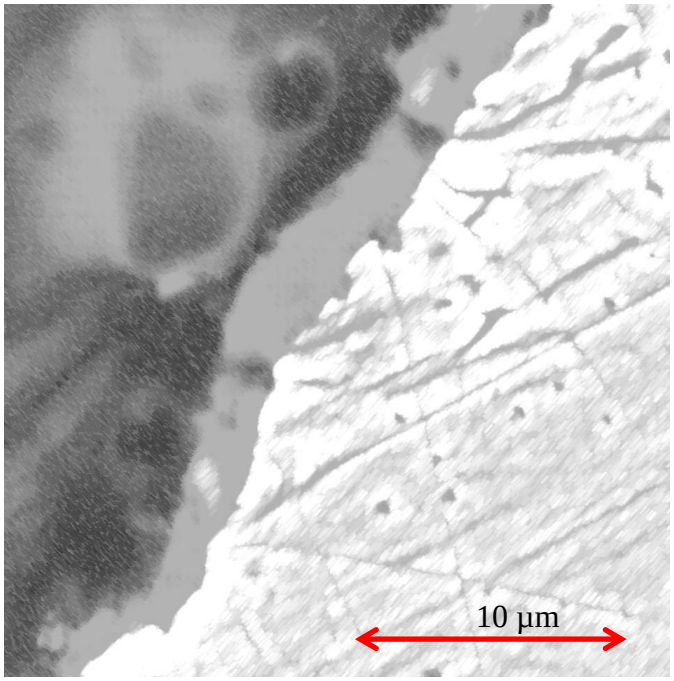

Figure 4.12 Cross-section of Fecralloy rod when oxidised at 1000 °C for 8 h.

A comparison of the oxide morphology on the Fecralloy rod post thermal oxidation at 1000 °C for 8 h and 16 h has been illustrated in Figure 4.13. The phase transformation from transient (η - ,γ - ,δ -) alumina to a more anhydrous, θ - and α - Al_2O_3 can clearly be seen. Although, it is important to note, that after oxidation at 1000 °C for 16 h, the phase transformation is not complete. The author would like to point out the occurrence of a mixed phase alumina layer i.e. presence of an underlying transient alumina layer which can be seen in Figure 4.13(b) and presence of a lower surface area phase.

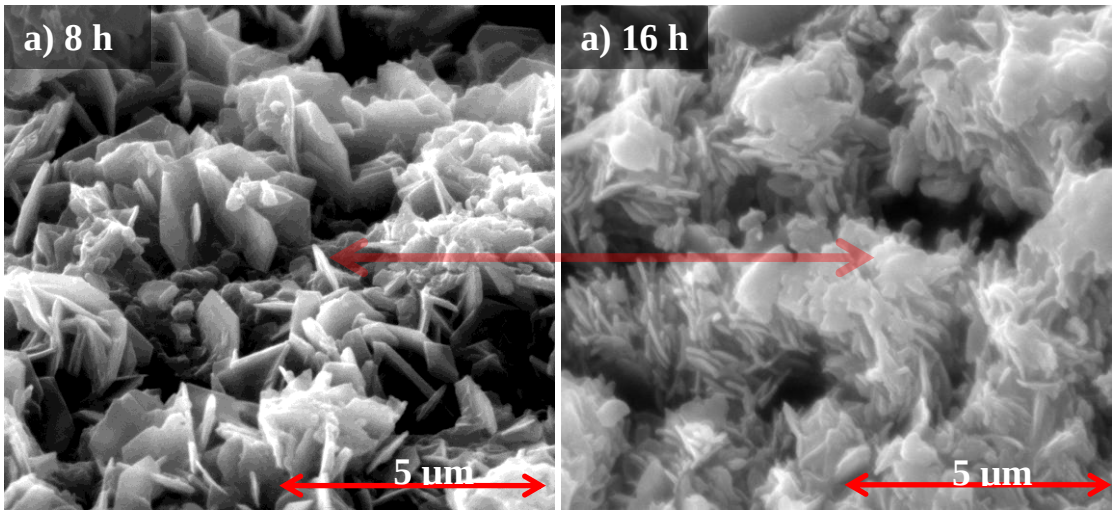

Figure 4.13 Comparison of oxide morphology on Fecralloy rod after thermal oxidation at 1000 °C for a) 8 h b)16 h.

The varied elemental composition on the surface of the Fecralloy rod post iso-thermal oxidation at 1000 °C for varied sampling times of 0.5 h - 8 h has been tabulated in Table 4.6. Initially there was a rapid increase in concentration of Al which stabilized with time. Results confirmed that with increasing time, as the thickness of the alumina layer increased, a decrease in concentration of Fe and Cr was observed.

	Weight%				
	O	**Al**	**Cr**	**Fe**	**Al/Fe**
0.5h	8.5	43.9	14.1	33.6	1.3
2h	32.8	61.4	2.3	3.5	17.7
8h	33.0	62.6	2.3	2.1	29.5

Table 4.6 EDX characterisation of the Fecralloy surface when oxidised at 1000 °C for 0.5 h - 8 h.

Using the EDX line scan programme in the *EDAX GENESIS* software package, the thickness of the oxide layer could be calculated (*Table 4.7*). The nature of the oxide layer grown on Fecralloy rod has been illustrated in Figure 4.14. With the passage of time the Al concentration present on the surface increased with time. Oxidation at 1000 °C for 8 h resulted in a rich transient alumina layer which had minimal concentrations of Fe and Cr.

Oxidation Time	**Alumina (Wt%)**	**Alumina layer thickness (µm)**
0.5h	52.4	0.4
2h	94.2	1.1
8h	95.6	3.7

Table 4.7 Thickness and composition of Alumina layer when oxidised at 1000 °C for 0.5 h - 8 h.

The data obtained from the line scan analysis was summarised in the form of bar charts which described the changing concentration of Fe, Cr and Al with time at 1000 C across the alumina scale grown on the Fecralloy rods (*Figure 4.15*). The figure illustrates the increased Al outward diffusion with time. During the initial stages of oxidation there was an increased presence of Fe and Cr present in the oxide layer, thus suggesting these cations are oxidised initially. However with the passage of time and increasing outward diffusion of Al, an alumina layer was formed with very minimal concentrations of Fe and Cr.

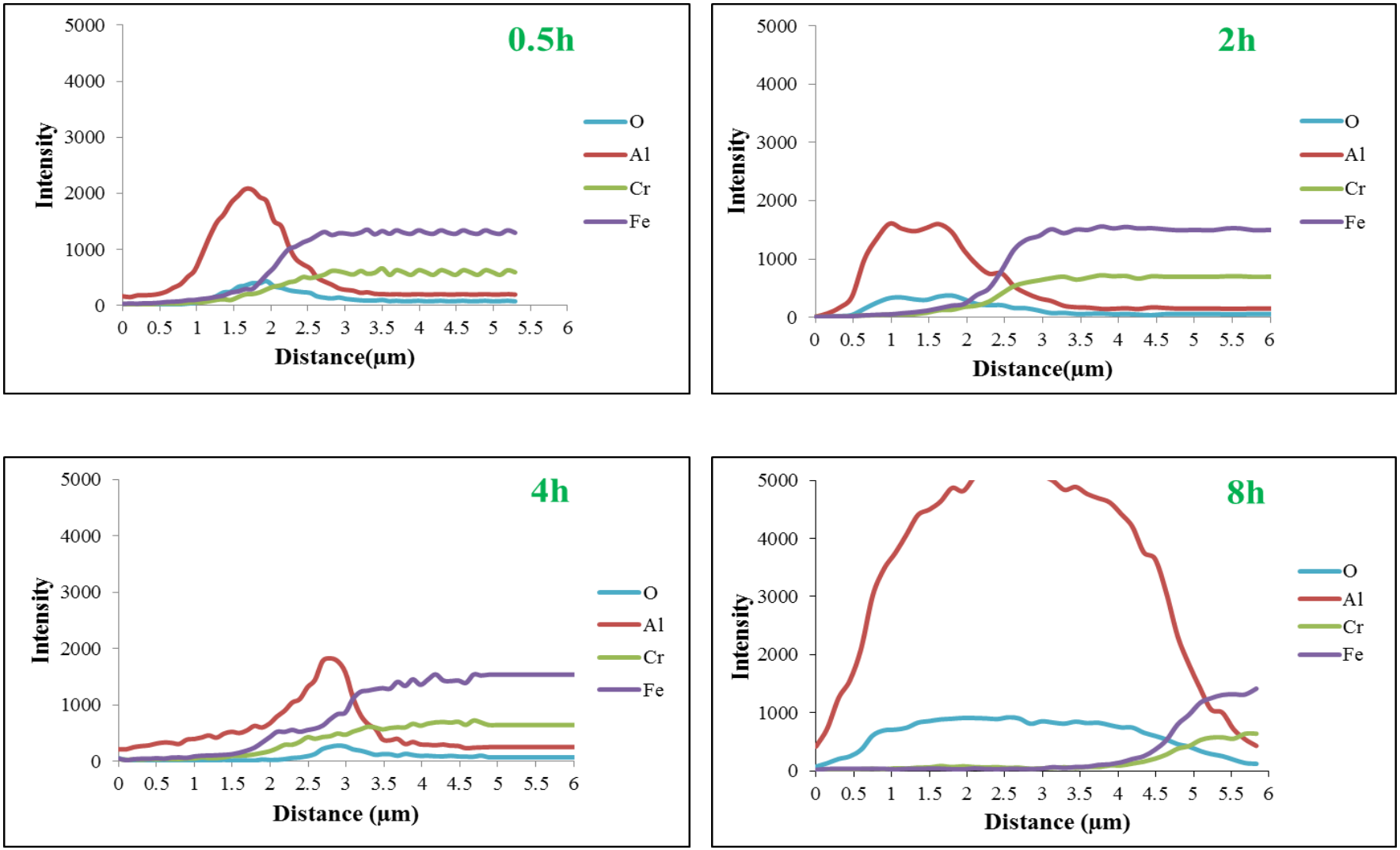

Figure 4.14 Line scan analysis of cross-section of Fecralloy rods oxidised at 1000 °C for 0.5 h - 8h.

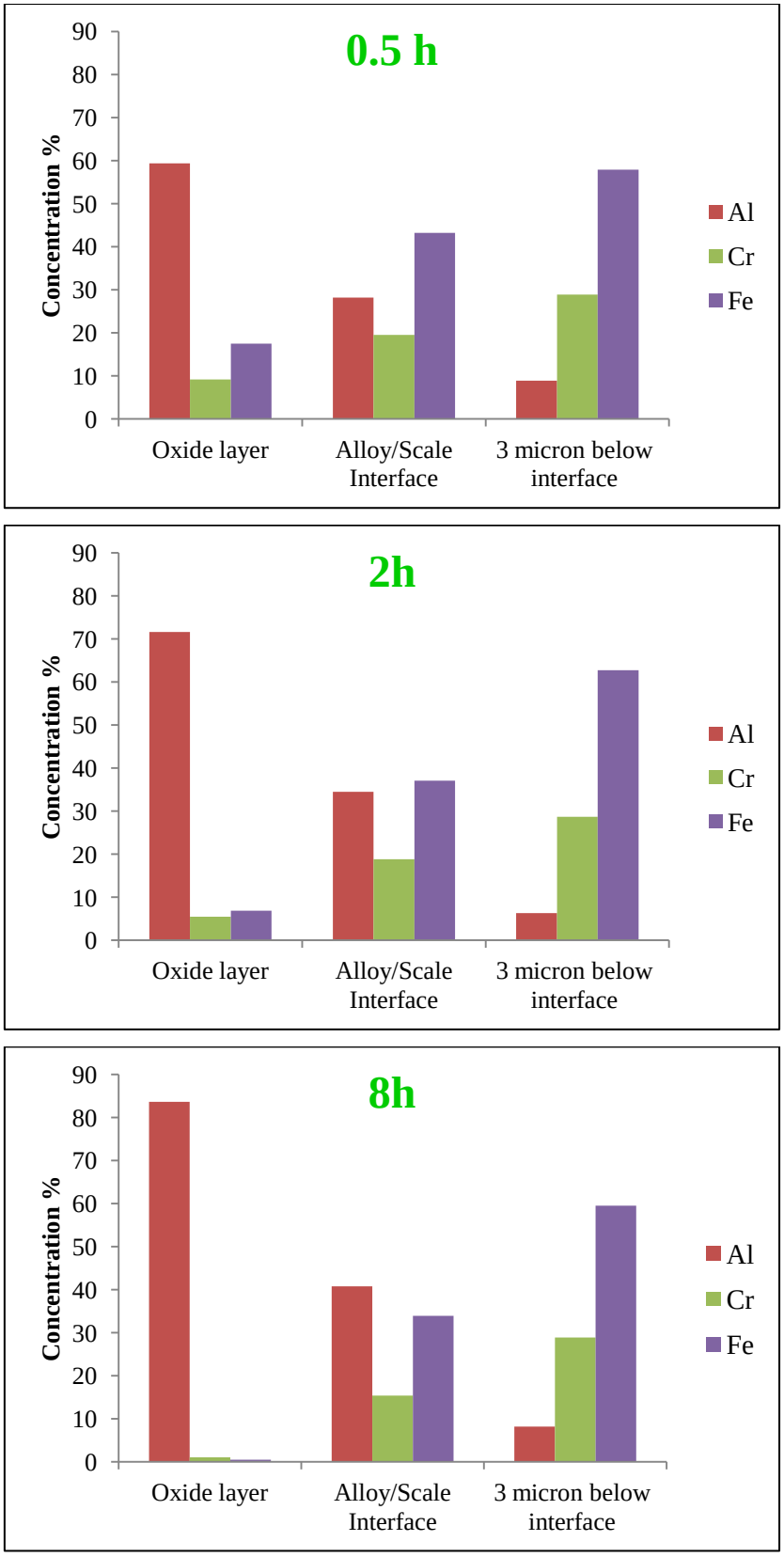

Figure 4.15 Changing concentration of Al, Cr and Fe across the Fecralloy rods when oxidized at 1000 °C for 0.5 h - 8 h.

The outward diffusion of Al and inward diffusion of O resulted in an outward growth of a transient alumina rich layer on the surface. XRD data showed the varying intensity of peaks when samples were oxidised isothermally at 1000 °C for 0.5 h - 16 h (*Figure 4.16*). With increasing time periods the peaks obtained appeared to be getting sharper indicating a phase transformation to a more crystalline lower surface area θ - and α - Al_2O_3.

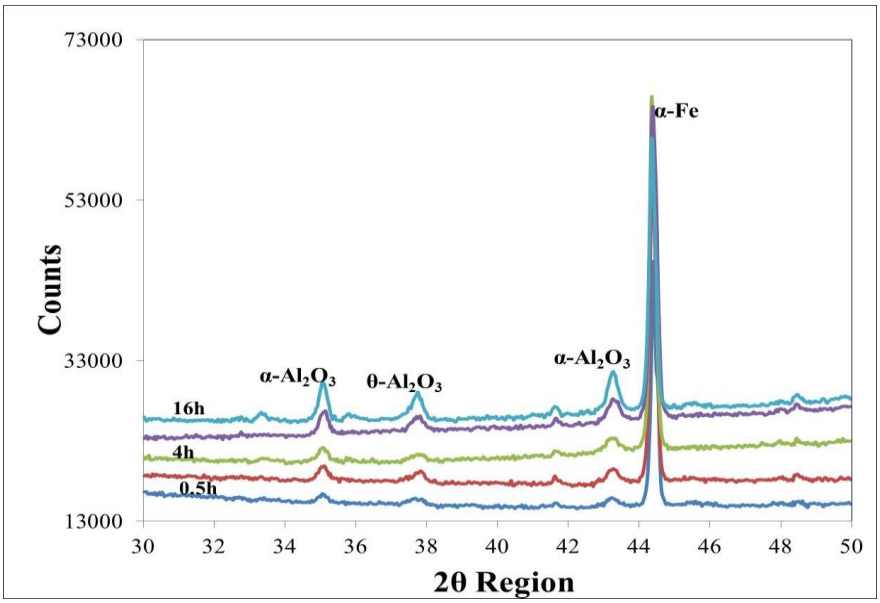

Figure 4.16 XRD peaks of Fecralloy oxidised at 1000 °C for 0.5 h – 16 h.

Oxidation at 1000 °C resulted in a varied surface morphology. After investigating all the characterisation results, the most suitable time and temperature of oxidation were found to be 8 h at 1000 °C. Thermal oxidation at these operating condition resulted in an increased concentration of Al on the surface in addition to the growth of long randomly oriented whiskers, thus making the surface suitable to be used as a catalytic support.

Summary of oxidation study of Fecralloy rods on a small scale

Based on the experimental data obtained from the thermal oxidation of Fecralloy, the oxide morphology formed at different temperatures and time periods could be schematically summarised, as shown in Figure 4.17. The graph is an indication of a suitable time period for different operating temperatures to obtain the required morphology. Solid line depicts where the morphology at the specific time and temperature are known and dotted lines are an extrapolation of available data sets where the experimental results are not available.

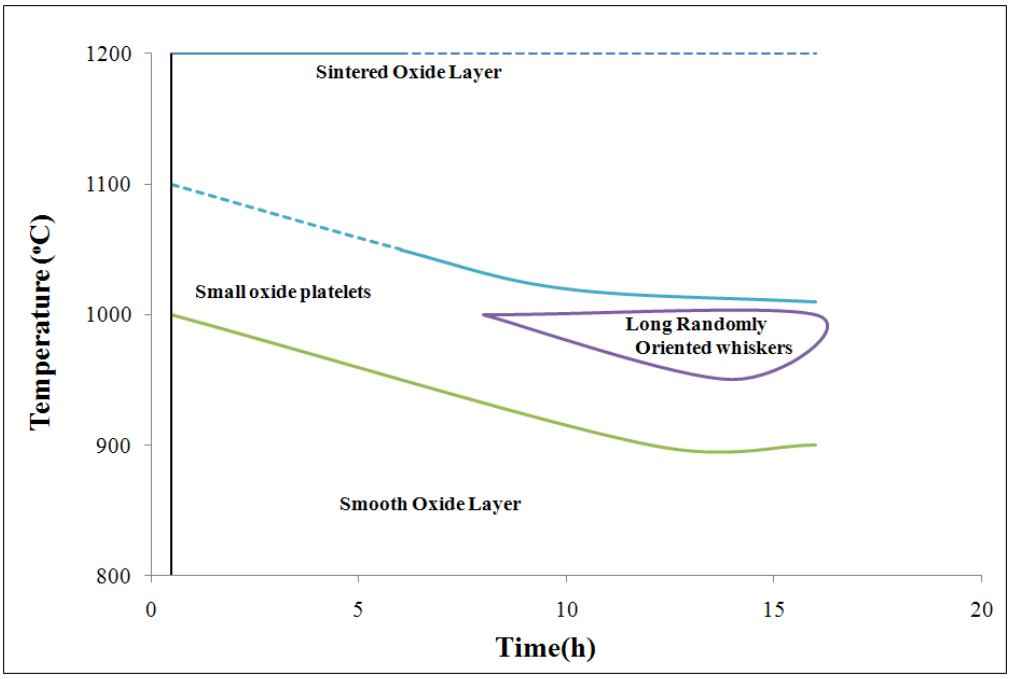

Figure 4.17 Oxide morphology formed at varied operating conditions of temperature and time.

To obtain suitable XRD spectra on a thin oxide layer grown on a curved surface is more complex than powdered samples. Given the very thin oxide layer grown on the Fecralloy rods, a quantitative phase analysis could not be done based on the crystallite size. Using Bragg's law, the inter-planar distances were calculated for the different peaks obtained from the XRD data for oxidation at 800 °C - 1200 °C for 16 h, and for oxidation at 1000 °C for varied time periods of 0.5 h - 16 h. The results have been tabulated and shown in Table 4.8 and were compared to the work done by Jedlinski in order to obtain a qualitative phase analysis (Jedliński et al., 2009). Strong maxima were detected when the samples were oxidised at 1000 °C - 1200 °C and for increased time of exposure. The maxima for transition aluminas were very strong for samples oxidised at 1000 °C for 8 h.

d_{hkl} [Å]	Temperature and time	Comments on UoM data compared with work by Jedlinski (2009)
2.55	900 °C - 1200 °C for 16 h 1000 °C for 1 h - 16 h	All aluminas present
2.38	900 °C - 1200 °C for 16 h 1000 °C for 1 h - 16 h	All aluminas
2.17	1000 °C for1 h - 16 h	Only transient aluminas, very strong at 1000 °C for 8 h and 16 h
2.09	900 °C - 1200 °C for 16 h 1000 °C for 1 h - 16 h	Only α - Al_2O_3, very strong at 1000 ^{o}C - 1200 ^{o}C for 16 h
2.04	800 °C - 1200 °C for 16 h 1000 °C for 1 h - 16 h	Underlying substrate, α - Fe, very strong

Table 4.8 Characterization of Alumina phase in terms of inter-planar distances.

Scale-up of Fecralloy thermal oxidation

Using the data summarised in Figure 4.17 and Table 4.8 and a method of trial and error, the author was able to scale-up the oxidation process from the TGA to a vertical tube furnace, i.e 50 mg samples to 2 g. Reproducing the controlled oxidation conditions present in the TGA to a tube furnace was challenging. Morphology of the alloy surface post oxidation treatment at 1000 °C for 8 h in a tube furnace revealed an oxide scale which appeared to be flat and a lower surface area phase. However by modifying the oxidation temperature and time, the author obtained a surface similar to morphology at 1000 °C for 8 h. The optimum conditions for scale-up were found to be 950 °C for 10 h under flowing air (50 ml/min). Oxidation at these conditions resulted in the growth of an oxide layer with a platelet morphology as shown in the ESEM image (*Figure 4.18*). The XRD spectra of the rods oxidised at 950 °C were compared to results of the rods oxidised at 1000 °C for 8 h (*Figure 4.19*) in order to ensure a phase transformation to a lower surface area α - Al_2O_3 had not taken place on the surface.

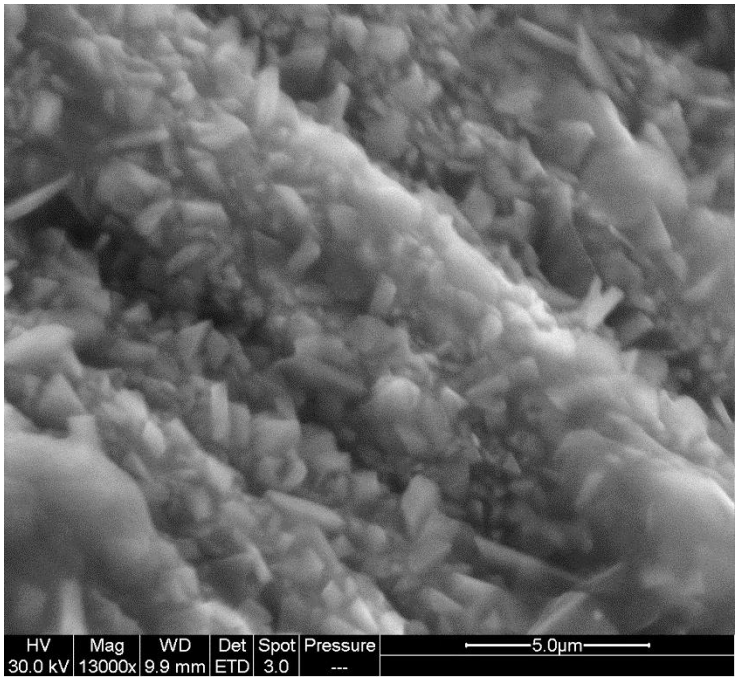

Figure 4.18 Morphology of Fecralloy rod when oxidised at 950 °C for 10 h.

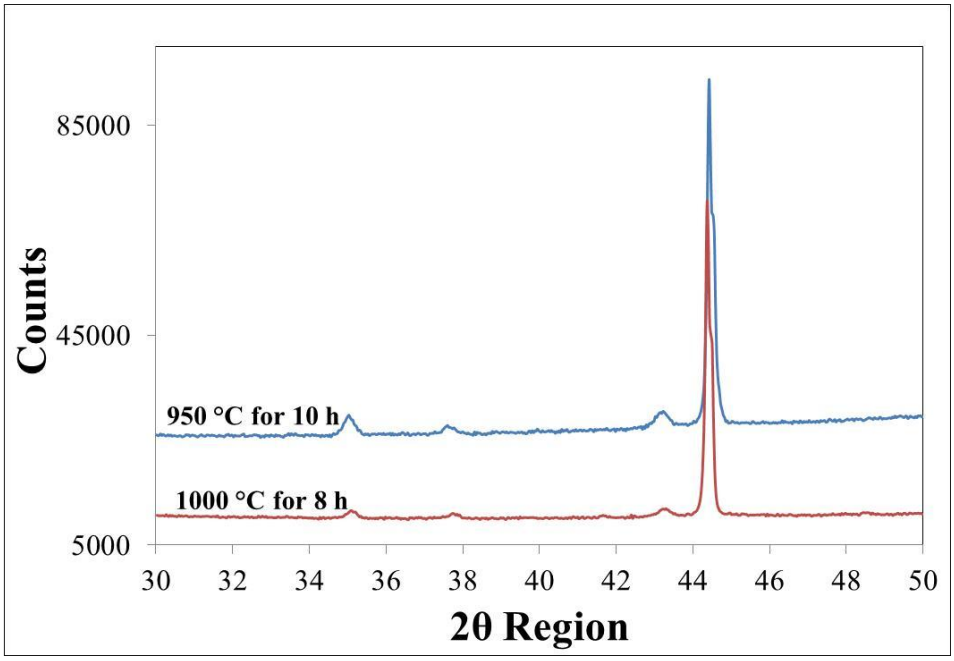

Figure 4.19 Comparison of XRD spectra for Fecralloy oxidised at 950 °C for 10 h and 1000 °C for 8h.

Thus to prepare the catalytic supports, the Fecralloy rods were packed into a quartz tube and oxidised in a suitably insulated vertical tube furnace (*Carbolite TZF 12/38/400*) under flowing air (50 ml/min) at 950 °C for 10 h.

4.3.3 Washcoat Optimisation

The third step involved in the preparation of the structured catalyst was the loading of an alumina washcoat. However, to ensure improved catalytic activity it was necessary to ensure the adherence of the washcoat. The following sections detail the work done by previous authors on loading of alumina washcoats on structured supports, subsequently detailing the experimental study done by the author to optimise the alumina washcoating step.

4.3.3.1 Loading of Alumina Washcoat-Literature Review

Various methods exist to coat a layer on to a support and the choice of method is very much dependent upon the support properties, coating properties and desired coating thickness. Adhesion of coatings on non-porous structures such as Fecralloy is non-trivial. Specific methods have been developed to load an alumina washcoat on the alloy support which are, suspension, sol-gel and hybrid methods.

A *suspension* technique is where the finished material to be deposited upon the surface is suspended within a liquid medium. Standard ingredients of a suspension technique include, powder (catalyst or support), binder, acid and water. The particle size of the material to be deposited is critical and has a major effect upon the adherence of the layer.

The *sol-gel* method is a technique where a solution or suspension is prepared containing a chemical precursor to the desired final wash coat material. To deposit alumina using this technique there are three different options for the chemical composition of the sol (Meille, 2006),

- hydrated aluminium oxides - pseudo boehmite or boehmite
- aluminium alkoxides
- aluminium chlorides and aluminium.

Hybrid methods are just a combination of the suspension and sol-gel techniques. The sol-gel method provides a thin primer layer to which the suspension can adhere to. This results in a thicker coating than could be obtained by either method. The sol acts as a binder but also affects the final coatings chemical and textural properties (Meille, 2006, Meille et al., 2005).

These three methods of deposition are usually conducted by dip coating, spray coating or brush coating. Dip coating is by far the most common method due to its ability to produce uniform and repeatable results. There are also known correlations between the thickness of the layer, viscosity of medium and withdrawal speed. The coatings can either incorporate the catalyst directly or act as a support upon which the catalytic phase may be deposited within. Table 4.9 classifies and details the work and findings of several authors for loading alumina on Fecralloy structures. All methods within the table attempt to build an alumina wash coat, which could be further impregnated with an active catalyst phase.

Author	**Deposition Method**			**Result**		
	Sol-Gel	Suspension	Hybrid	Uniform	Adherent	Thickness
Meille et al., 2005	Y			Y	Y	<1 µm
Wu et al., 2001		Y		Y		~50 µm
Zhao et al., 2003			Y	Y	Y	~50 µm
Jia et al., 2007			Y	Y	Y	50 - 60 µm
Valentini et al., 2001			Y	Y	Y	~60 µm
Liu et al., 2003			Y	Y	Y	~20 µm

Table 4.9 Summary of methods to deposit Alumina on Fecralloy.

From previous work shown in Table 4.9, Meille et al achieved a thin layer of alumina deposited on Fecralloy fibres however, there were significant cracks observed even within such a thin layer (Meille et al., 2005). The coated fibres were further impregnated with platinum and it was found this step was not detrimental to the integrity of the coating. It was also found that the alumina precursor used to produce the sol should not be thermally pre-treated. From the observations it was proposed the thermal pre-treatment of the alumina

resulted in elimination of hydroxyl groups thus reducing the potential number of surface chemical bonds between the sol and support - the result being a non-uniform non-adherent layer.

The sol's viscosity was also found to play a crucial role in the thickness developed, an increase in viscosity resulted in increased thickness of the layer. The viscosity was found to be controlled through the alumina concentration and pH of the slurry. Wu and co-workers achieved a significantly thicker coating than that by Meille and co-workers by using a suspension method opposed to sol-gel (Meille et al., 2005). However even with the addition of high temperature stabilisers, such as, TiO_2, CeO_2, La_2O_3, SiO_2 and ZrO_2 an adherent layer could not be achieved. The non-adherence of the layer could be attributed to the large alumina particle size used in the study; which was in the range of 38 - 80 μm. Agrafiotis and Tsetsekou in their research suggested that to attain an adherent layer the particle size should not exceed 5 μm (Agrafiotis and Tsetsekou, 2000).

Zhao and co-workers claimed to have produced a layer of similar thickness to that of Wu and co-workers and was claimed to be adherent by the use of a hybrid method (Wu et al., 2001, Zhao et al., 2003). In an excellent review by Meille, it was stated that the hybrid methods could be used to build the thickness whilst remaining adherent to a greater degree than that obtainable by the sol or dispersion methods (Meille, 2006). The study concluded that the thermal pre-treatment of the support was key, with three controlling factors with respect to the adhesion, namely

- the specific surface area of the pre-oxidised layer
- matching of the crystal grain of the metallic support and pre-oxidised layer
- matching between the crystal grain of the pre-oxidised layer and γ-alumina coating.

Jia and co-workers also claimed to have produced a uniform highly adherent layer of similar thickness to that of Zhao and co-workers and Valentini and co-workers (Jia et al., 2007, Valentini et al., 2001, Zhao et al., 2003). The research teams thermally oxidised the alloy support prior to using a hybrid deposition method. They found the optimal temperature for oxidation to be 900 °C and 10 h.

Valentini and co-workers in their research suggested a two-step methodology for the loading of an alumina washcoat onto a structured support which has been schematically shown in Figure 4.20. Samples were withdrawn from the primer sol and alumina slurry at a constant speed of 3 cm/min which resulted in a thick alumina washcoat. The alumina slurry was prepared by dispersing a sub-micronic γ - Al_2O_3 powder in nitric acid (in a fixed molar ratio), followed by vigorous stirring in a closed reactor for 16 h at 18 °C.

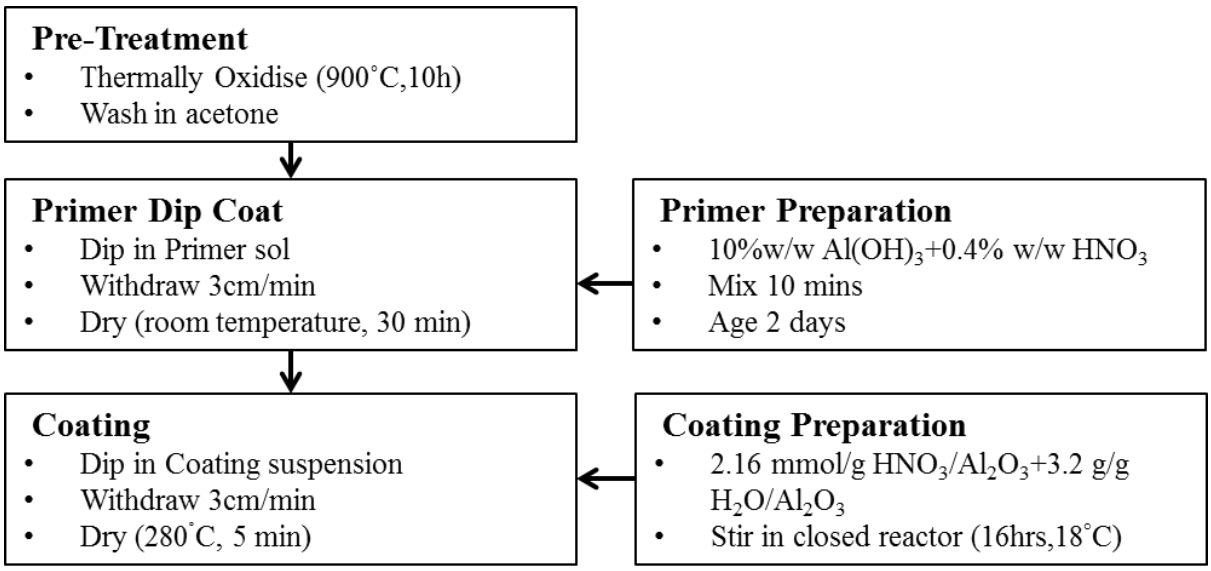

Figure 4.20 Hybrid deposition method for alumina washcoating.

Valentini et al in their research further suggested that the optimum molar ratio to prepare the alumina slurry (after a range of options were tested), was HNO_3/Al_2O_3 = 2.16 mmol/g with a ratio of H_2O/Al_2O_3 = 3.2 g/g (Valentini et al., 2001). They found, an increase in the ratio of H_2O/Al_2O_3 resulted in a decreased degree of deposition. As shown in Figure 4.21, the maximum degree of deposition was achieved at a ratio of 2.8 g/g, however they found the layer to be non-adherent. The ratio which produced the most adherent layer was found to be 3.2 g/g.

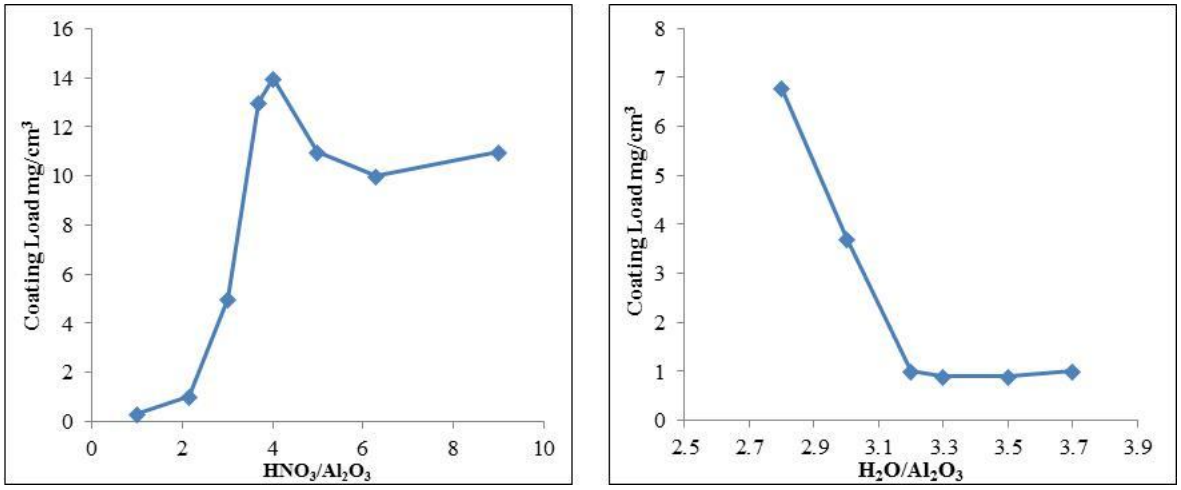

Figure 4.21 Change in coating load with varying proportions of HNO_3 (aq), Al_2O_3 and H_2O (Valentini et al., 2001).

Zhao et al and Jia et al did a detailed study on the effect of the different parameters such as support pre-oxidation and alumina particle size on the sol-layer and slurry layer loading. In their work both of the research groups, followed the two step hybrid deposition method suggested by Valentini et al. They were able to achieve alumina washcoats with a coating load of 20 wt%. However the coating was non-adherent (weight loss > 25%) and consisted of several cracks as shown in Figure 4.22. Thus rendering it unsuitable to be used as a catalytic support.

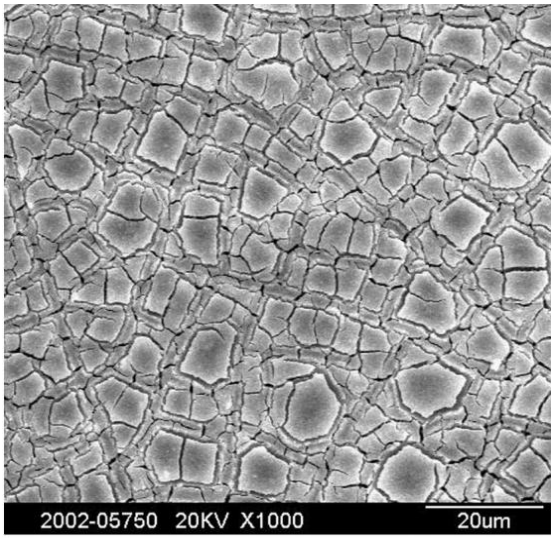

Figure 4.22 Calcined Coating Layer (Zhao et al. 2003).

Contrary to the two-step method suggested by previous researchers, Liu et al in their US patent suggested a novel 1-step hybrid method to deposit an alumina washcoat onto Fecralloy supports (Liu et al., 2003). Liu et al in their patent suggested the preparation of a coating slurry which consisted of a boehmite sol and alumina suspension agitated in a fixed ratio. The slurry was aged for a time period of 8 h and the final pH of the slurry was 3.27. The boehmite sol acted as a binding agent, to improve the adhesion of the alumina washcoat. Various metallic substrates such metallic plate heat exchangers, monoliths and stainless steel supports were coated with the prepared slurry. The coated samples were calcined at temperatures between 500 °C - 650 °C for 2 h. Depending on the thickness of the alumina washcoat required multiple washcoats were applied. Liu et al were able to achieve an adherent washcoat with thickness which was between 10 - 30 µm. Thus, rather than depositing a primer layer followed by an alumina washcoat layer, Liu et al were successfully able to achieve the deposition of an adherent washcoat through a single step.

After studying the various methods of washcoating a Fecralloy support with an adherent alumina layer, it was attempted to optimise and load an adherent alumina washcoat on the Fecralloy methods. This is has been detailed in the following section.

4.3.3.2 Optimisation of the washcoat procedure-Experimental Study

The Fecralloy rods prior to being loaded with an alumina washcoat are subjected to a thermal treatment step as detailed earlier on in the chapter. Initially the two step hybrid method as suggested by Valentini and co-workers was attempted to achieve an adherent coating.

Two step Hybrid method

A primer was used to improve the adherence of the alumina washcoat layer. The primer sol, consisted of a dispersion of 10% (w/w) of a commercial aluminium hydroxide (DISPERAL, *Sasol*) powder in a 0.4% (w/w) HNO_3 aqueous solution. The mixture was vigorously agitated for 30 minutes to obtain a stable dispersion. The observed pH rose from 1 to 3.5 over a period of 2 days, which was in accordance to the supplier's specifications.

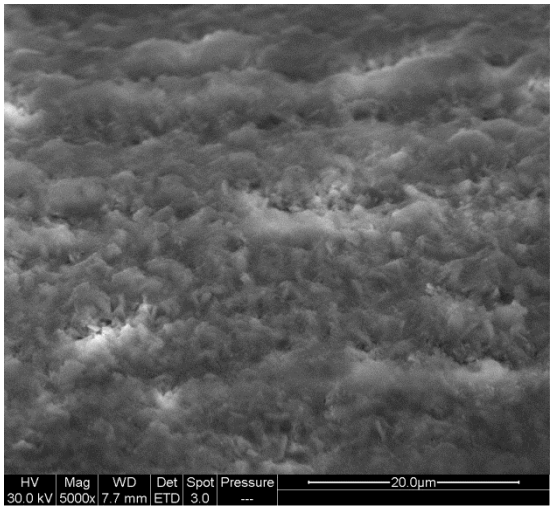

Figure 4.23 Fecralloy coated with a Primer.

The calcined Fecralloy rods were cut into strips of 2.5 cm and fitted onto ceramic blocks. These blocks were dip-coated in the prepared primer sol and withdrawn at a constant speed of 3 cm/min. Following which, they were calcined at 650 °C for 2 h to form a thin adherent layer which was characterized by ESEM (*Figure 4.23*).

This was followed by dip-coating the Fecralloy rods in an alumina slurry. Commercially manufactured sub-micronic γ-Al_2O_3, diameter 5µm (PURALOX, *Sasol*) was used to prepare the washcoat slurry. The alumina was dispersed in HNO_3 and distilled water in a fixed molar ratio of: HNO_3/Al_2O_3 = 2.16 mmol/g and H_2O/Al_2O_3 = 3.2 g/g

The mixture was gently agitated over a period of 24 h - 72 h and the rods, fitted onto ceramic blocks, were dipped in the slurry, for 1 minute and were withdrawn at a constant speed of 3 cm/min. The samples were flash dried in a GC oven for 5 minutes at 150 °C before dipping into the slurry for a repeat washcoat (*Figure 4.24*). The flash drying temperature had to be above 100 °C so as to remove any water and increase the adherence of the layer. Samples which were dried at 30 °C revealed a very thin and poorly adherent layer.

Figure 4.24 Fecralloy rods with alumina washcoat.

Multiple washcoats were applied onto the Fecralloy support to increase the coating load. The coated samples were calcined in a furnace for a period of 2 h to form a well adherent γ - Al_2O_3 layer. The calcination temperature had to be in the range of 500 °C - 800 °C to result in the formation of a γ - Al_2O_3 layer, temperatures higher than this range would result in the formation of a mixed phase alumina layer comprising of δ -,θ -, α - Al_2O_3.

The coating load varied with slurry ageing time and with the number of washcoat layers as summarized in Table 4.10. As expected the washcoat thickness increased with ageing of the slurry. When the slurry was aged for 24 h, the washcoat thickness increased with the number of dipcoats. However for the slurry aged 48 h, the second dipcoat yielded an increase but subsequent dipcoats resulted in reduced thickness. The slurry aged for 72 h showed a reduction in the washcoat thickness with increasing number of dipcoats.

	Coating Load (%)			
	Washcoat Layers			
	1	**2**	**3**	**4**
24 h	0.84	0.89	0.97	2.1
48 h	0.81	1.11	0.69	0.61
72 h	1.42	1.34	1.09	1.04

Table 4.10 Summary of coating load at varied slurry ageing time and washcoat layers.

ESEM images of the Fecralloy rods with a washcoat layer at different periods of ageing of the slurry have been illustrated with in Figure 4.25. The ESEM images revealed cracks to be prevalent in the alumina layer. The presence of cracks would retard the catalytic activity of the alumina coated supports.

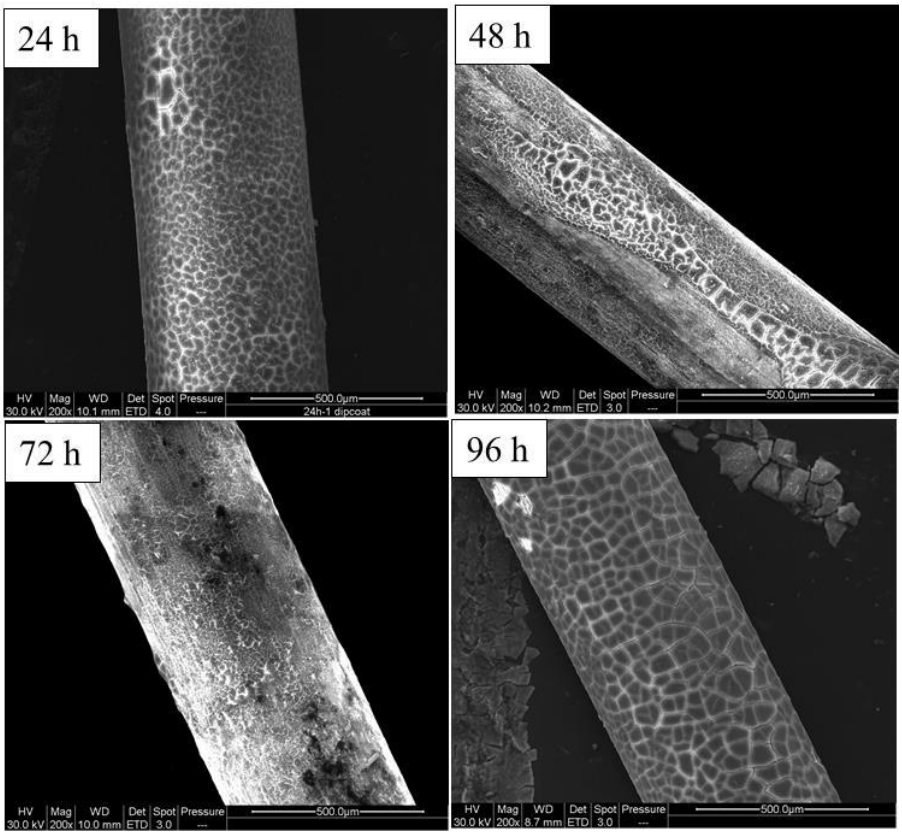

Figure 4.25 SEM images of washcoated Alumina layer on FeCralloy after different periods of ageing.

Following the trial of the two step alumina washcoating method, a one-step method as suggested by Liu and co-workers was attempted. The author tried both methods in order to compare and obtain the optimum method for coating the Fecralloy rods.

<u>One Step deposition method</u>

To attempt to improve the adherence of the washcoat layer, and also to increase the loading of a more uniform layer in one step, the novel hybrid method suggested by Liu et al in their US patent was used and extended by washcoating the Fecralloy rods in a 24 h aged slurry and a 48 h aged slurry (Liu et al., 2003).

A binder sol was prepared which was added to the washcoat slurry to increase the loading. The binder sol comprised of 4 % (w/w) boehmite powder (DISPERAL) dispersed in 16 % (w/w) conc.HNO_3 and 80 % (w/w) distilled water. The binder sol was gently agitated for 24 h at 25 °C. The slurry was prepared by dispersing 23 % of the binder sol prepared, in 23 % (w/w) γ - Al_2O_3 powder (PURALOX) and 54 % (w/w) distilled water. The alumina slurry thus prepared was stirred gently for 48 h at 50 °C prior to dip-coating, with the pH of the alumina slurry remaining stabilised at 3.7. Nijhuis et al in their work suggested that in order to obtain an adherent washcoat the pH of the slurry should be maintained between 3 - 4 (Nijhuis et al., 2001). The steps involved in loading of the alumina washcoat are summarised in Figure 4.26.

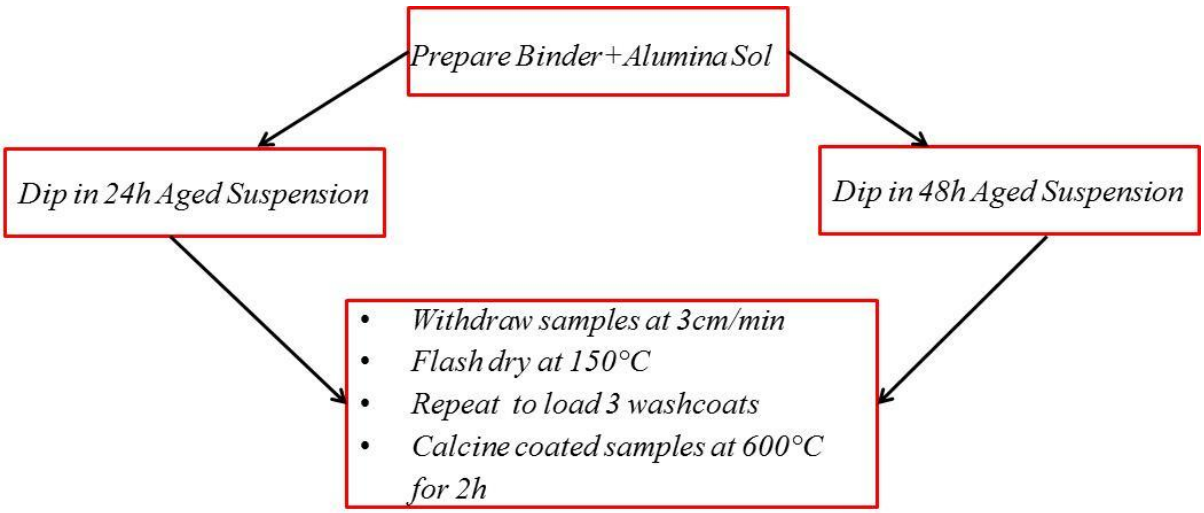

Figure 4.26 Steps involved in Alumina coating deposition.

The one step deposition method resulted in a uniform alumina washcoat. The coating load after washcoating in the 24 h aged slurry was 0.8 wt% and the final coating load following washcoating in the 48 h aged slurry was found to be 1.3 %. The samples were embedded in a resin to obtain the thickness of the alumina layer as illustrated in Figure 4.27. ESEM analysis revealed an alumina washcoat that was uniformly coated in addition to being free from cracks on the surface. The thickness of the layer was found to be ~6 µm which was found to be much lesser than the thickness achieved by Liu et al in their patent. This could be attributed to the difference in the final coating slurry, which could be due to a difference in alumina particle size used by Liu et al in their patent and in this research. The resulting

alumina layer, despite being thin could still be suitable to be used as a support for the dehydrogenation of MCH, due to the fast nature of the reaction.

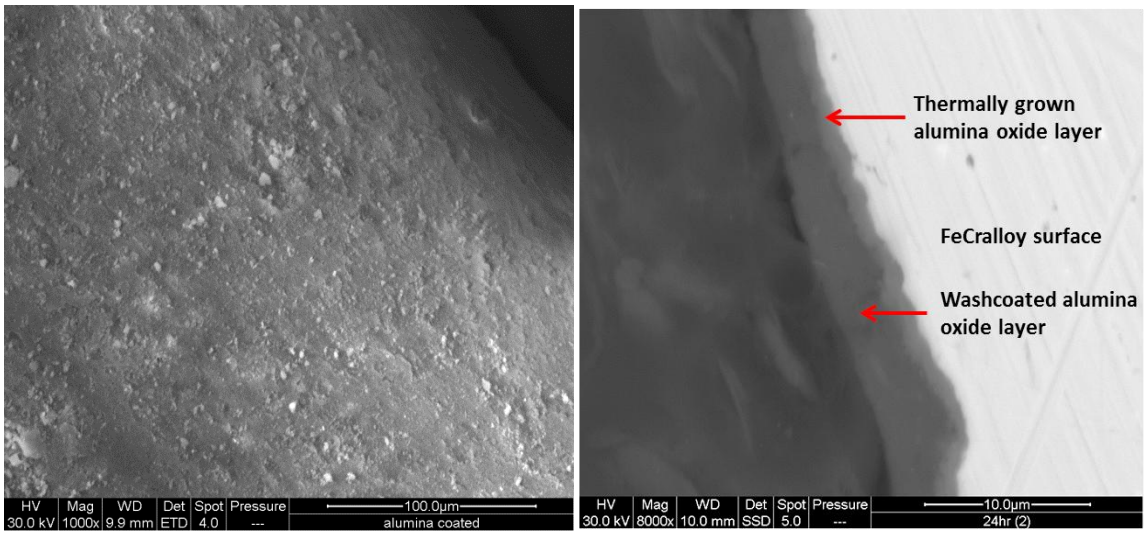

Figure 4.27 Alumina washcoated Fecralloy through one step deposition method (LHS : SEM image; RHS : SEM cross section).

Therefore the one-step deposition method was adopted to load the alumina washcoat onto the thermally oxidised supports. The layer appeared to be free of cracks in addition to being adherent. Thus confirming, the alumina washcoat layer and the thermally grown oxide layer on the Fecralloy support had a matching crystal grain structure. This method was repeated twice; both times the results were identical hence confirming reproducibility of the results.

4.3.4 Preparation of metal loaded alumina of Fecralloy support

The dispersion of the active catalytic phase on a high surface area support is commonly carried out by one of four methods (Richardson, 1989),

- precipitation
- adsorption
- ion exchange
- impregnation

In *precipitation* the objective is to create a reaction between a metal salt solution and the support resulting in a metal hydroxide or carbonate on the surface of the carrier support. It is a preferred route when a loading greater than 10 - 20% is required, below this, other techniques are usually preferred (Richardson 1989). Deposition via *adsorption techniques* is achieved through equilibrium controlled adsorption of metal ions in solution on to support adsorption sites. It is an excellent way of achieving low loadings with uniform dispersion. In addition to this no additional washing and filtration steps are required (Bartholomew and Farrauto, 2006, Richardson, 1989). Deposition by *ion exchange* is achieved by the exchange of low valence ions with that of higher charged ions. It is particularly useful when either harmful agents are required to be removed or for addition of promoters. However it can often involve multiple stages (Richardson 1989; Bartholomew and Farrauto 2006). *Impregnation* is the simplest and most direct method of deposition. However the pore volume and diameter must be determined in order to optimise the drying process. Failure to optimise the drying process results in irregular and uneven distribution of the catalytic phase. When there is a large pore size distribution within the support, as with alumina, optimisation of the drying process is often not possible.

Sinfelt in his study of turnover number for methylcyclohexane dehydrogenation mentioned that a typical 0.3 - 0.6 wt% platinum with a particle size of 1 - 2 nm was necessary for a good performance of the Pt/Al_2O_3 catalyst (Sinfelt, 2000).

The preparation protocol of monometallic catalysts have been reported previously (Tsakiris, 2007). Platinum was loaded onto the catalytic support by wet impregnation in order to obtain a uniform γ - Al_2O_3 catalyst. The impregnating solution was prepared by dissolving $H_2PtCl_6.(6H_2O)$ (*Sigma Aldrich*), which was the metal pre-cursor in deionized water. The final concentration of the solution prepared was 0.0001M. 50 ml of this solution was required to load 0.1 g of alumina. The coated rods were added to this solution and gently stirred for 30 minutes at 35 °C by which point the pH remained constant at 3.28, which suggested that equilibrium pH had been reached and no further adsorption of the metal could take place. It is important to note that the impregnation process was performed in darkness to minimize degradation and decomposition of the hexachloroplatanic acid solution (Schwarz and Heise, 1990).

The next step in the impregnation procedure was catalyst drying. This process was done by heating the mixture gently to 70 °C with gentle agitation for 2 h to gradually evaporate the water. During the vaporization process, the mixture was gently stirred every 15 minutes until the mixture was nearly dry. The mixture was thoroughly dried in an oven at 120 °C for 12 h.

4.3.4.1 Characterisation of Platinum loading and dispersion

EDX analysis on different spots on the alumina coating indicated approximately 1 % platinum loading with an accuracy of ± 1%. STEM analysis was used to confirm that platinum was loaded onto the surface and was highly dispersed across the surface of the metallic rod. Transmission electron microscope (TEM) imaging (*Figure 4.28*) demonstrated that the platinum was deposited on the alumina coating. The dark spots in Figure 4.28 represent the platinum dispersion which was an aggregate consisting of many rod-shaped nanoparticles.

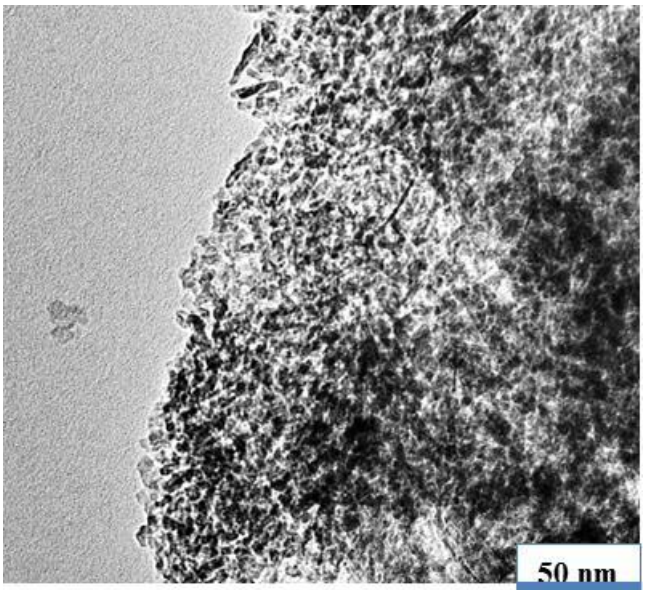

Figure 4.28 Bright field transmission electron microscope image.

Using the high angle annular dark field (HAADF) imaging mode in the STEM it was possible to obtain high resolution images which revealed a uniform dispersion of bright sub-nanometre clusters associated with the alumina support (*Figure 4.29(a&b)*). Unlike in

conventional TEM imaging, the intensity of the HAADF STEM signal was highly sensitive to the local atomic number, suggesting that the brighter regions observed in the images were likely to be associated with the deposited platinum metal. The images at two different magnifications show bright spots indicating clusters of atoms of different sizes.

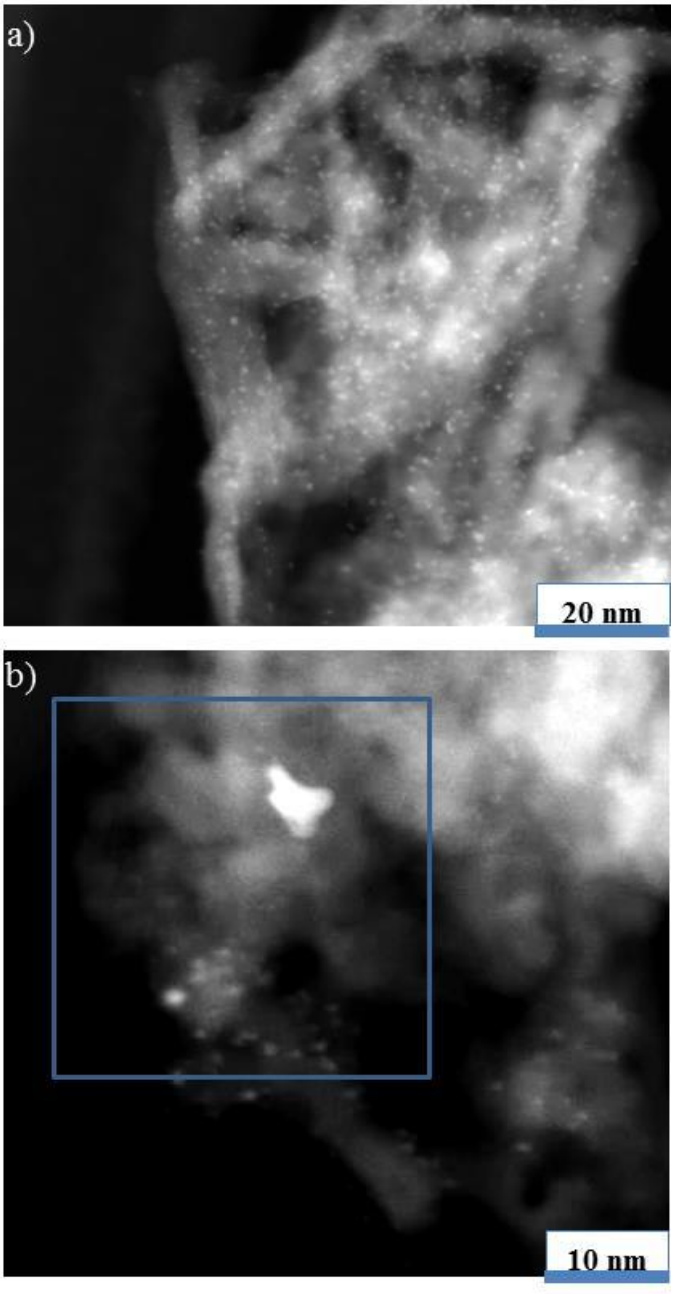

Figure 4.29 High angle annular dark field scanning transmission electron microscope images showing the Pt deposited alumina coating at a) 20 nm and b) 10 nm.

This was confirmed by elemental mapping using the energy dispersive x-ray STEM spectral imaging. The elemental mapping established that the platinum being found was associated with, the bright sub - 1 nm clusters and with the less-common larger nanometre sized particles (4 - 7 nm) as shown in Figure 4.30.

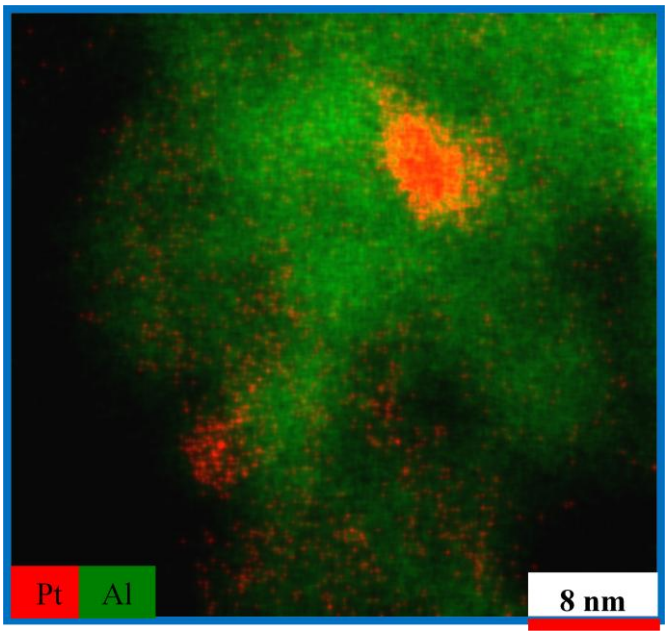

Figure 4.30 Elemental distribution of Pt and Al mapped using EDX STEM spectral.

It was found that the fine scale platinum metal clusters were highly mobile, rearranging in sequential frames due to the energy of the electron beam. Figure 4.31(a) & (b) describe the same area with images taken 17 seconds apart, thus demonstrating that the platinum was highly mobile and able to rearrange under the action of the electron beam. The occasional streaking was where atoms moved during image acquisition. Arrows in Figure 4.31(b**)** highlight regions where the changes between Figure 4.31(a**)** and Figure 4.31(b**)** are most obvious. Baker et al in their work suggested the increased mobility of platinum atoms in the presence of an electronic beam could be attributed to the formation of a Pt-Al alloy (Baker et al., 1979).

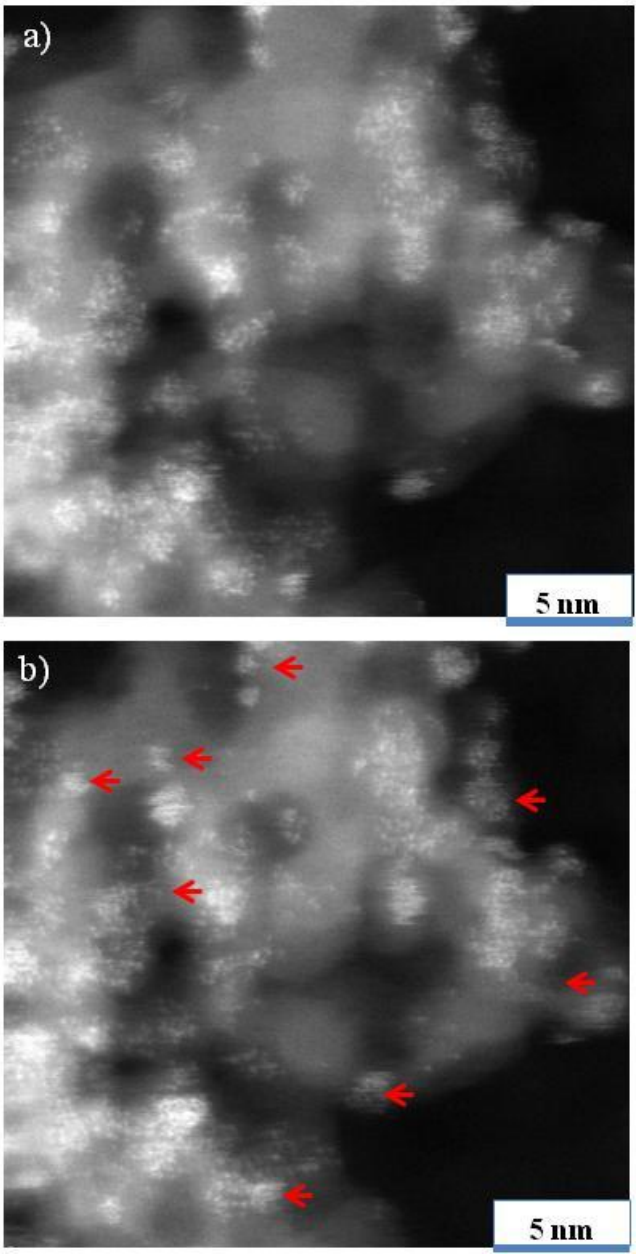

Figure 4.31 Atomic resolution HAADF STEM images showing the presence of both individual Pt atoms and Pt metal clusters on the alumina support.

The size of the individual platinum clusters were found to be 1 - 2 nm and were found to be well dispersed in the alumina coating as shown in Figure 4.32(a). Tschudin et al and Perez et al found that by determining the particle size of platinum it was possible to estimate the dispersion of the metal on the support (Pérez et al., 1983, Tschudin et al., 1999). By analysing different clusters, the average cluster size of the platinum crystal was found to be 1.5 nm. Using the mathematical relation derived in the work by Perez et al the dispersion of the platinum on the support was estimated to be 75 %. Figure 4.32(b) describes the dispersion

to be in the form of clusters of platinum atoms. From the image (*Figure 4.32(b)*) each cluster was found to have approximately 15 - 25 atoms and a size of approximately 2 nm.

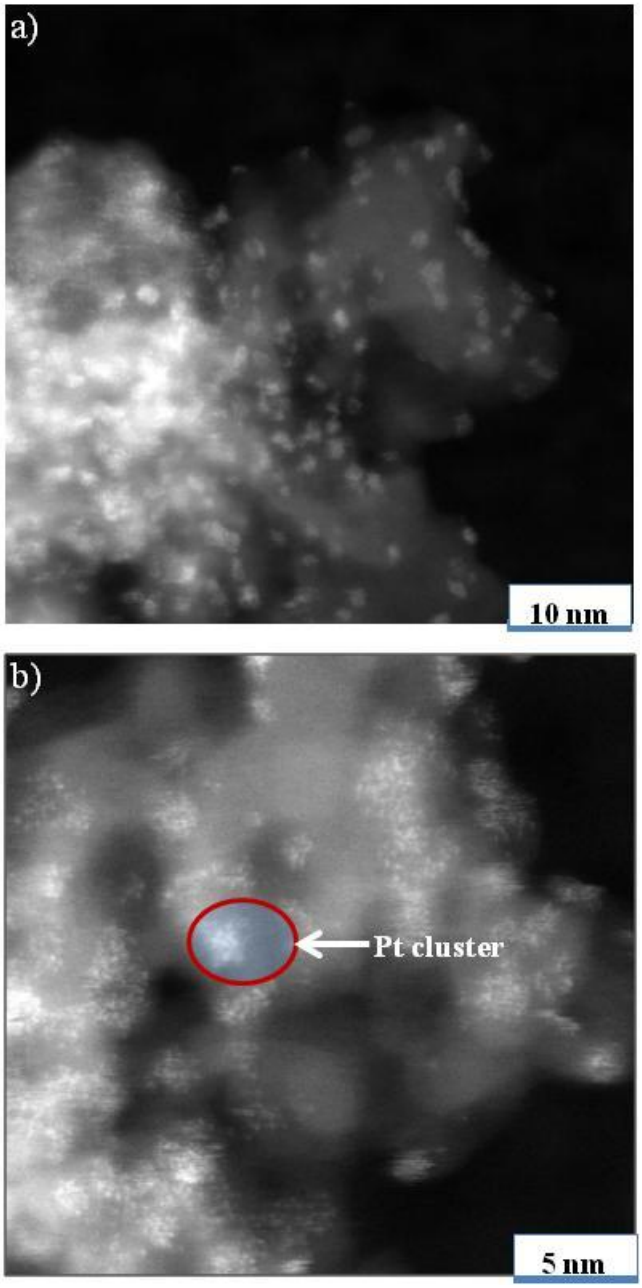

Figure 4.32 HAADF STEM images reveal a) good Pt dispersion (10 nm scale) b) Clusters of Pt crystals (5 nm scale).

Using HAADF STEM imaging, it was found the platinum was well dispersed (~75%) in the form individual atoms as well as clusters of platinum atoms. Arai et al in their work suggested that supported metal clusters coalesced to form large crystallites (Arai et al., 1980). Desai and Richardson in their research showed that an increase in cluster size led to an increase in cyclohexane dehydrogenation and benzene hydrogenolysis whilst the fine particles below 1.5 nm were more selective to the formation of dimethylcyclopentanes (Desai and Richardson, 1986). The platinum crystallites exist as cubo-octahedra, which consist of a distribution of low co-ordination sites and face sites (Richardson, 1989, Yacamán and Gómez, 1984). The low co-ordination sites consisted of steps and kinks and were found more in fine particles of size 1 - 2 nm. Desai and Richardson in their work found that an increase in crystallite size led to an increase in face sites and a decrease in low co-ordination sites. Thus the platinum cluster size had an effect on its morphology (Desai and Richardson, 1986). Somorjai and Blakley described in great detail the effect of the morphology of the platinum particles on the selectivity of the catalyst (Blakely and Somorjai, 1976). In their research they showed, that depending on the platinum particle size, it was possible to estimate the different concentrations of the kink, step and terrace sites. The concentration of these sites had an impact on the selectivity of the catalyst. This has been detailed further in chapter six.

The developed catalyst was loaded into a dehydrogenation rig (*described in Chapter five*) and tested for the dehydrogenation of methylcyclohexane. The activity of the catalyst and its selectivity towards toluene formation was studied and has been reported in detail in Chapter six.

5 Catalytic Testing

5.1 Introduction

Assessment of catalytic processes and catalyst screening takes place usually in pilot reactors. In short term experiments catalytic properties such as activity, selectivity, and diffusion characteristics are determined, while long-term experiments are employed to determine the rate of catalyst deactivation. This work investigates the dehydrogenation of methylcyclohexane (MCH) over Pt/Al_2O_3/Fecralloy and conventional Pt/Al_2O_3 catalysts. The methodology was based on experimental work that was conducted in a micro pilot reactor (dehydrogenation unit). It can operate with either pure methylcyclohexane feed or diluted with a suitable carrier gas, such as H_2 which prevent the catalyst from deactivating.

5.2 Apparatus

To thoroughly study the activity, selectivity and kinetics of MCH dehydrogenation on the prepared structured Pt/Al_2O_3/Fecralloy catalyst, activity and life tests have been conducted. The activity and life tests were performed in an atmospheric-pressure dehydrogenation unit. The design details of the rig have been illustrated in the following sections.

5.2.1 Catalytic dehydrogenation rig

The catalyst was tested in a catalytic dehydrogenation rig which was designed and built by the author (*Figure 5.1 and Figure 5.2*). The design specifications of the rig are listed in Table 5.1 and the process instrumentation diagram in Figure 5.1.

Design Parameter	Specification
Design Pressure	1.013 bar
Design Temperature	550 °C
Operating Pressure	1.013 bar
Operating Temperature	300 °C - 500 °C
MCH Flowrate	0.01 - 0.5 ml/min
H_2 Flowrate	0 - 500 ml/min
Air Flowrate	0 - 500 ml/min

Table 5.1 Design speciation of Dehydrogenation rig.

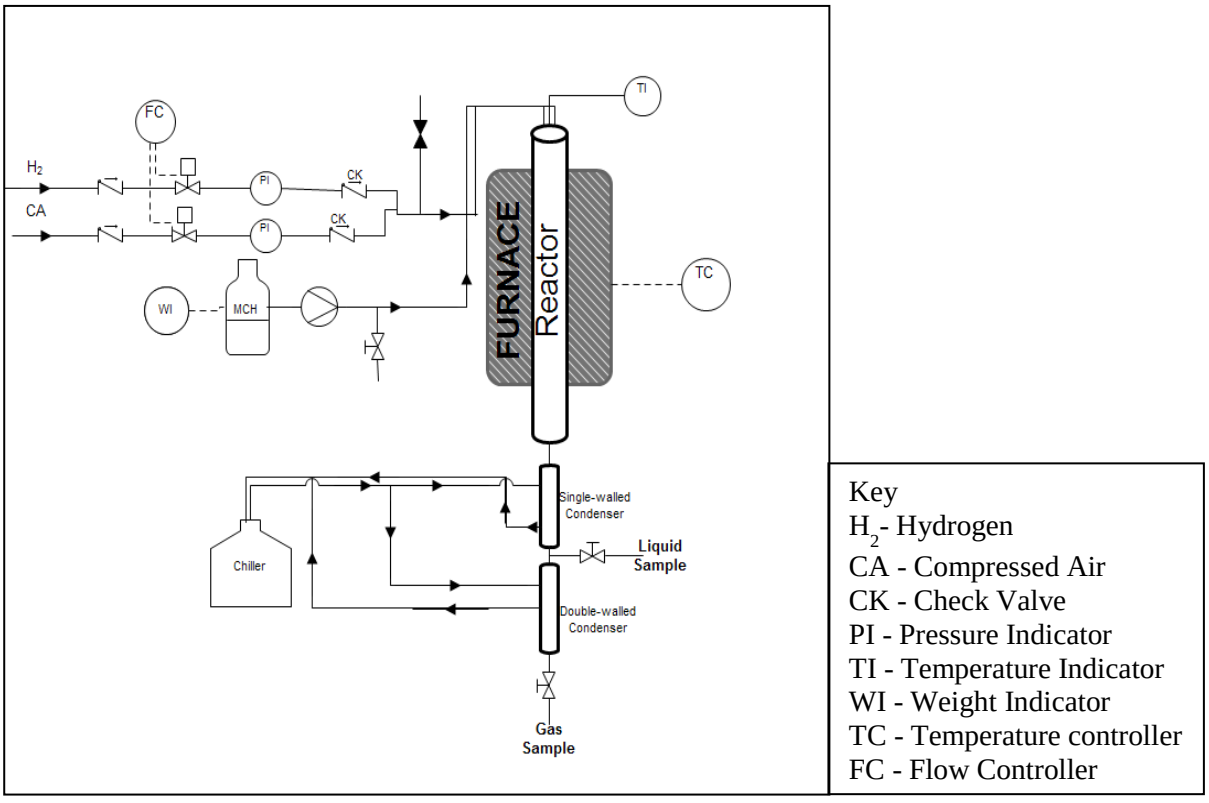

Figure 5.1 P&ID of Catalytic Dehydrogenation Rig.

Figure 5.2 Atmospheric pressure dehydrogenation rig.

The dehydrogenation rig, consisted of four main units, the liquid and gas feed modules, the reactor unit and the separation unit. A brief description of each module has been detailed in the following sections while a bill of materials is given in Appendix A1.1.

5.2.1.1 Liquid Feed Module

Methylcyclohexane is a colourless hydrocarbon liquid (C_7H_{14}). The physical properties of the feedstock are listed in Appendix A1.2. The MCH used was purchased from Sigma Aldrich and had a purity of 99.8%. The liquid feed is pumped into the reactor using a high pressure liquid chromatography (HPLC) pump. The pump calibrated and used in this system was a *JASCO PU-980* pump. MCH was stored in a 1 litre feed bottle and was placed on a weighing balance, to confirm the amount of liquid being pumped into the reactor system as illustrated in Figure 5.3. The feed was pumped by a HPLC pump from the reservoir through an inline filter to the reactor.

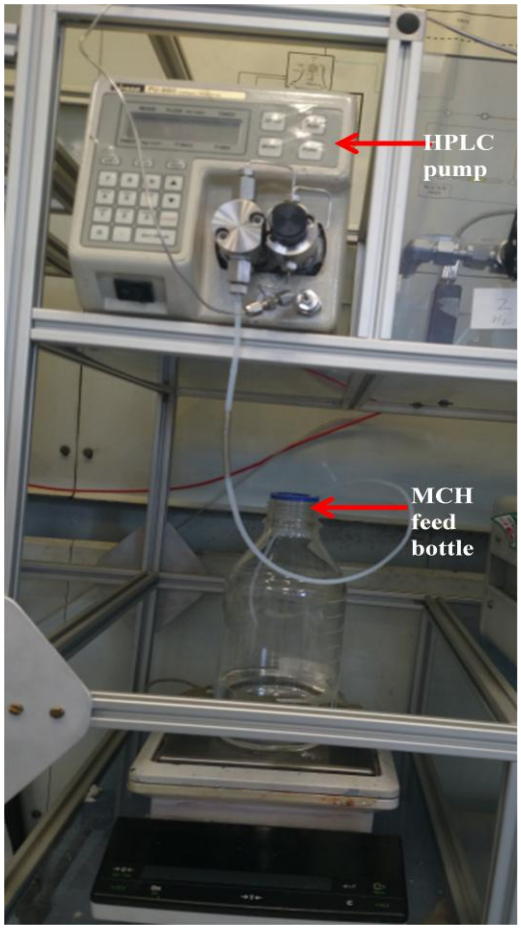

Figure 5.3 Liquid feed module to pump MCH to the reactor system.

5.2.1.2 Gas Feed Module

The gas feed module, allowed the supply of pressurised gases (typically 1-9 bar) namely hydrogen (99.995% purity) and air to the unit from high pressure cylinders (150 - 200 bar) which were ordered from BOC. The properties of the gases are listed in Appendix A1.3. The pressure of the supply gases were brought to the operating pressure of 1 bar using pressure regulators and the flow of air and hydrogen was controlled by a *Brooks Instruments 5850 TR* mass flow controllers connected to a *Brooks Instruments Read out & Control Device 0154*. The channels were fitted with pressure gauges required to monitor the operating pressure of the gases going to the unit. Check valves were installed at the end of the lines to avoid mixing of by-products with the main gas supply should there be any reverse flow. The mass flow controller was calibrated for hydrogen and the calibration chart has been listed in Appendix A1.4.

5.2.1.3 Reactor Module

The reactor module is the most critical zone of the unit. MCH and H_2 are fed through separate reactor inlets as illustrated in Figure 5.4. The mixture passes through the reactor in down-flow mode. The reactor was made of Pyrex and was connected with stainless steel Swagelok end fittings for gas and liquid inlet connections, the design has been illustrated in Figure 5.4. The glass reactor was designed by the author and manufactured at the University of Manchester. The reactors specifications of the rig are described in Table 5.2. The glass reactor ends consisted of ground glass joints in order to form leak-proof seals with the Swagelok fittings. In addition, the base of the reactor was fitted with an inner 14/23 ground glass joint which connected to the separation section and was sealed using PTFE sleeves. The glass reactor module was fitted inside a furnace (*Carbolite TZF 12/38/400)* which had three zones controlled by a fully eurotherm controller. The catalyst bed temperature was monitored by a calibrated thermocouple that was inserted through a ceramic thermowell, which was fitted during catalyst loading and detailed later in this chapter.

Description	**Specification**
Body Material	Glass-Pyrex
Reactor Total Length	60 cm
External Diameter	1.51 cm
Internal Diameter	1.12cm
Thermowell length	55cm
Reactor Total Volume	49.5 ml
Maximum Operating Temperature	550 °C
Allowable Working Pressure	1.013 bar

Table 5.2 Reactor specifications of Dehydrogenation rig.

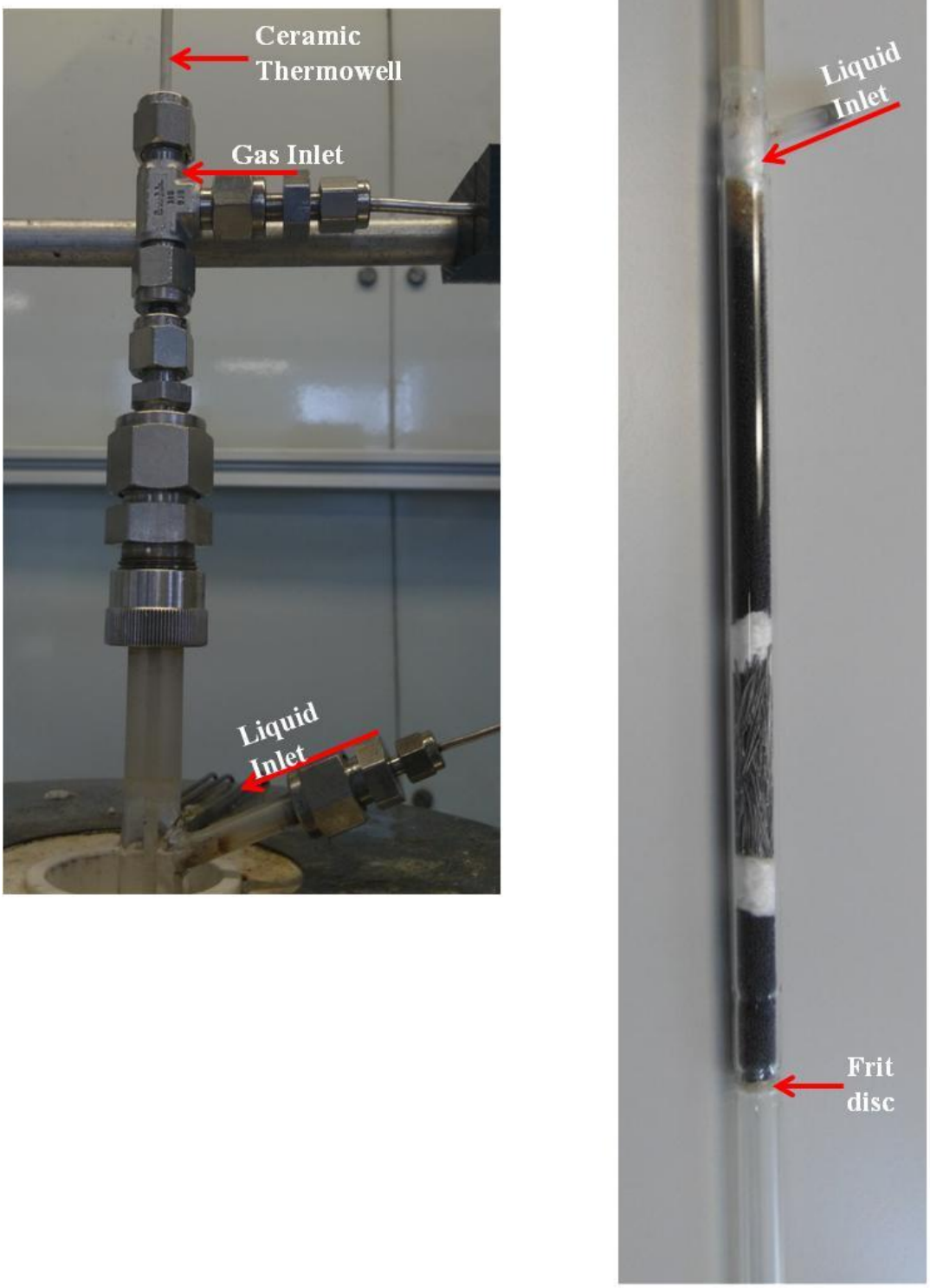

Figure 5.4 Glass reactor tube detailing gas and liquid inlets, central thermowell and glass fitted disc supporting catalyst.

5.2.1.4 Separation Module

This module was designed to separate the liquid reactant and products from the hydrogen gas. It consisted of a chiller (*Camlab*) with ethylene glycol (40%) and water (60%) mixture as the coolant to allow sub-ambient operation. This mixture has a viscosity of -0.310 Pa s at -20 °C, and a freezing point -25 °C. It was used as an anti-freeze to operate the chiller below 0 °C without freezing the coolant. The coolant mixture was continuously stirred constant speed using a digital agitator (*Eurostar digital IKA labortechnik*). The coolant was pumped (motor pump fitted on chiller) continuously into a single walled glass condenser connected in series with a double walled glass condenser, as shown in Figure 5.5. The glass condensers were made of Pyrex and were manufactured at the University of Manchester. The ends of the condenser consisted of 14/23 inner and outer ground glass joints. The glass condensers and reactor tube outlet were connected through the ground glass joints. All the joints were fitted with PTFE sleeves (*Fisher Scientific*) in order to ensure leak-proof seals. The chiller was typically operated at a temperature of -17 °C.

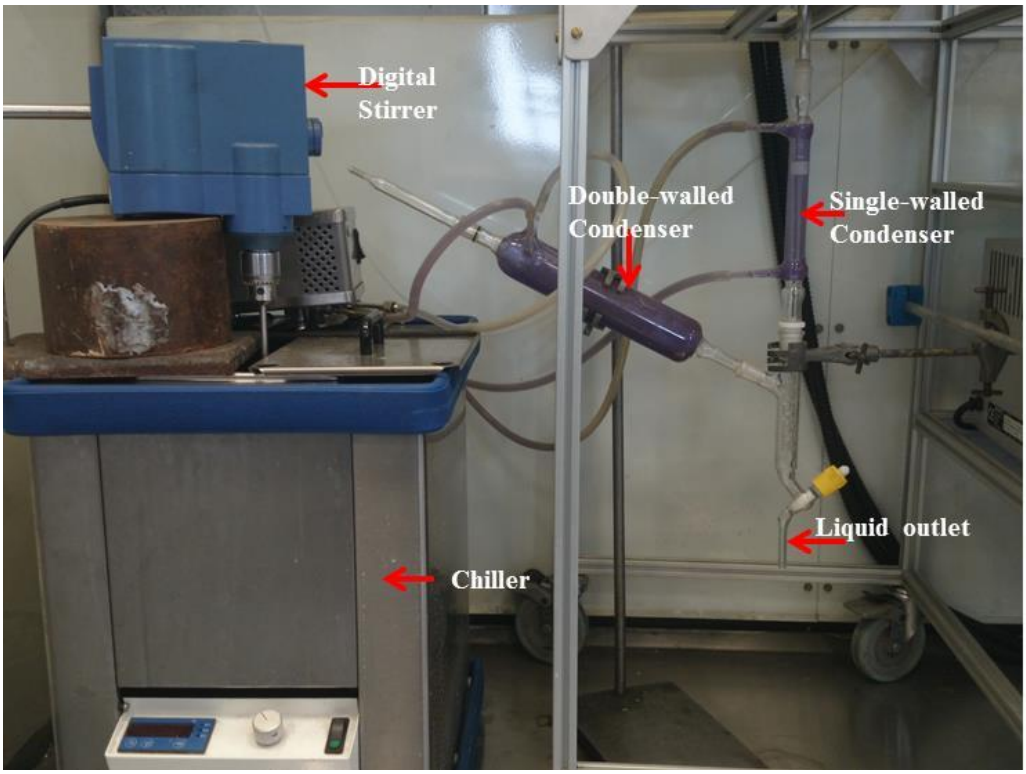

Figure 5.5 Glass Condenser Unit.

5.3 Catalytic testing – MCH dehydrogenation

In order to improve the efficiency of the MCH dehydrogenation reaction, Pt/Al_2O_3 catalyst was supported on a conductive metallic alloy has been used. The activity, selectivity and stability of the developed catalyst were compared with pelleted, commercial and in-house prepared, Pt/Al_2O_3 catalysts. The catalysts which were used have been listed in Table 5.3. The catalytic details and preparation of the supported catalyst have already been addressed in chapter three. The coated Fecralloy rods were approximately 2.5 cms long and 0.5 mm wide. The preparation of the in-house pelleted catalyst is described in Appendix A2.1. The alumina used to prepare the in-house catalyst was PURALOX, which was used to prepare the alumina coating on the Fecralloy support as detailed in chapter four. The commercial catalyst and in-house prepared Pt/Al_2O_3 catalyst were initially in a powder form. Prior to loading, both these catalysts were pressed using a catalytic press at a pressure of 2.5 tons. Following this, the catalysts were crushed using a mortar and pestle gently and passed through a sieve to obtain spherical catalyst particles of size 0.2 mm.

Catalyst	Supplier
1 wt% Pt/Al_2O_3/Fecralloy	In-house
1 wt% Pt/Al_2O_3	In-house (pelleted)
1 wt% Pt/Al_2O_3	Commercial (pelleted)

Table 5.3 Catalysts used in study.

5.4 Experimental Program

As previously indicated, the dehydrogenation of MCH over Pt/Al_2O_3/Fecralloy was investigated in two ways, activity and life time tests. The activity tests were short-term tests that mainly investigated the catalytic activity, short-term selectivity and indications of deactivation of the catalyst. The life time tests were an extended study that helped give a better understanding of the long-term stability of the developed catalyst, the long-term selectivity and long-term deactivation. Life time tests were also performed on the pelleted powdered catalysts in order to compare the activity and selectivity of the different catalysts.

Prior to addressing the details of these tests, catalyst loading into the reactor will briefly be discussed.

5.4.1 Catalyst Loading

In order to achieve the optimum catalytic performance the catalyst loading is very important. The catalyst particle size and the packing of the catalyst influence the mass and heat transfer phenomena in the reactor. Wall-channelling of the reactants might cause a drastic reduction of the reaction rate if the catalyst particles are too loosely packed or if the particle size is relatively large compared to reactor diameter. On the contrary, if the catalyst particles are too tightly packed or if the particle size is too small, excessive pressure-drop in the reactor limits the ability to vary the reactor space time (*W/F*) over the range of interest. Given the geometry of the Fecralloy rods, the catalyst loading was more complex. It was aimed to pack the rods as tightly as possibly, so as to have a reduced bed voidage and avoid excessive channelling.

The reactor was divided into three zones. The bottom zone contained glass beads (1-1.3 mm in diameter) and was typically 5 cm long, while the zone just above (middle zone) was filled with the coated catalyst rods. The top zone was approximately 10 cm long and was filled with glass beads of the same size as the bottom zone and worked as a pre-heater and distributor of the feed. The three zones in the reactor (top, middle, and bottom) were separated by layers of glass-wool to prevent the mixing of the catalyst and glass beads. The loaded catalyst and packing has been shown in Figure 5.6. The glass beads post catalytic testing turn black due to coke deposits as can be seen in Figure 5.6.

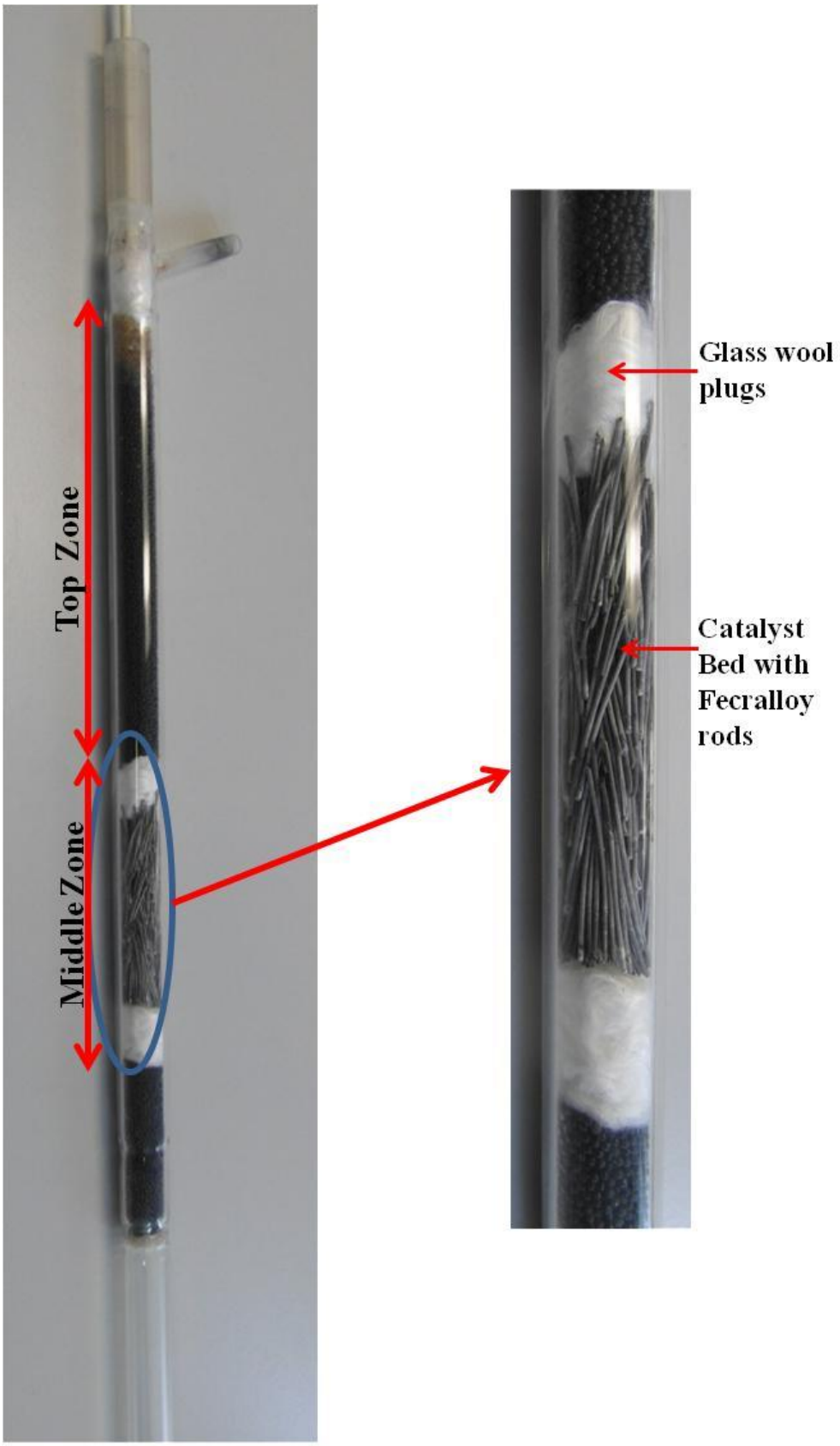

Figure 5.6 Packed Reactor Tube.

5.4.2 Catalyst Activation

Prior to starting the catalytic runs a two-step catalytic activation treatment was carried out. The treatments involved a calcination step and a reduction step and were carried out in-situ. Both the steps are very important for the catalytic performance. The activation procedure has been illustrated in Figure 5.7.

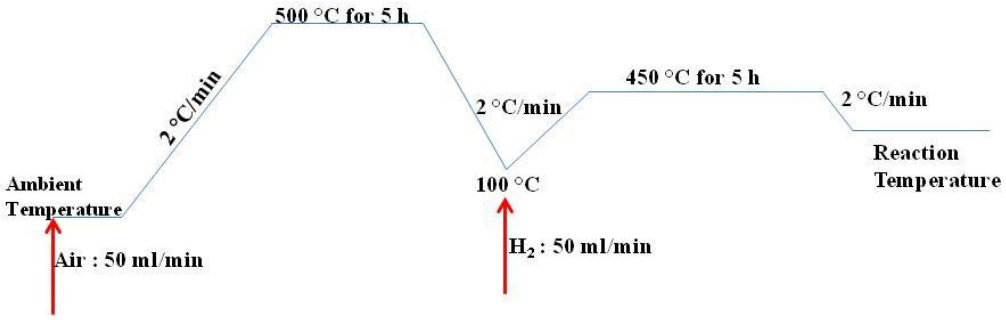

Figure 5.7 Catalyst activation procedure.

The calcination step was required to decompose the platinum precursor ($H_2PtCl_6.nH_2O$) and also to remove any adsorbed volatile components. During the calcination stage the platinum metal deposited on the support was converted to its oxide form. This step was achieved by heating the catalyst in air to 500 °C. The selection of a suitable calcination temperature was important as sintering of the metal crystallites could occur. According to Pinna in order to achieve the optimum dispersion of metal in Pt/Al_2O_3, the calcination temperature should not exceed 500 °C (Pinna, 1998). The heating rate in the calcination process was 2 °C/min and the air flow rate was maintained at 50 ml/min.

Catalyst reduction was the second stage of the activation procedure. During this stage the metal oxide was reduced to the metal (active form), which was achieved by thermally treating the catalyst in hydrogen. The heating rate, final temperature, time of reduction, hydrogen flow rate, hydrogen concentration, and hydrogen purity can affect this process. The catalyst oxidised in air was allowed to cool to around 100 °C before the gas flow was switched to hydrogen (50 ml/min). The catalyst was then heated at a slow rate of 2 °C/min to 450 °C and held overnight at this temperature before gradually (2 °C/min) bringing down the temperature to the reaction temperature.

5.4.3 Activity Tests

The activity tests have been conducted in the dehydrogenation rig described at varied operating conditions. Each test or experiment had four runs, R1, R2, R3 and R4. The four runs of the experiments were performed at fixed temperature but different MCH and/or H_2 flowrates. R1 was the run conducted at the lowest MCH flowrate while R3 was the run conducted at the fastest flowrate. The MCH flowrates for R1, R2 and R3 were 3 ml/h, 4.5 ml/h and 6 ml/h respectively. The hydrogen flowrate varied between 80 ml/min and 240 ml/min depending on the H_2/MCH molar ratio. The operating conditions and variables have been listed in

Table 5.4.

Operating Variable	Value Range
Temperature	340 °C - 400 °C
Pressure	1.013 bar
MCH flowrate	3 - 6 ml/h
H_2 flowrate	80 - 240 ml/min
H_2/MCH molar ratio	0 - 9

Table 5.4 Range of Operating Conditions for activity tests.

The experiments normally started with R1 and then proceed to R2, R3 and finally R4 which was a repeat of R1 to assess the extent of catalyst deactivation at the end of each experiment. To allow reactor stabilisation and accurate estimation of mass balance, the time duration of each run was three hours with liquid samples collected every hour. The total number of activity tests conducted in this study were 62.

5.4.4 Life time Tests or Deactivation Tests

The life time tests or deactivation tests were used to determine the catalyst stability and long term selectivity of the three catalysts listed in Table 5.3. Five long-term deactivation tests have been conducted. The operating conditions of the life time tests have been listed in Table 5.5 and ran for approximately 400 h. In the first eight hours of the study samples were collected every hour to study the initial phase of deactivation. After that samples were collected every 24 hours. In addition, the temperature profiles of the catalyst bed were also recorded during sample collection.

Operating Variable	**Value**
Temperature	400 °C
Pressure	1.013 bar
MCH flowrate	3 ml/h
H_2 flowrate	80 ml/min
H_2/MCH molar raio	0 - 9

Table 5.5 Operating conditions for life tests.

5.4.5 Sample Analysis

To obtain a detailed quantitative assessment of the selectivity toward the formation of toluene at various operating conditions, all samples were analysed in a Gas Chromatography-Mass Spectroscopy (GC-MS). The GC-MS was manufactured by *Agilent Technologies* (*Model-6890N*) and was equipped with a *HP-5MS* capillary column (50 m x 0.00025 m i.d., 5 % Phenyl and 95 % methylpolysiloxane). The GC-MS was calibrated by running samples of known concentrations. Standard mixtures of key products (0.005 %v/v - 0.1 %v/v) such as methylcyclopentane, heptane, methylcyclohexene benzene, xylene (o.p-) and biphenyl were dissolved in dichloromethane (*Analytical Reagent 99% Purity, Sigma Aldrich*). The calibration charts have been included in Appendix A3.1

6 Selectivity and By-products

6.1 Introduction

Reaction Selectivity is a very important factor in chemical processes. The selectivity of a process is usually enhanced by choosing a suitable catalyst that promotes the formation of the desired product and inhibits formation of by-products. The selectivity of MCH dehydrogenation bears directly upon the economics of production, since it determines the efficiency of the reactant conversion. The selectivity of a process is defined as the ratio between desired products yield and total product which can be expressed as ratio of yield of toluene and total conversion.

The research project has led to the development of a novel catalyst and has been tested for the dehydrogenation of MCH. In order to get a better understanding of the stability of the catalyst and more importantly the effect of the prepared catalyst on the by-product yields, a thorough investigation of the reaction selectivity and by-product yield at various operating parameters has been carried out. The results have been compared with a commercial catalyst and an in-house prepared catalyst for the same operating conditions. The alumina (PURALOX) used to prepare the in-house catalyst is similar to the alumina used to coat the Fecralloy rods as described in chapter five. In the majority of experiments conducted, for the Pt/Al_2O_3/Fecralloy catalyst, toluene selectivity in MCH dehydrogenation was maintained above 99%. The selectivity of the structured catalyst dropped to 98% during the life time tests after a time period of about 150 h and finally to 96% after 400 h.

6.2 Reaction Pathways

Before addressing the effect of operating parameters on reaction selectivity it is important to identify the main side reactions associated with the dehydrogenation of MCH. These side reactions can be identified by examining the results of the GC-MS. These results indicate that the by-products that are formed can be lumped into six main groups as indicated in Table 6.1. After reviewing the work done previous researchers on the by-products formed during MCH dehydrogenation a reaction pathway was proposed as illustrated in Figure 6.1 (Pacheco and Petersen, 1984a, Parera and Beltramini, 1988, Rebhan and Haensel, 1988, Sinfelt et al., 1960).

Lump	Composition
Benzene	Benzene
Paraffin	Methyl hexane and n - heptane
Substituted-Cyclopentane	Dimethylcyclopnetane isomers and ethylcyclopentane
Methylcyclohexene	Methylcyclohexene
Xylene	Xylene isomers (o-, p-, m-)
Substituted-biphenyl	Biphenyl, methylbiphenyl and dimethylbiphenyl isomers

Table 6.1 Composition of by-product lumps.

The by-products obtained from MCH dehydrogenation can be classified into two main categories,

- Products derived from the reactant - Methylcyclohexane
- Products derived from the product - Toluene

The by-products derived from MCH are methylcyclohexene, paraffin and substituted cyclopentanes while the products derived from toluene are benzene, xylene and substituted biphenyls. A brief review of the formation of these by-products is addressed in the following sections.

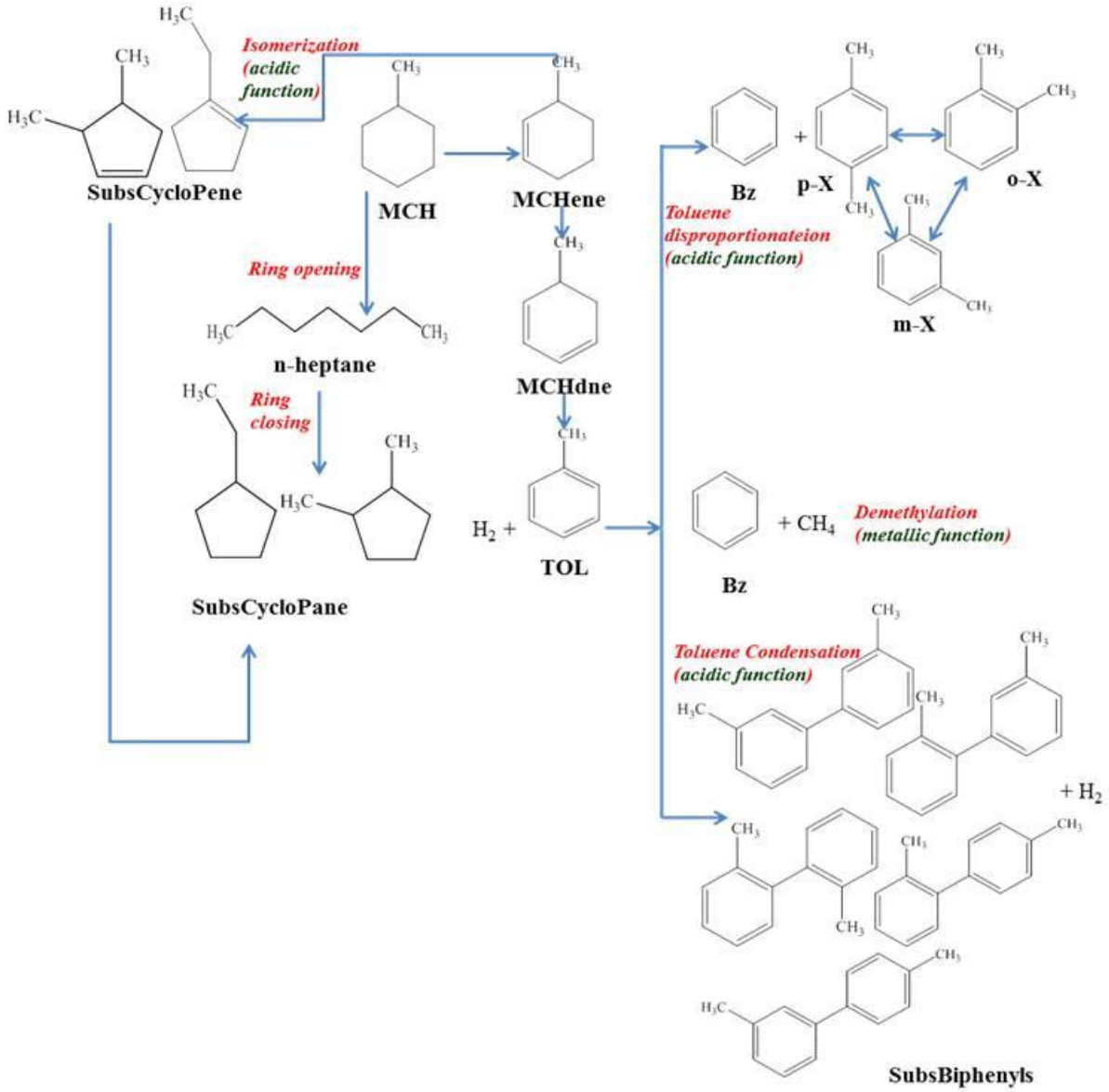

Figure 6.1 Reaction pathways in methylcyclohexane dehydrogenation and associated side reactions. (MCH: methylcyclohexane; MCHene:Methylcyclohexene; MCHdne: methylcyclohexadiene; TOL: toluene; Bz: benzene; o-X: ortho-Xylene; m-X: meta-Xylene; p-X: para-Xylene; SubsCycloPene: Substituted Cyclopentenes; SubsCycloPane: Substituted Cyclopentanes; SubsBiphenyls: Substituted Biphenyls) (Tsakiris, 2007).

6.2.1 Products derived from MCH

The by-products derived from MCH are methylcyclohexene, paraffin and substituted cyclopentanes. Methylcyclohexene is a reaction intermediate that is formed due to partial dehydrogenation of MCH. Paraffins are formed when methylcyclohexane undergoes a ring opening reaction yielding n-heptane and methylhexane. Substituted cyclopentanes are either formed from a ring closing reaction of paraffins or by the hydrogenation of dimethylcyclopentene isomers which are formed by the ring opening and ring closing reactions of methylcyclohexene (Rebhan and Haensel, 1988). Parera and his co-workers reported that cyclopentanes are coke precursors in bifunctional catalysts due to the dehydrogenation ability of the metallic function and the condensation ability of the acidic function (Parera and Beltramini, 1988). This results in the formation of polyaromatic compounds from cyclopentanes which over time produce a graphitic coke deposition causing irreversible deactivation of the catalyst. Traces of poly-aromatic compounds were found in some GC-traces but the concentrations were very low.

6.2.2 Products derived from Toluene

The main by-products derived from toluene are benzene, xylene and substituted biphenyls. Toluene formation resulted in three potential reaction pathways. The first is a demethylation reaction, in which the methyl group is removed yielding benzene and methane. The demethylation reaction is characteristic of the metallic function at temperatures higher than 300 °C. The second is toluene disproportionate (TDP) reaction which is highly attributed to the Lewis acid sites of the catalyst (Liang and Weng, 1993). In this process, two molecules of toluene react and form benzene and xylene (dimethylbenzene). The TDP reaction produces three xylene isomers, ortho -, meta -, and para - as illustrated in Figure 6.2.

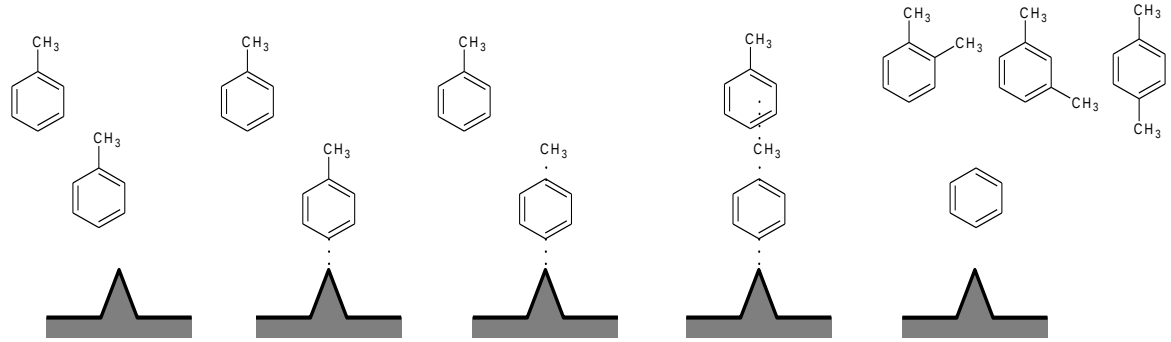

Figure 6.2 Toluene Disproportionation reaction on Lewis acid site, (Liang and Weng, 1993).

The third reaction pathway is a condensation reaction, in which two molecules of toluene condense to form substituted dimethylbiphenyls and hydrogen. The condensation reaction is believed to be attributed to the acidic function of the support, similar to toluene disproportionation. Further dehydrogenation of the substituted dimethyl - biphenyls may lead to carbon deposition on the active surface in a graphitic structure (hydrogen deficient), which is responsible for an irreversible deactivation of the catalyst.

6.3 Effect of Operating Parameters on by-product yields

To thoroughly study the effect of the operating parameters on toluene selectivity we need to investigate the effects on these parameters on the formation of by-products. Two types of catalytic tests have been employed, short term activity tests and life tests. The short term activity tests investigated the effect of reactor space time (*W/F*), temperature and H_2/MCH ratio on by-products yield. The life tests were used to assess the effect of time-on-stream (TOS) or catalyst deactivation on reaction selectivity. To easily differentiate between the catalysts tested a set colour coding as shown in Table 6.2 was used.

Catalyst*	Supplier	Support	Abbreviation	Symbol
1 wt%Pt/Al_2O_3/FeCralloy	In-house	FeCralloy	Pt(S)	▲
1 wt%Pt/Al_2O_3	In-house	PURALOX	Pt(P)	◆
1 wt%Pt/Al_2O_3	Commercial	NA	Pt(C)	●

Table 6.2 Symbols and abbreviations used to distinguish between catalysts. *Pt content confirmed by STEM analysis as shown in *section 4.3.4*.

6.3.1 Short term activity tests

The short term activity tests have been conducted at various operating parameters and have been used to investigate the effect of each of these parameters on reaction selectivity and by-product yield. Activity tests were performed on the structured catalyst and the commercial pelleted catalyst. This enabled a comparison of catalytic activities at the different operating parameters in addition to the by-product yield. Both the catalysts showed similar catalytic activity however; there was a difference in the by-product yield. The concentration of the by-product yield was significantly higher for the structured catalyst. This has been discussed in detail in the following sections. For better clarity on the by-product yield when testing the commercial pelleted catalysts, the concentration profiles of the resulting by-products formed when using this catalyst have been included in Appendix A3.2. Additionally, the difference in by-product yield with the different operating parameters (increasing *W/F* and *T*) has been schematically shown through the reaction mechanism; where the red arrows indicate an increase in yield and the green arrows describe a decreasing in yield.

6.3.1.1 Effect of reactor space time

Reactor space time is a very important kinetic parameter. It is the ratio of the weight of the catalyst to the feed molar flow rate (*W/F*) [$g_{cat/(}$mol $_{MCH}$ feed/sec)]. The reciprocal of the space time is known as space velocity (i.e. WHSV). The effect of reactor space time on reaction selectivity and by-product yield has been investigated by varying the reactor space time while fixing the operating parameters of temperature (400 °C), pressure (1 bar) and H_2/MCH molar ratio of 9. The catalyst activity of the structured and pelleted catalysts at different reactor space times has been illustrated in Figure 6.3. The varied by-product yield formed with increasing *W/F* is described in Figure 6.5.

As expected, conversion rapidly increased with *W/F* as illustrated in Figure 6.3. With increasing *W/F*, the contact time is increased thus enhancing MCH dehydrogenation and improving the reaction conversion. In order to check on the repeatability of the results obtained from the GC analysis, sample analysis was repeated twice and the results were found to be similar with a difference of $\pm$ 2%.

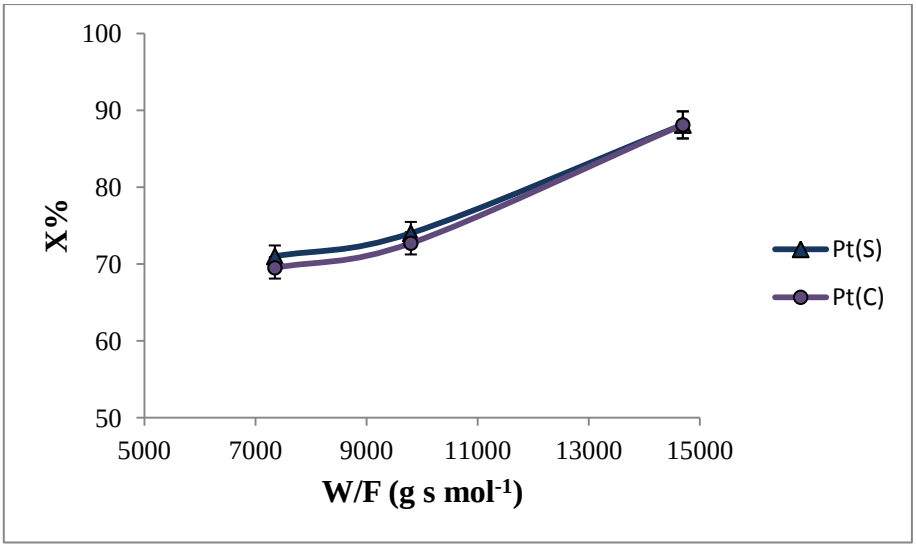

Figure 6.3 Reaction conversion increases for increasing reactor space time: T = 400 °C, P = 1 bar and H_2/MCH = 9.

The by-products obtained from toluene increased with reactor space time whilst the by-products obtained from methylcyclohexane depicted a different trend, the by-products either increased with time (xylene, benzene, substituted biphenyls), or decreased with the reactor space time (methylcyclohexene, substituted cyclopentanes). This has been schematically shown in Figure 6.4. The change in by-product concentrations, obtained from toluene and methylcyclohexane has been described graphically in Figure 6.5. The by-products yield with the commercial catalyst was 50 % lower than the yield of by-products with the structured catalyst The effect of reactor space time (*W/F*) on by-products yield for both the commercial catalyst and structured catalyst depicted a similar trend. Hence only the concentration profiles of the by-products, resulting from the dehydrogenation of methylcyclohexane over a structured catalyst have been included and the results can be summarised as follows:

- Xylene and benzene concentration increased with reactor space time and the molar ratio of benzene to xylene was 1. Hence implying both the products were formed simultaneously from toluene disproportionation reaction. As *W/F* increased, there was an increase in toluene formation which further resulted in an increase in toluene disproportionation. Analysis of the gaseous products showed only traces of methane present thus confirming, that the benzene yield was from toluene disproportionation.

- Methylcyclohexene and paraffin yield significantly dropped with increasing *W/F*. Thus increased reaction holding time improved the rate of complete MCH dehydrogenation hence decreasing the formation of reaction intermediaries methylcyclohexene, substituted cyclopentanes paraffins.

- Since increased *W/F* resulted in increased toluene formation there was an increase in the formation of biphenyls. Toluene undergoes a condensation reaction on the acidic function of the catalyst to produce substituted biphenyls.

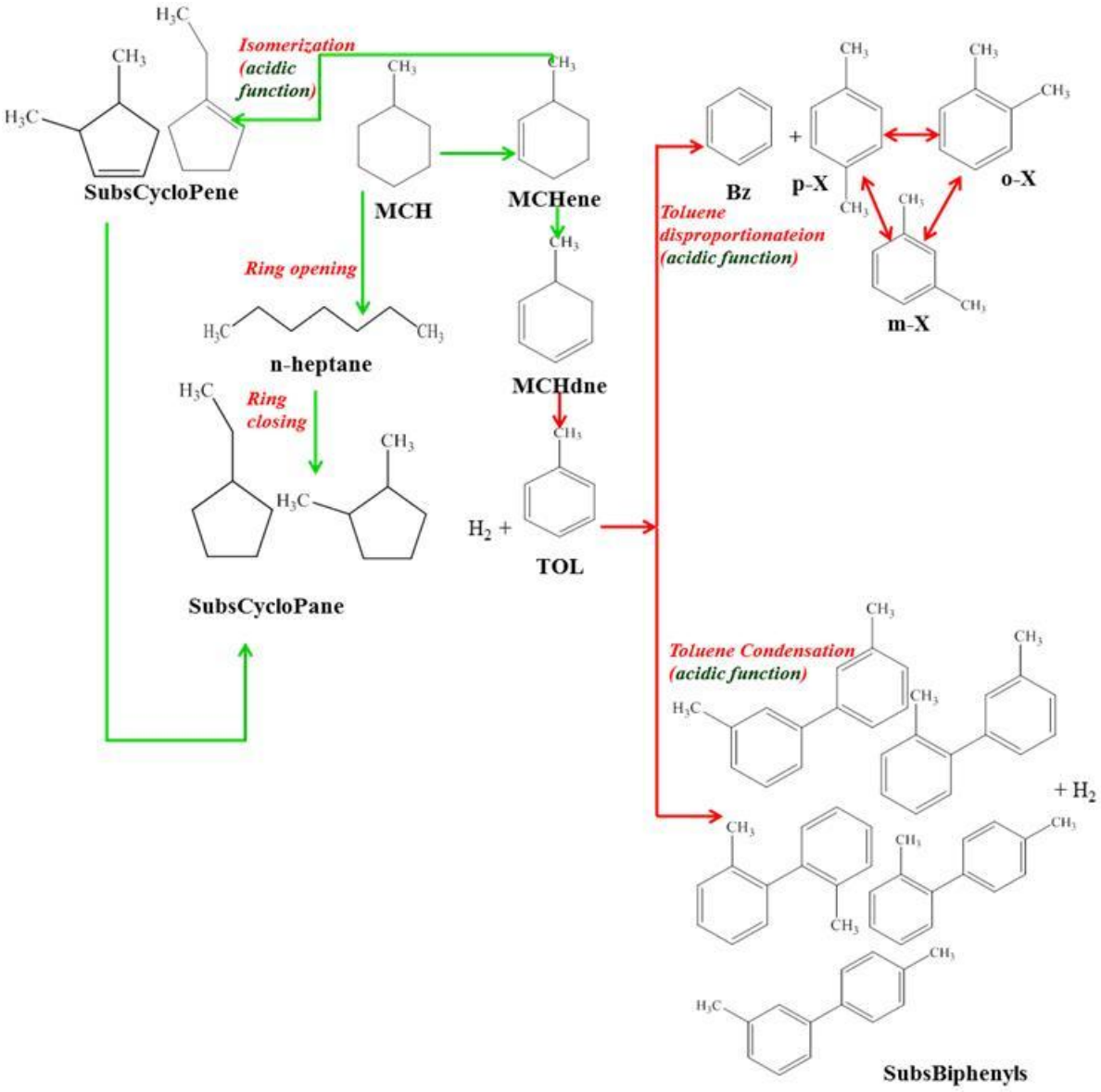

Figure 6.4 With increasing W/F yield of products derived from TOL increased and products derived from MCH decreased (red arrows describe increase in yield, green arrows describe decrease in yield).

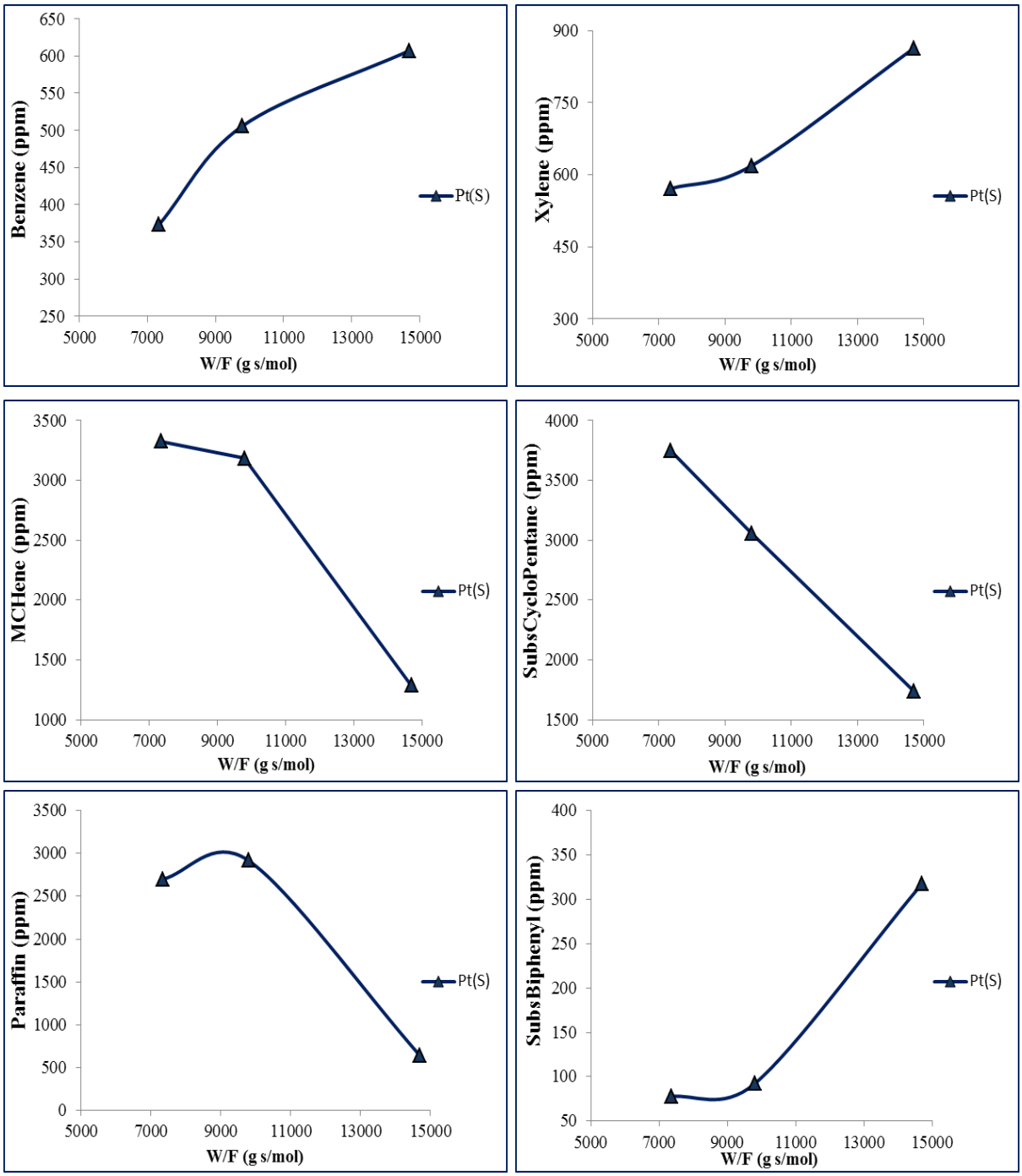

Figure 6.5 Effect of W/F on by-product yields and conversion at T = 400 °C, P = 1bar and H_2/MCH = 9

6.3.1.2 *Effect of Temperature*

The effect of temperature has been investigated by testing the catalyst at 340 °C - 400 °C at 1 bar and H_2/MCH molar ratio of 9 and fixing the reactor space time at 14690 g s mol^{-1}. Figure 6.6 illustrates the increasing conversion with increasing temperature at the fixed operating parameters. The structured catalyst described an improved conversion profile when compared to the commercial catalyst. This difference could be attributed to the reduced thickness of the alumina washcoat (~ 6 µm) on the Fecralloy rods thus reducing the resistance to diffusion when compared to the spherical commercial catalyst particles which have an approximate diameter of 200 µm.

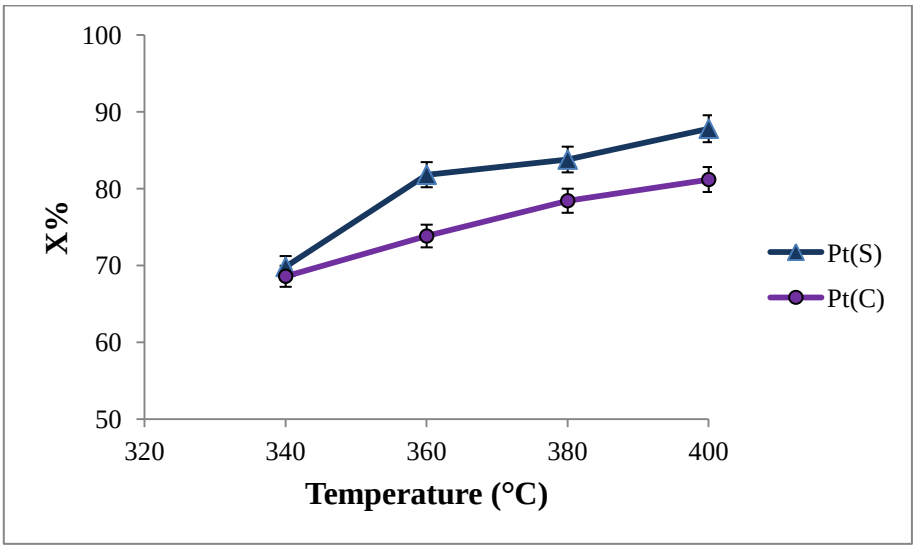

Figure 6.6 Reaction conversion increases for increasing temperature: W/F = 14690 g s mol^{-1}, P = 1 bar and H_2/MCH = 9.

Figure 6.7 and Figure 6.8 describe the effect of increasing temperature on the reaction mechanism for the structured catalyst and by-product concentration (both the catalysts) respectively. The main observations noted from these figures are:

- Much lower concentrations of by-products for the commercial catalyst.

- The increasing concentration (for both catalysts) of benzene and xylene suggest that toluene disproportionation is temperature dependent. The ratio of benzene to xylene

(molar) yield was approximately 1. Thus suggesting the formation of benzene was primarily from toluene disproportionation and not toluene demethylation reaction. Gas samples of the products were subjected to GC analysis, the results did not show traces of methane thus confirming absence of toluene demethylation reaction.

- For the structured catalyst, methylcyclohexene concentration decreased with temperature however there was a significant increase in the formation of substituted cyclopentanes with temperature. Methylcyclohexane undergoes a ring opening reaction to produce n-heptane which further undergoes a ring closing reaction to give substituted cyclopentanes. However this reaction appears to be inhibited with increasing temperature. Methylcyclohexene isomerizes to produce substituted cyclopentenes which further hydrogenate to give substituted cyclopentanes. Comparison of the reaction mechanism with the by-product yield, suggested that with increasing temperature the isomerization ability of the structured catalyst increased. Hence an increase in temperature resulted in the formation of substituted cyclopentanes from two plausible reaction routes.

- For the commercial pelleted catalyst, methylcyclohexene concentration increased slightly with temperature despite the significant increase in conversion to toluene. This suggests the beginnings of catalyst deactivation.

- The yield of substituted biphenyls, for both the structured and commercial catalyst increased with increasing temperature and toluene conversion, and, thus implying toluene condensation is temperature dependent.

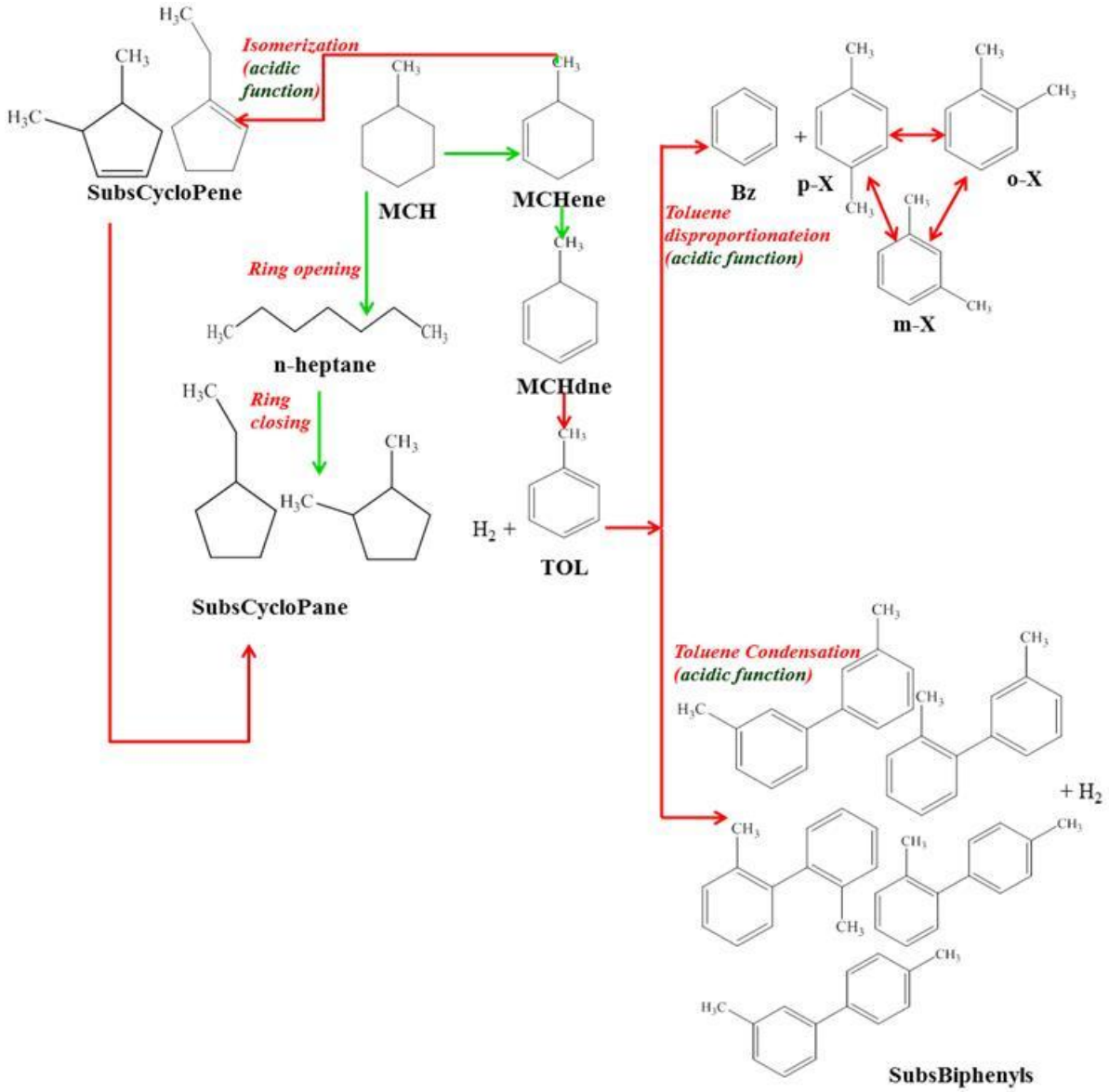

Figure 6.7 With increasing temperature dehydrogenation and isomerization activity of structured catalyst was enhanced (red arrows describe increase in yield, green arrows describe decrease in yield).

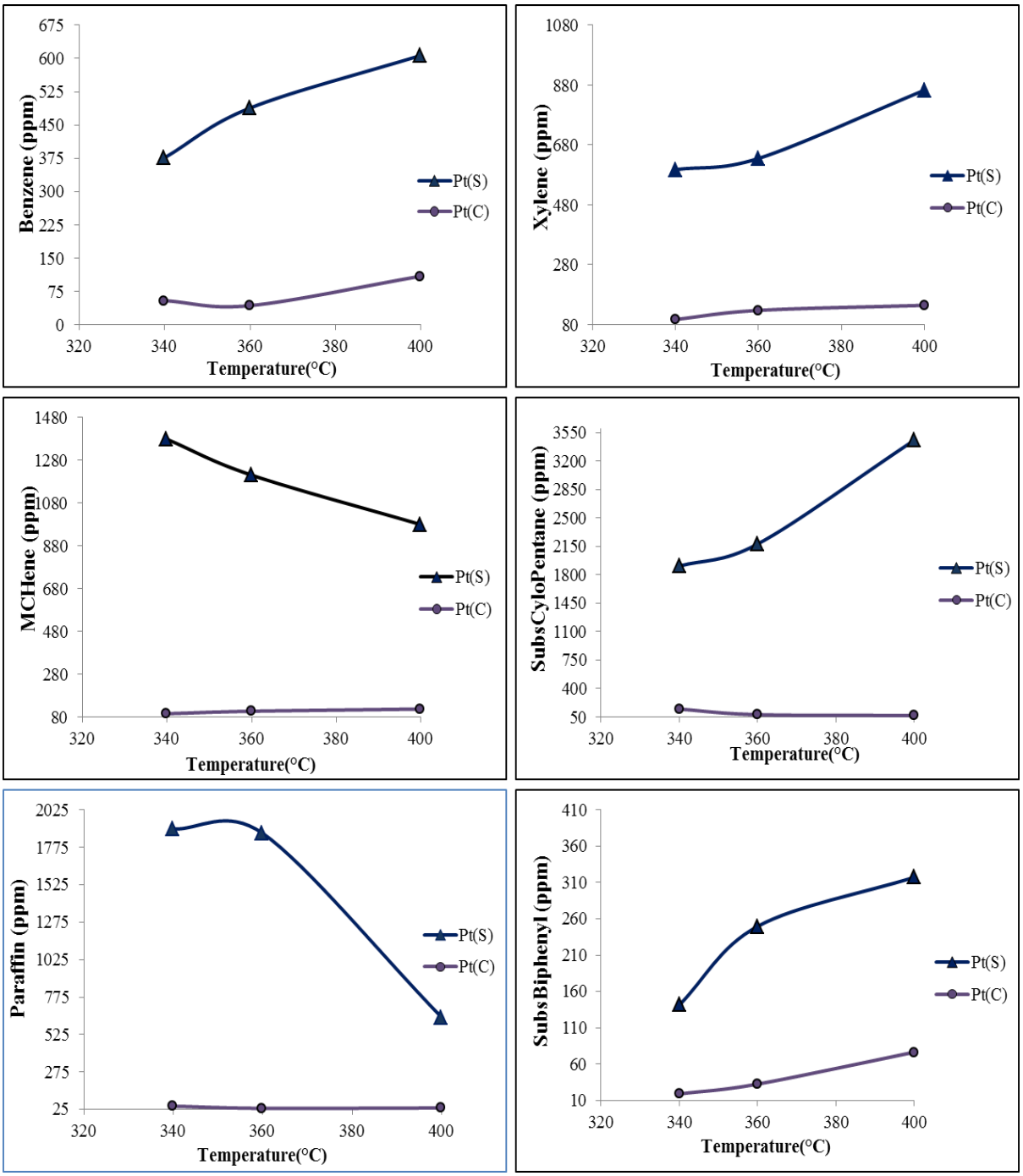

Figure 6.8 Effect of temperature on by-product yields and conversion at W/F = 14690 g s mol^{-1}, P = 1 bar and H_2/MCH = 9.

6.3.1.3 *Effect of H_2/MCH molar ratio*

The reaction selectivity and by-product yields were studied at different H_2/MCH ratios at a fixed temperature of 400 °C, pressure 1 bar and *W/F* of 14690 g s mol^{-1}. The comparison of the catalyst activity and selectivity was done at the operating conditions which were likely to cause the highest catalyst deactivation

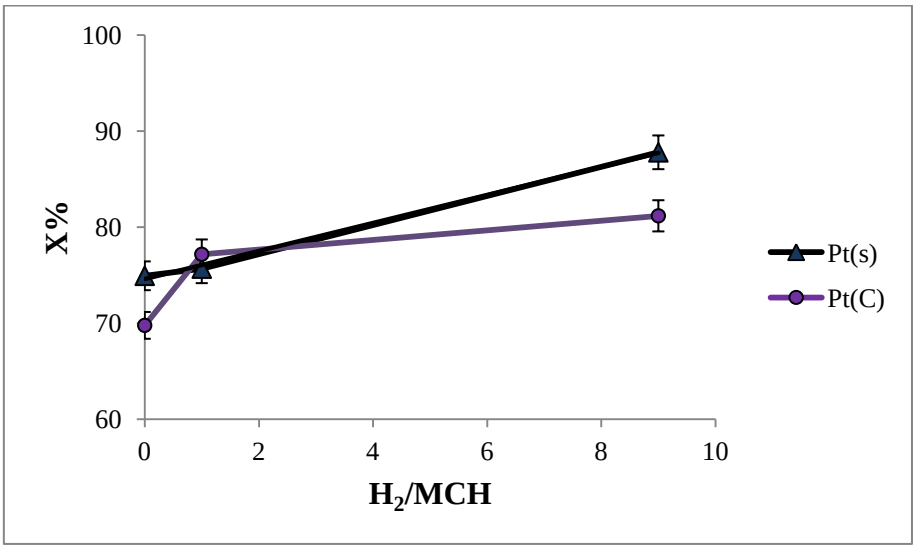

Figure 6.9 Reaction conversion increases for increasing ratio of H_2/MCH ratio: W/F = 14690 g s mol^{-1}, P = 1 bar and T = 400 °C.

Figure 6.9 illustrates the increasing conversion with increasing H_2/MCH ratio at the fixed operating parameters. Figure 6.10 describes the effect of increasing H_2/MCH ratio on the yield of by-product concentrations. The main observations noted from these figures are:

- For the structured catalyst, increasing H_2/MCH ratio resulted in an increased formation of benzene and xylene. At H_2/MCH ratio of 0 and 1, the molar ratio of benzene to xylene was approximately 5 and 4 respectively. This suggests that in the absence of hydrogen toluene demethylation reaction was enhanced and the increased H_2/MCH ratio supressed this reaction. However, for the commercial pelleted catalyst the molar ratio of benzene to xylene was 1.5 at H_2/MCH ratio of 0 which reduced to 1 with increase in H_2/MCH ratio. Thus suggesting there were a differences in activity of the metallic function between both the catalysts.

- The concentration of paraffins (for both the catalysts) increased with increasing H_2/MCH ratios which subsequently resulted in an increase in substituted cyclopentane yield for the commercial catalyst through ring closing mechanism. Thus implying, absence of hydrogen inhibited methylcyclohexane from undergoing a ring-opening reaction.

- For the structured catalyst, the yield of substituted cyclopentanes decreased with increase in H_2/MCH ratio. The formation of substituted cyclopentanes is through two mechanisms, the ring opening and closing of methylcyclohexene and isomerization of methylcyclohexene (Rebhan and Haensel, 1988). Therefore, the decrease in substituted cyclopentane concentration when using the structured catalyst can be attributed to the decrease in isomerization activity in the presence of excess hydrogen.

- The methylcyclohexene yield (for both the catalysts) increased with increasing the H_2/MCH ratio which can be attributed to the increase in incomplete dehydrogenation of MCH. Based on Le-Chatelier principle increasing the H_2/MCH ratio increases the reaction rate and hence the reaction in the forward direction which results in an increase in incomplete dehydrogenation of MCH.

- With increasing H_2/MCH ratio the conversion to toluene increased thus resulting in an increase in toluene condensation and formation of substituted biphenyls which was very marked in the Fecralloy catalyst. The commercial catalyst showed an increase in biphenyl yield when H_2 was added, but the change in concentration when the H_2/MCH ratio was increased from 1 to 9 was only very little.

- It is also important to note, that in an increased hydrogen atmosphere, there is a decreased coke formation. There is more likely to be an increased formation of saturated products rather than unsaturated products as can be seen in Figure 6.10. Unsaturated products are more reactive and tend to form irreversible carbonaceous layers over the catalyst. Thus the catalyst was more active and stable when the H_2/MCH ratio was increased.

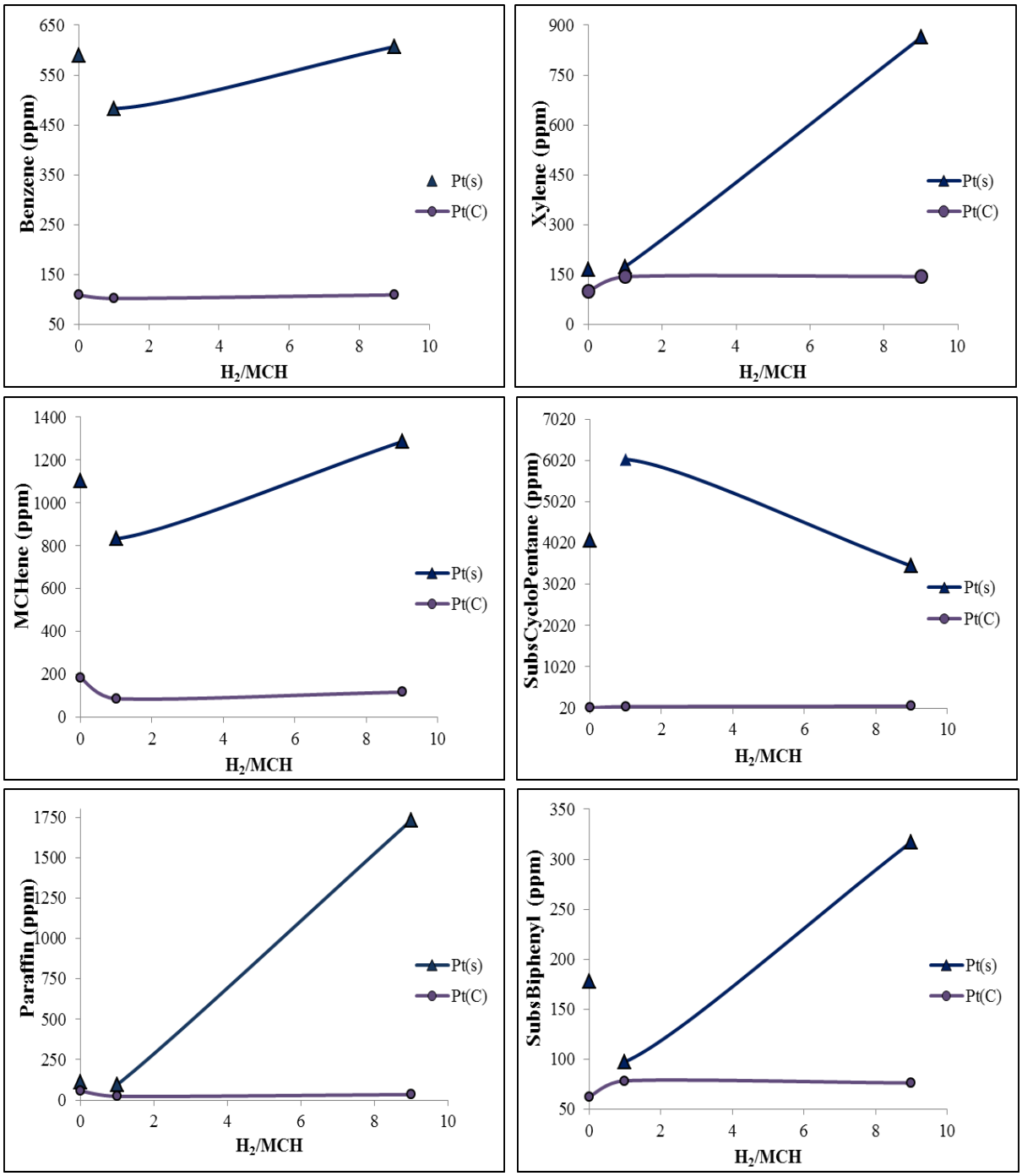

Figure 6.10 Effect of H_2/MCH ratio on by-product yields and conversion at W/F = 14690 g s mol^{-1}, P = 1bar and T = 400 °C.

6.3.2 Long term life tests

The life time tests have been used to assess the effect of time-on-stream (TOS) or catalyst deactivation on reaction selectivity. To explain the difference in catalytic activity and selectivity of the different catalysts as it deactivates, one has to consider the effect of surface deactivation on dehydrogenation, ring-opening and isomerization activities. Long term life tests have been performed on the structured catalyst and pelleted, in-house and commercial catalysts. Thus it was possible to compare the effect of TOS on reaction selectivity for the different catalysts.

6.3.2.1 Effect of time-on-stream on Conversion

The effect of catalyst deactivation on reaction selectivity and by-product yields has been investigated by conducting long term deactivation tests. The deactivation tests on all the catalysts were conducted at identical operating conditions. Figure 6.11 illustrates the deactivation pattern of the three catalysts that were tested. All the catalysts depicted a similar two phase deactivation pattern. The first phase of deactivation was characterized by a steep deactivation curve with a loss of activity of around 20%, within a relatively short period of time (around 100 h). The second phase of deactivation, the "plateau", was characterized by a slower deactivation rate and hence a loss of activity of around 10% over a period of 300 h. The initial sharp deactivation resulted in a significant loss in catalytic activity in the plateau. The deactivation patterns illustrated in Figure 6.11 are only valid for the given operating conditions. At different operating conditions or at higher pressure, the deactivation patterns are bound to be altered.

In order to get an improved understanding on the stability of the developed catalyst, additional life tests were conducted on the structured catalyst at different operating parameters. Figure 6.12 illustrates the catalyst deactivation profile over a period of 250 h at two different flowrates and fixed operating parameters of, temperature (400 °C), pressure (1 bar) and H_2/MCH (9).

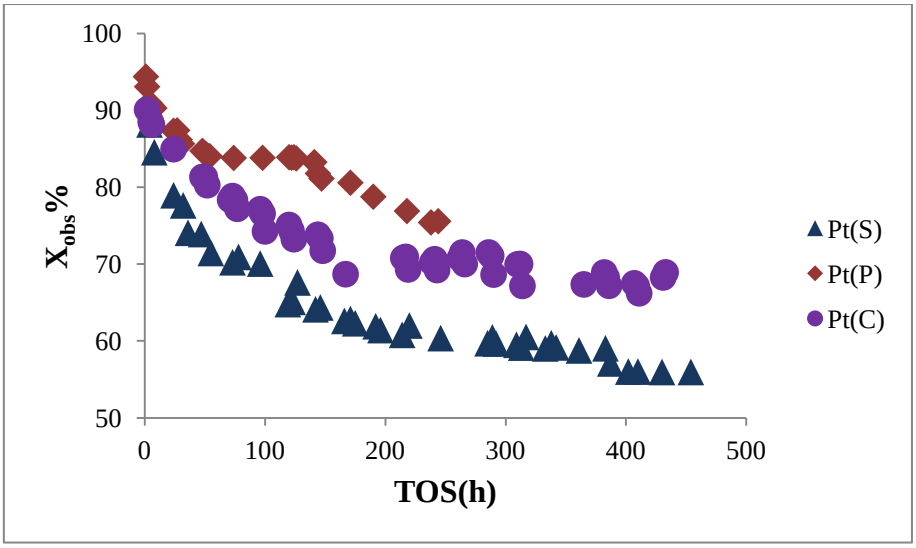

Figure 6.11 Deactivation rate of catalysts tested at: W/F = 14690 g s mol^{-1}, T = 400 °C, H_2/MCH = 9 and P = 1bar.

As expected, the conversion to toluene is higher with increased *W/F*. However, the catalyst describes a similar deactivation profile when tested at different *W/F*. Figure 6.13 describes the deactivation profile when the structured catalyst was tested without any hydrogen in the feed i.e. H_2/MCH = 0. In the absence of hydrogen the catalyst rapidly deactivated within a period of 48 h. This could be attributed to the increased formation of unsaturated by-products that resulted in formation of graphitic structures on the acid function of the catalyst as well as the metallic function.

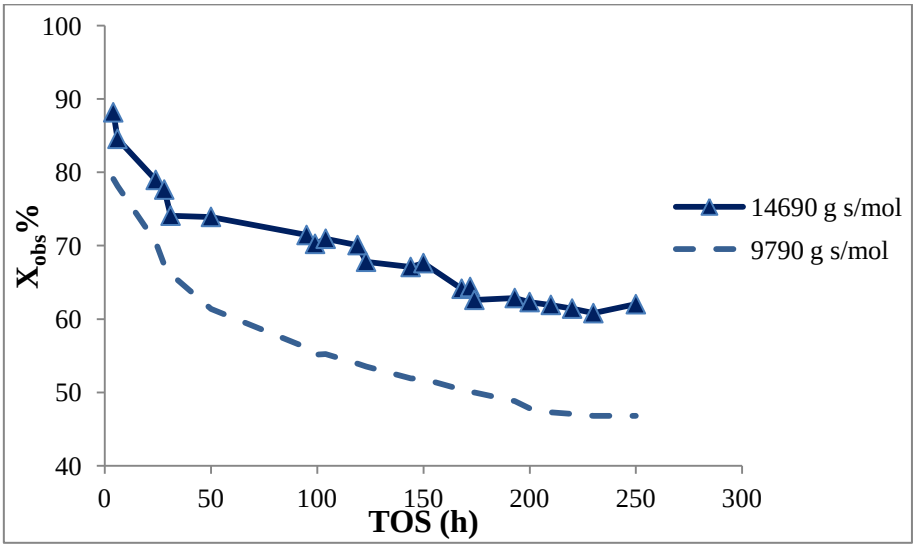

Figure 6.12 Life test on structured catalyst at W/F = 14690 - 9790 g s mol^{-1}, T= 400 °C, P = 1 bar and H_2/MCH = 9.

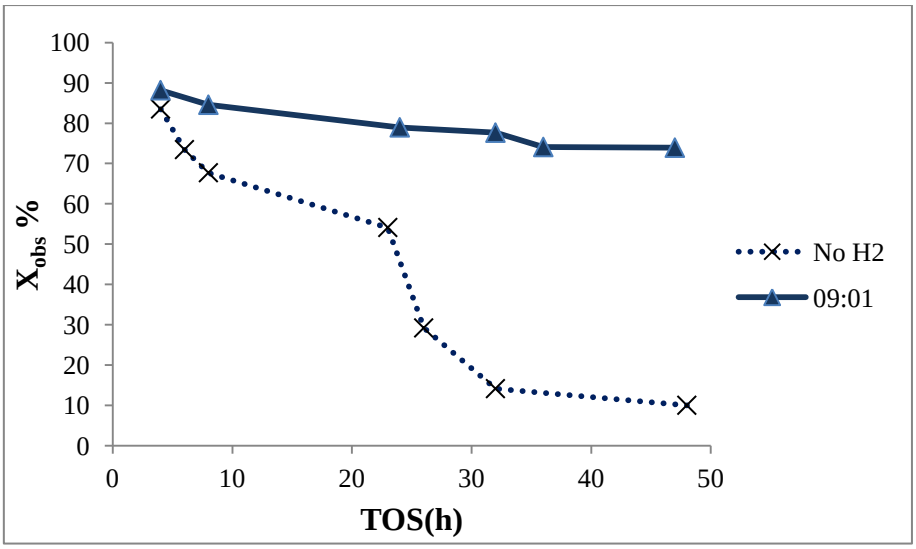

Figure 6.13 Life test on structured catalyst at W/F = 14690 g s mol^{-1}, T = 400 °C, P = 1 bar and H_2/MCH = 0 and H_2/MCH = 9.

6.3.2.2 Effect of time-on-stream on reaction selectivity

The effect of catalyst deactivation on long term selectivity is illustrated in Figure 6.14. The commercial catalyst and in-house catalyst (made using PURALOX) showed similar stable high selectivity of > 99% and were relatively unchanged despite a loss of 30% activity. The Fecralloy catalyst showed a steady decline of 4% selectivity over the same loss of conversion. As stated earlier, platinum loading and dispersion in addition to the support acidity are key aspects to consider in order to achieve a good selectivity.

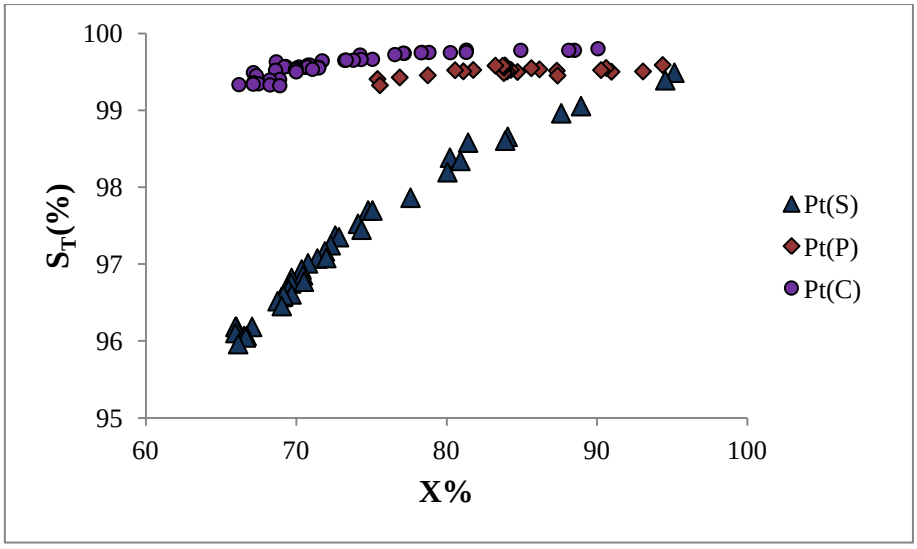

Figure 6.14 Selectivity towards toluene as catalyst deactivates at :W/F = 14690 g s mol^{-1}, T = 400 °C, H_2/MCH = 9 and P = 1bar.

6.3.2.3 Effect of time-on-stream on by-product formation

To obtain a better understanding of the difference in long term selectivity of the different catalysts, the by-product yields of the deactivation tests were assessed against time on stream. The GC-MS chromatograms detail the by-product distribution for the different catalysts with increasing TOS and are shown in Figure 6.15 - 6.17. A detailed inspection of the results indicated the following:

- Presence of Benzene in the GC-MS chromatograms suggested the presence of toluene demethylation. As the catalyst deactivated there appeared to be a decrease in the xylene peaks indicating a decrease in toluene disproportionation. Xylene formation decreased with catalyst deactivation. Toluene disproportionation is caused by the acidic function of the catalyst. Thus with time, as the active metal sites deactivate, the acidic function of the catalyst undergoes deactivation as well. The yield of xylene was higher for the in-house pelleted catalyst when compared to the commercial catalyst.

- Methycyclohexene peaks in the GC-MS chromatograms confirm the enhancement of partial dehydrogenation of methylcyclohexane as the catalyst deactivated. The yield of methylcyclohexene increased with time, as the catalyst deactivated. The increase in partial dehydrogenation of MCH suggests that as the catalyst deactivated there could

be an increased formation of a carbonaceous overlayer over the metal sites which subsequently limited the formation of toluene and favoured the reaction intermediate.

- The formation of substituted cyclopentanes increased simultaneously with the enhancement of partial MCH dehydrogenation. This suggested that formation of substituted cyclopentanes was from the isomerization of methylcyclohexene to substituted cyclopentenes which further hydrogenated to form substituted cyclopentanes. There was an increased formation of the reaction intermediate methylcyclohexene and substituted cyclopentanes in the structured catalyst when compared to the pelleted catalysts, which was consistent with greater deactivation of the metallic function of the structured catalyst.

- Formation of substituted biphenyls, for all the catalysts, decreased as the catalyst deactivated which could be attributed to the deactivation of the more active platinum sites which resulted in a decrease in toluene condensation. The initial phase of sharp deactivation could be attributed to the formation of biphenyls. As the catalyst deactivated the yield of biphenyls decreased suggesting increased coking of the acid sites of the catalysts. Biphenyls yield was significantly higher for the in-house pelleted catalyst. Biphenyls and xylenes are formed on the acidic function of the catalyst that is the alumina support. There was also increased formation of these by-products when the in-house pelleted catalyst was used suggesting a difference in support acidity between the pelleted catalysts.

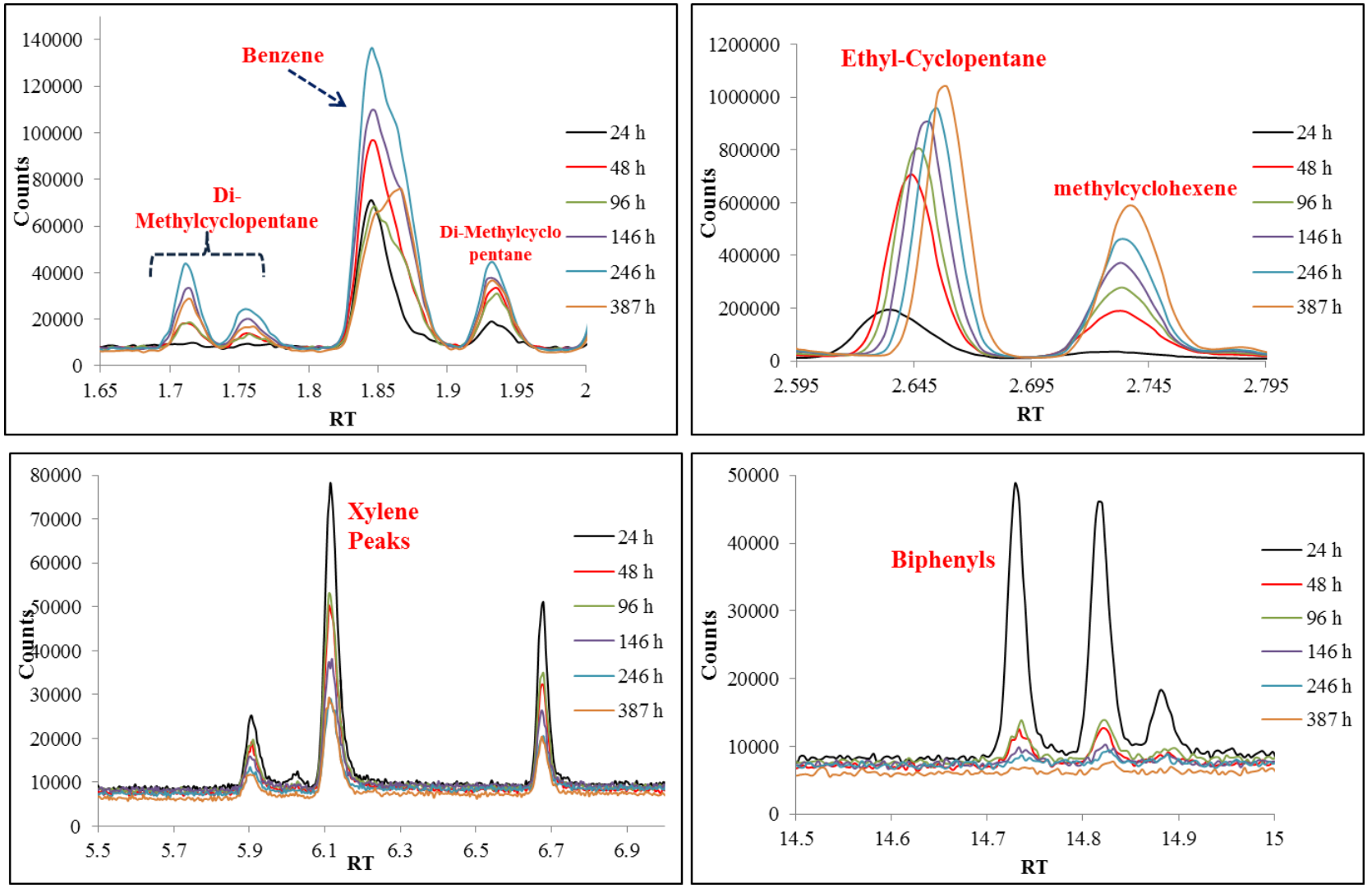

Figure 6.15 GC-MS chromatograms describing change in the by-products distribution with increasing TOS for the structured catalyst at T = 400 °C, P = 1 bar and W/F = 14690 g s mol $^{-1}$.

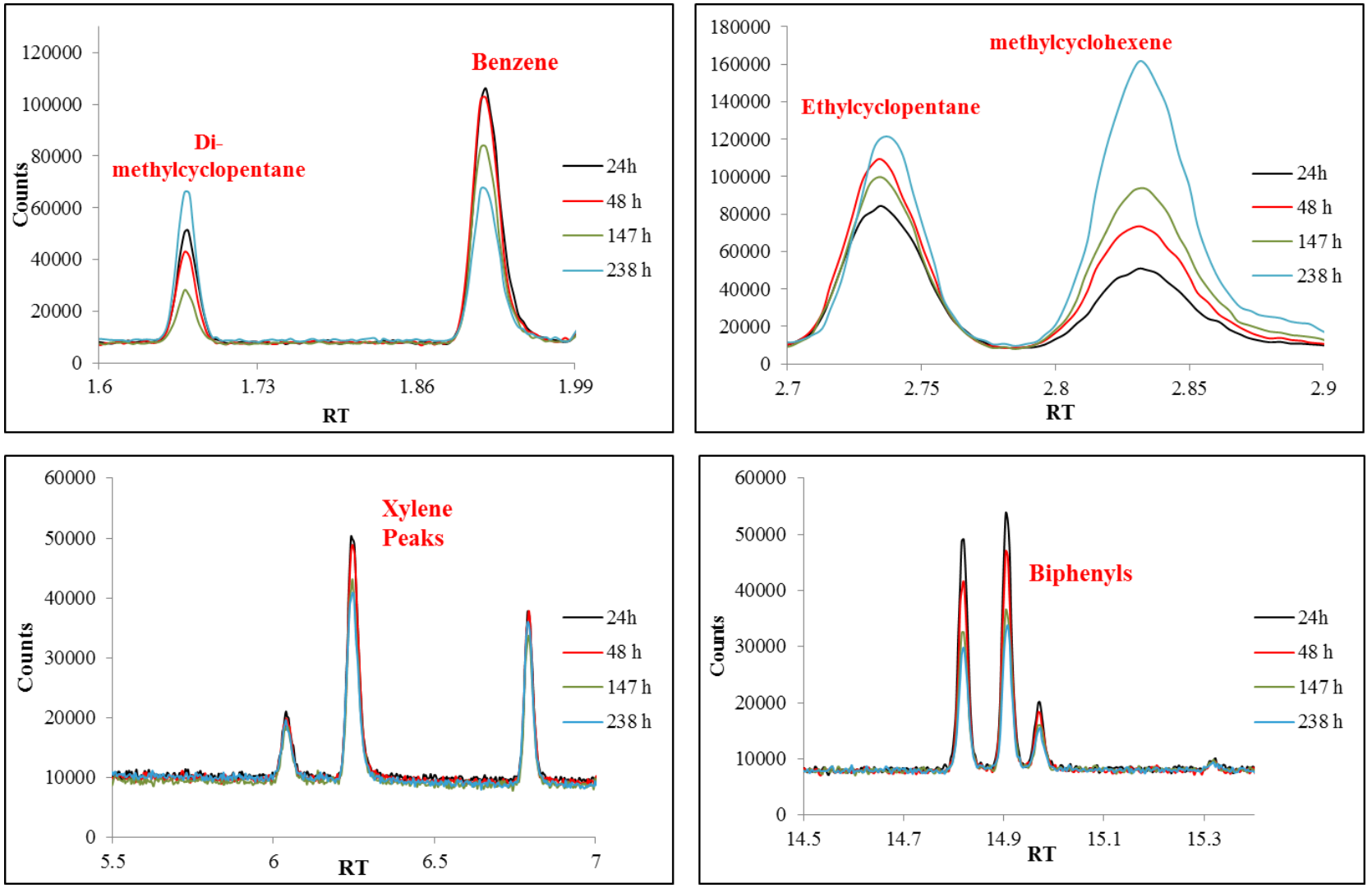

Figure 6.16 GC-MS chromatograms describing change in the by-products distribution with increasing TOS for the in-house pelleted catalyst at T = 400 °C, P = 1 bar and W/F = 14690 g s mol $^{-1}$.

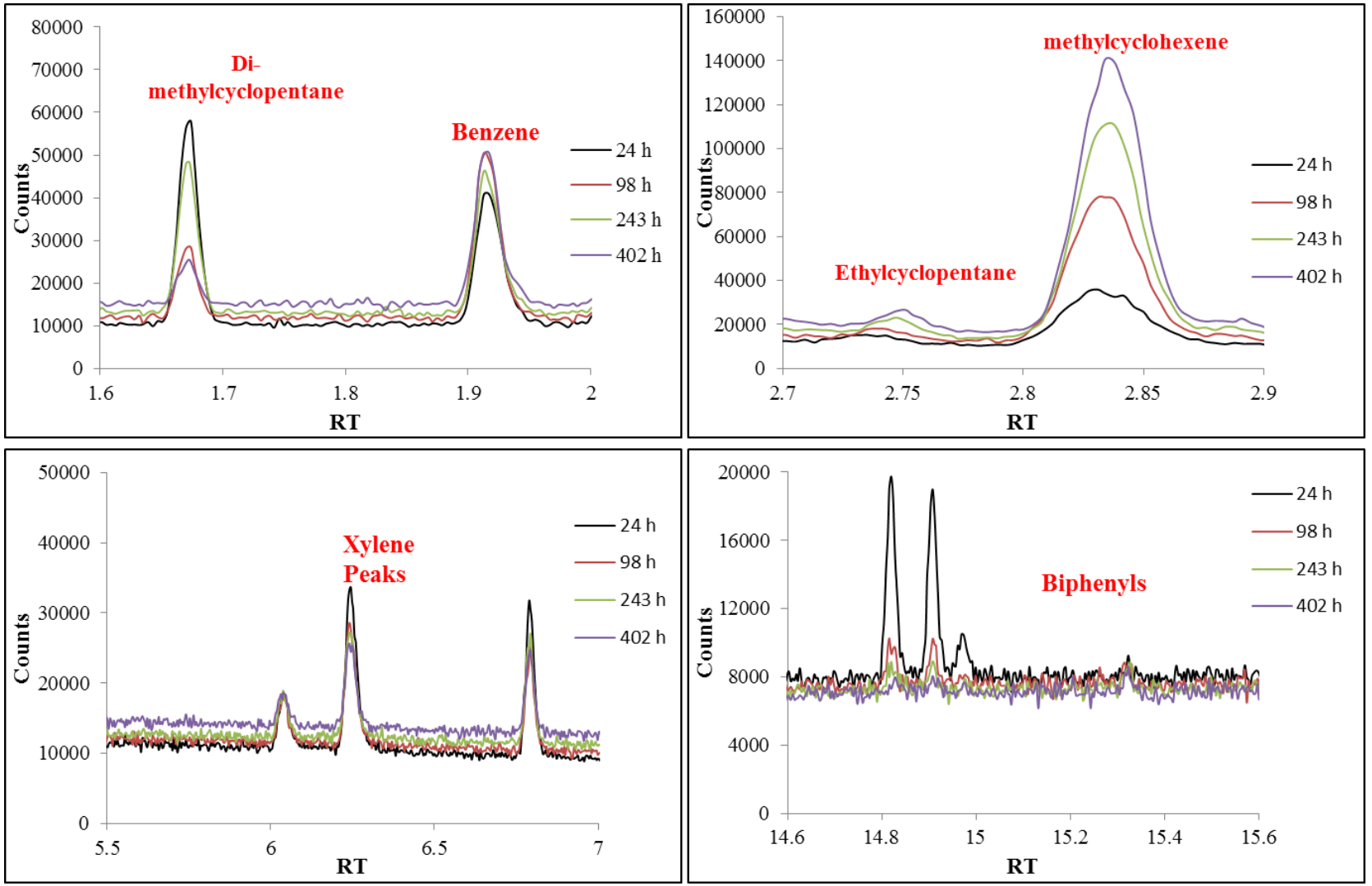

Figure 6.17 GC-MS chromatograms describing change in the by-products distribution with increasing TOS for the commercial pelleted catalyst at T = 400 °C, P = 1 bar and W/F = 14690 g s mol $^{-1}$.

6.3.2.4 *Effect of time-on-stream on by-product yield*

Following the qualitative comparison of the by-products yields, a quantitative comparison of the by-products was done to study the change in concentration of the different by-products as the catalyst deactivated over time. In addition this comparison enabled a better understanding on the difference in acidity of the pelleted catalysts and the difference in activity of the metallic functions between the three catalysts.

Effect of time-on-stream on Benzene and Xylene Yield

By plotting the benzene and xylene yield with time, there were clear indications of differences between the three catalysts. The structured catalysts gave a higher xylene yield initially but after a time period of 100 h, they described a similar yield as that of the in-house pelleted catalysts. Both the in-house prepared catalysts typically yielded around 200 ppm of xylene after 100 h which was approximately twice that of the commercial catalysts. Thus the difference yield of these by-products suggests a difference in the nature of the support alumina between the in-house prepared catalysts and commercial catalysts.

Benzene and xylene were initially formed in equal amounts suggesting that they were formed through toluene disproportionation which took place on the acidic function of the catalyst. With increasing time-on-stream, all three catalysts showed reduced yields of xylene suggesting with increasing time the acidic function of the catalyst was deactivating (*Figure 6.18)*. The results suggested that the in-house structured and pelleted catalysts had a higher acidity, when compared to the commercial pelleted catalyst.

Initially the benzene yield for both the in-house prepared catalysts were similar, however the benzene yield for the structured catalyst, after a time period of around 72 h, rapidly increased with time as illustrated in Figure 6.15 and Figure 6.19. The benzene yield for both the pelleted catalysts increased only slightly over time. A comparison of the changing benzene to xylene molar ratio with time (*Figure 6.20*) suggested that initially benzene was formed equally with xylene, however as the catalyst began to deactivate the xylene yield decreased, but the benzene yield did not. Therefore with increasing time on

stream benzene was increasingly formed through toluene demethylation reaction which is known to take place on the metallic function of the catalyst.

The molar ratio was significantly higher for the structured catalyst (ranging from 1 to 4.5) when compared to pelleted catalysts (ranging from 1 to 2). The increased toluene demethylation taking place on the structured catalyst possibly indicates a deactivation of acid sites however such a large difference could also be attributed to a difference in activity of the metallic function of the catalysts, where the dispersion and morphology of the platinum metal on the support play an important role. This has been discussed later on in this chapter.

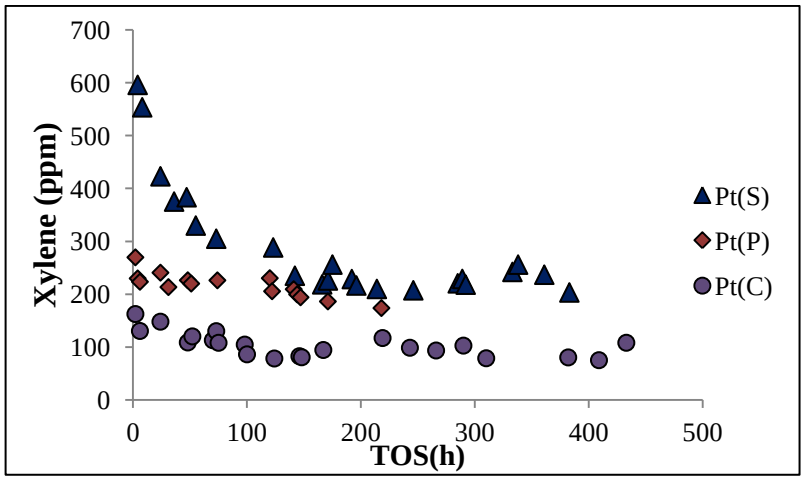

Figure 6.18 Change in Xylene concentration with TOS at T = 400 °C, P = 1 bar, W/F = 14690 g s mol^{-1}.

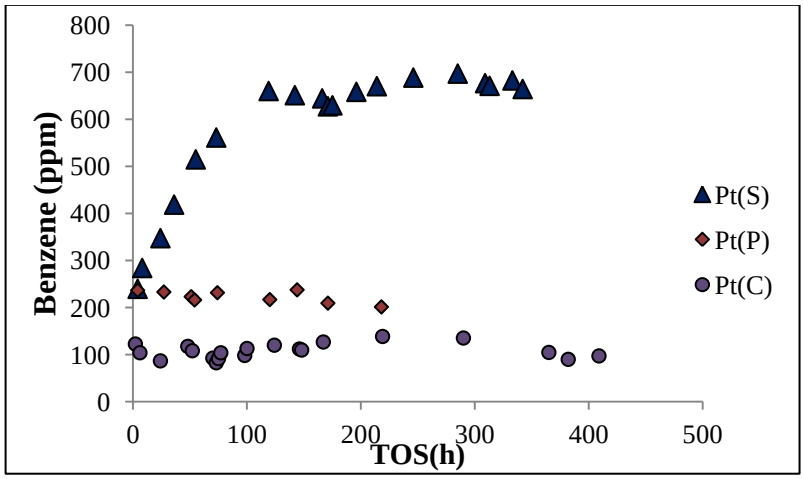

Figure 6.19 Change in Benzene concentration with TOS at T = 400 °C, P = 1 bar, W/F = 14690 g s mol^{-1}.

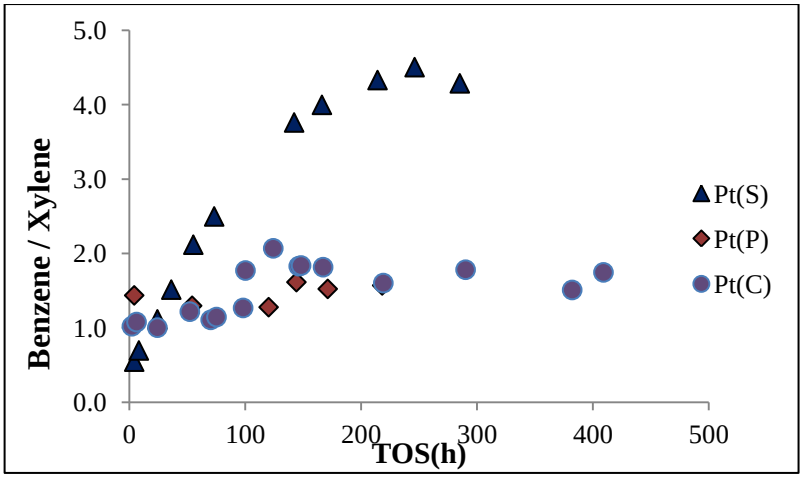

Figure 6.20 Change in Benzene/Xylene molar ratio with TOS at T = 400 °C, P = 1 bar, W/F = 14690 g s mol^{-1}.

Effect of time-on-stream on Substituted Cyclopentanes and Methylcyclohexene yield

With increasing TOS and as the catalyst deactivated there was an increase in the formation of reaction intermediates derived from methylcyclohexane. Figure 6.21 describes the change in paraffin concentration with TOS. As the structured catalyst deactivated there was a significant increase in the yield of paraffins. Thus suggesting that with the decreasing dehydrogenation activity of the catalyst there was an increase in methylcyclohexane concentration which builds up and undergoes a ring-opening reaction to yield n-heptane which further undergoes a ring closing reaction to produce substituted cyclopentanes. Hence the n-heptane yield is mirrored with a significant increase in substituted cyclopentanes yield with TOS as shown in Figure 6.22.

Only the structured catalyst showed a significant increase in formation of the methylcyclohexene (*Figure 6.23*), hence implying an increase in partial dehydrogenation of methylcyclohexane most likely due to, deactivation of the active metal sites caused by the formation of heavier higher boiling, by-products which eventually would yield carbonaceous overlayers. Given the increased isomerization ability of the structured catalyst, the increase in methylcyclohexene yield resulted in an increase in the formation of substituted cyclopentenes which further hydrogenated to give substituted cyclopentanes.

The paraffin yield for both the pelleted catalysts was significantly lower than the structured catalysts and remained fairly constant with time. With increasing TOS, there was an increase in concentration of methylcyclohexene for both the pelleted catalysts. One noticeable difference was that the concentration of substituted cyclopentanes was higher for the in-house prepared pelleted catalyst. Thus indicating, that the in-house prepared pelleted catalyst had an increased isomerization activity when compared to the commercial catalyst. This higher isomerization activity of the in-house prepared catalyst could be attributed to the increased acidity of the catalyst.

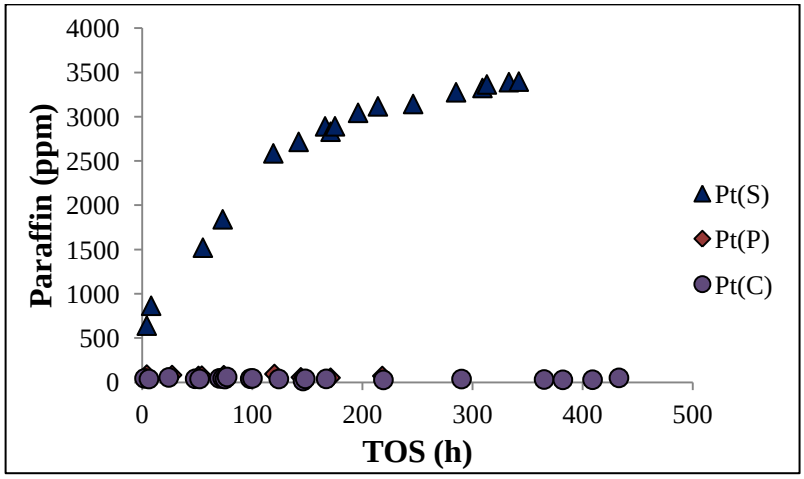

Figure 6.21 Change in yield of Paraffin with increasing TOS at T = 400 °C, P = 1 bar and W/F = 14690 g s mol^{-1}.

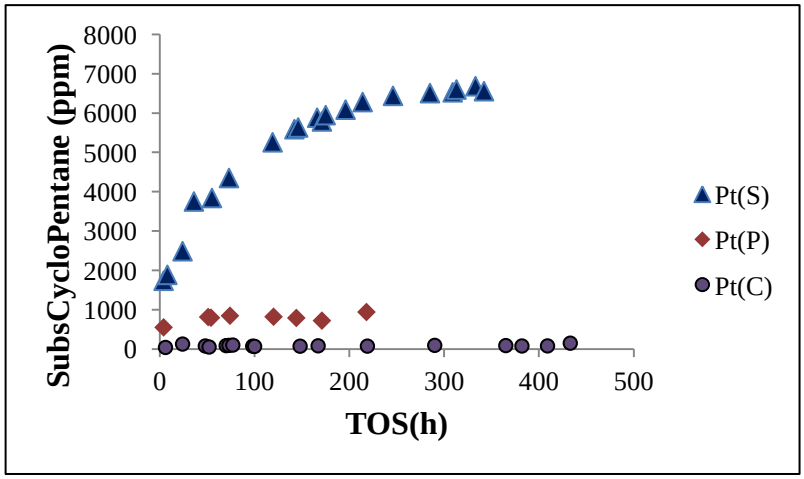

Figure 6.22 Increasing concentration of substituted cyclopentane as catalysts deactivated at T = 400 °C, P = 1 bar, W/F = 14690 g s mol^{-1}.

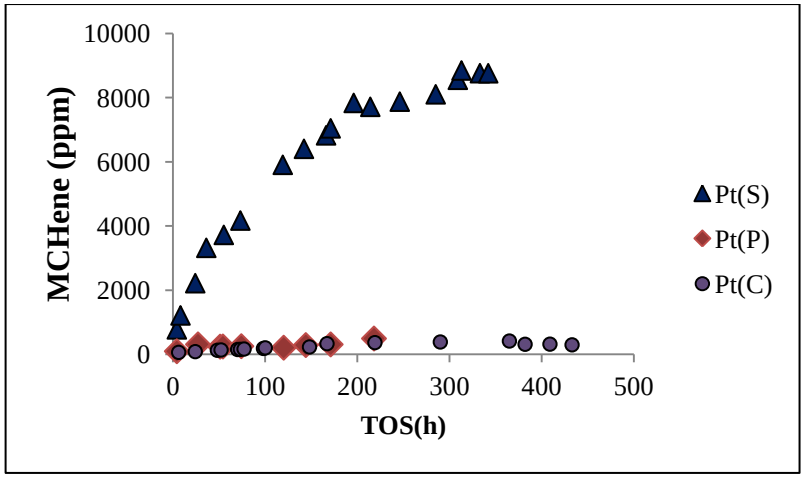

Figure 6.23 Increasing methylcyclohexene concentration as catalysts deactivated at T = 400 °C, P = 1 bar, W/F = 14690 g s mol^{-1}.

Effect of time-on-stream on Substituted Biphenyl Yield

With increasing TOS as the catalyst deactivated the conversion to toluene decreased which resulted in a decrease in toluene condensation reaction and subsequently a decrease in yield of biphenyls (*Figure 6.24*). Biphenyls are coke precursors and tend to form graphitic structures over the active metal sites over time thus causing catalyst deactivation. Very different yields of substituted biphenyls were observed with TOS. However both the pelleted catalysts, showed a similar rate of decline of the biphenyl yield. The initial steep phase of catalyst deactivation can be attributed to the formation of biphenyls. Both the in-house prepared catalysts initially gave a similar yield of biphenyls, however the yield for the structured catalyst rapidly declined over a time period of around 50 h suggesting rapid deactivation.

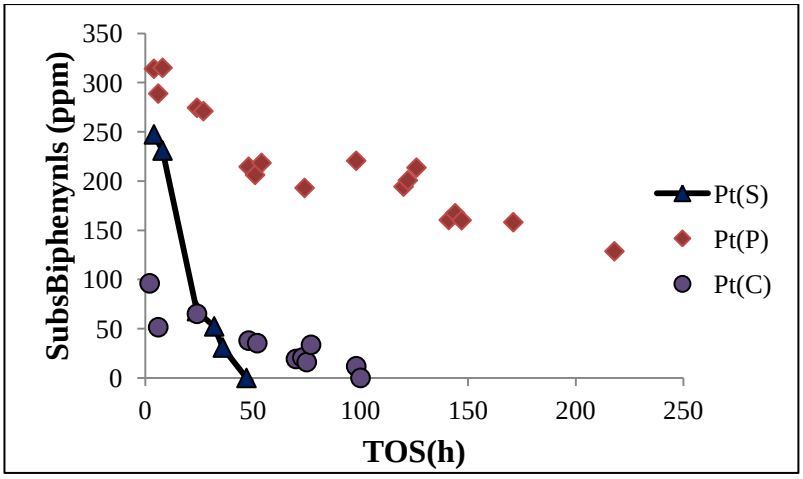

Figure 6.24 Decreasing concentration of substituted biphenyls as catalyst deactivated at T = 400 °C, P = 1 bar and W/F = 14690 g s mol^{-1}.

6.4 Catalyst effect on by-product yields

The previous sections have shown the effect of operating parameters on the by-product distribution which varies with the different catalysts. This variation suggests there are other variables that influence selectivity of reaction such as platinum morphology, effect of support acidity and effect of structured alloy support which have been detailed in the following section. Previous authors have suggested that the dehydrogenation mechanism did not vary if it was taking place on the single crystal platinum surface or if the platinum was dispersed on a high surface area support (Blakely and Somorjai, 1976, Herz et al., 1981, Sinfelt, 2000). However Baker et al in their research showed that the platinum particles when dispersed on a high surface area support such as γ - Al_2O_3, during increased temperature of reaction (T > 600 °C), tended to migrate towards each other to form larger crystallites which had an effect on the selectivity of the catalyst (Baker et al., 1979). Cussamano et in their work suggested that the metal support interaction for Al_2O_3 supports was not profound (Cusumano et al., 1966). Based on the findings in literature, the author has ruled out the effect of metal-support interaction on the by-product yields.

6.4.1 Effect of Platinum size

Desai and Richardson in their work showed that the rate of methylcyclohexane dehydrogenation increased with increase in platinum crystal size (Desai and Richardson.,1986). Rocherfort et al concurred with their work and indicated that dehydrogenation rate of methylcyclohexane at T = 300 °C, increased by a factor of 6 with increasing particle size from 1 to 3 nm (Rochefort et al., 1992). Rocherfort et al attributed this effect to the increase in chemisorbed hydrogen atoms which blocked the accessibility of the metal surface to the MCH molecules, as the crystallite size decreased. Arai et al in their work examined the effect of the platinum particle size on dehydrogenation of methylcyclohexane (Arai et al., 1980). They found the individual fine particles (< 1.5 nm) to be more selective to the formation of methylcyclopentanes. In addition Arai et al noticed a 'cluster' effect i.e. groups of platinum atoms coalescing to form a larger platinum crystallite (Arai et al., 1980). The formation of larger crystallites could lead to loss of active surface area available for dehydrogenation to take place and further sintering of the metal resulting in deactivation of the catalyst.

As described previously in Chapter four (*Figure 4.32*), the platinum dispersed on the alumina were in a range of sizes, there are large particles of size 5 - 8 nm, smaller particles in around 1.2 nm and some very fine particles with a size < 1.2 nm. Based on the platinum dispersion on the support, the deactivation of methylcyclohexane which was characterized by two phases could be correlated with the size of the platinum particle. The initial steep phase can be linked to the reaction taking place on fine particles and the more active sites which probably deactivate rapidly due to coking. With the passage of time, the fine particles tend to coalesce to form larger crystallites, as suggested by previous authors, thus reducing the active metal surface area of the catalyst and further reducing the activity of the catalyst. The second phase of the deactivation which is slower would therefore, probably take place on these larger crystallites. These larger particles slowly deactivate as the metal particles tend to sinter and the coke deposits potentially poison the catalyst.

6.4.2 Effect of platinum morphology

The surface of the platinum crystal is structurally heterogeneous with different types of active sites as described in chapter three. The platinum surface consists of flat or terrace, step and kink sites. The concentration of the different types of sites is dependent on the size of the platinum crystal especially in the size range of 1 - 4 nm (Herz et al., 1981). Based on the findings given in literature, the author has proposed a four site hypothesis which could describe the reaction mechanism taking place on the different sites of the platinum crystal.

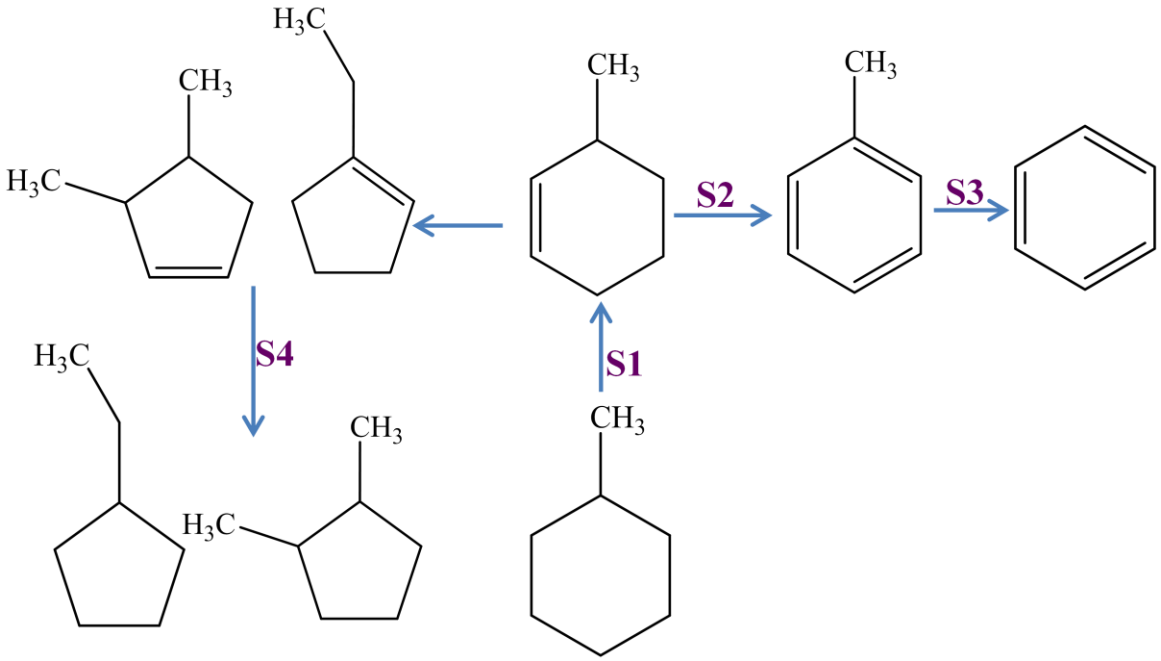

Figure 6.25 Dehydrogenation of MCH taking place on different sites of Pt.

The dehydrogenation of MCH takes place on three active sites of the platinum crystal which are S1, S2, S3 and S4 and have different deactivation rates. The reaction mechanism taking place on these sites has been illustrated in Figure 6.25. S1 is used to describe the sites on which the partial dehydrogenation of MCH takes place, Blakely and Somorjai found this to be a structure insensitive reaction (Blakely and Somorjai, 1976). S2 is the step site on which the fast dehydrogenation of methylcyclohexene to toluene takes place. S3 is the kink site on which hydrogenolysis of toluene occurs and S4 is the step site on which the hydrogenation of substituted cyclopentenes to substituted cyclopentanes takes place.

During the early stages of deactivation, S2 is highly active thus there is a good yield of toluene. This high activity also results in the formation of biphenyls which are coke precursors and can result in the formation of carbonaceous overlayers. Previous researchers have shown that the carbonaceous overlayers that are formed initially are ordered (active carbon monolayer) but, they tend to become more disordered (graphitic carbon layer) with the time (Blakely and Somorjai, 1976, Herz et al., 1981). In this work; if the carbonaceous overlayers were formed then it did not appear to disrupt the formation of toluene, however as the catalyst deactivated the toluene formation decreased which supports the concept of the formation of a disordered overlayer which poisoned the S2 step site. This deactivation of the S2 site resulted in an increased formation of the reaction intermediates (methylcyclohexene and methylcyclohexadiene) on the S1 site. The increase in methylcyclohexene was noticed on the GC-MS chromatograms, however the formation of methylcyclohexadiene was not found due to its strong adsorption on the catalyst surfaces (Land et al., 1989). As methylcyclohexene accumulated it isomerized to form substituted cyclopentenes which subsequently hydrogenated on the S4 site to form substituted cyclopentanes which then hydrogenated to form substituted cyclopentanes. The proposed mechanism is in agreement with the work done by Sinfelt who suggested in his research that in the presence of cyclohexene, cyclopentene will form due to equilibrium consideration. Toluene undergoes hydrogenolysis on the kink sites S3, to form benzene (Sinfelt, 1964). The formation of carbonaceous overlayers did not appear to disrupt the formation of benzene thus suggesting the hydrogenolysis taking place on the S3 site was insensitive to the ordering of the carbonaceous overlayer.

The different catalysts tested described a varied yield in the by-product formation which could be attributed to the difference in platinum dispersion and the mixed concentration of the different sites on the platinum particle. The structured catalyst appeared to have an increased presence of kink sites and step sites. The pelleted catalyst was more selective to the formation of toluene suggesting an increased presence of step sites.

6.4.3 Effect of support acidity

The acidity of the catalyst is factor that could affect the reaction selectivity. Platinum supported on γ - Al_2O_3 is a bifunctional catalyst that has a metallic and acidic function. The acidity of the γ - Al_2O_3 in platinum supported catalysts is usually dependent on the chlorine concentration (Sinfelt, 2000). Okada et. al, in their work suggested that the support acidity had no role in the dehydrogenation activity and that the reaction is mainly dependent on the metallic function (Okada et al., 2006). Sinfelt suggested that an increase in acidity of the support resulted in a decrease of reaction selectivity by the promotion of other reforming reactions (Sinfelt, 2000). Contradicting the work of Sinfelt and Okada et al, Ali and his co-workers in their research showed that by using the right amount of support acidity, the dehydrogenation reaction was enhanced (Ali et al., 1999).

In this research, the in-house prepared structured and pelleted catalyst appeared to have a higher acidity than the commercial catalyst. The preparation of the structured catalyst required the loading of an alumina washcoat consisting of boehmite powder (DISPERAL) dispersed in an alumina slurry (PURALOX and aq.HNO_3) as detailed in chapter four. The alumina used to prepare the support (according to manufacturer's specifications) consisted primarily of Lewis sites. In addition, the calcination step involved during the catalyst preparation could result in a further increase in the presence of Lewis sites. Liang and Weng in their work showed that the toluene disproportionation reaction took place on the Lewis sites of the catalyst (Liang and Weng, 1993). Thus the increased formation of xylene on the structured catalyst when compared to the pelleted catalysts suggests a difference in concentration of Lewis sites between the three catalysts. Previous work by Tanabe has suggested that the difference in concentration of Lewis sites greatly affects the selectivity and activity of the catalyst (Tanabe, 1970). This increased acidity of the catalytic washcoat on the structured catalyst could be attributed to the increase in by-product formation and increased coke formation. In addition, the Cl^{-1} ions which are added on during impregnation of the active phase, could also contribute to the acidity of the catalyst. The coke that is formed tends to form graphitic structures on the different sites of the catalyst resulting in catalyst deactivation.

The in-house prepared pelleted catalyst appeared to have a higher acidity when compared to the commercial pelleted catalyst. The difference in acidity between the two catalysts could be attributed to the acidity contribution by Cl^- ions during impregnation of the active phase which could have increased the acidity of the γ - Al_2O_3 support.

Thus the preparation of the in-house catalysts would require to be optimised in order to adjust the acidity of the support which would further reduce the by-product yield and coke formation and prevent the catalysts from deactivating. In addition characterization of the acid sites by pyridine adsorption would help give a better understanding on the concentration of the acid sites present in the alumina of three catalysts tested an hence improved knowledge on their respective effect on the selectivity in the dehydrogenation reaction.

6.4.4 Effect of structured alloy support

Yu et al, Enchave et al, Smorgyo et al, Martinez et al and Sirijaruphan et al have compared the activity of Fecralloy supported catalysts with that of powdered catalysts (Martínez T et al., 2010, Sirijaruphan et al., 2005, Smorygo et al., 2009, Yu et al., 2007). The alloy supports post thermal oxidation treatment were coated with an alumina washcoat and further impregnated with Platinum. Enchave et al and Yu et al in their work indicated the Pt/Al_2O_3 supported on Fecralloy foams, when tested for methanol steam reforming depicted a lower activity when compared to the powdered Pt/Al_2O_3 catalysts. The researchers attributed the lower activity to the diffusion of Fe and Cr to the surface resulting in the formation of inter-metallic alloys between Pt-Fe and Pt-Cr. However Sirijaruphan et al suggested the contrary and that the underlying alloy did not influence the reaction. Enchave et al suggested a hypothesis that the underlying alloy substrate could directly participate in the reaction, and to check this, Enchave et al tested the thermally treated Fecralloy foams without any catalytic material on it. The un-coated catalytic material showed neglible activity thus ruling out the hypothesis.

The author, tested the Fecralloy rods for dehydrogenation of MCH without any catalytic material on it, the activity of the catalyst was negligible (<1%). Thus confirming the underlying alloy had no influence on the reaction. The washcoat layer that was applied onto the Fecralloy rods was very thin and during catalytic testing there could be a possibility that

parts of the coating were non-adherent. The Fecralloy rods (without any catalytic material on) showed negligible activity for dehydrogenation of MCH suggesting the underlying alloy oxides (Fe_3O_4 and Cr_2O_3) were not active for dehydrogenation of MCH. However there is likelihood, of the underlying alloy oxides (Cr_2O_3 and Fe_3O_4) interfering and taking part in the side reactions thus resulting in an increased by-product yield. Cr_2O_3 oxides are active in cyclization reactions and Fe_3O_4 oxides have low dehydrogenation activity and which could possibly cause partial dehydrogenation of MCH. In addition the underlying Fe, in the presence of excess lewis acid sites could act as promoter for coke formation thus resulting in deactivation of the acid sites (Tanabe, 1970).

7 Reaction Kinetics and Catalyst Deactivation

7.1 Introduction

The previous chapters have detailed the preparation of a structured catalyst and its activity and selectivity towards the dehydrogenation of methylcyclohexane. The developed catalyst was subjected to long term deactivation tests and the activity and selectivity of the catalyst was compared with conventional pelleted Pt/Al_2O_3 catalyst. All the catalysts were packed in a fixed reactor bed and tested under a range of operating conditions as detailed in Chapter five.

This chapter details the temperature profiles obtained during the catalytic testing process in addition to the kinetic parameters that are calculated from the experimental data. An assessment of the rate of the dehydrogenation of MCH over the Pt/Al_2O_3/Fecralloy has been done. Further, the author has studied the catalyst deactivation mechanism and attempted to obtain an empirical curve-fit to reaction data.

7.2 Kinetic Parameters

To study the kinetics of MCH dehydrogenation two types of kinetics parameters are required independent variables and dependent variables. The mean bed temperature (T_m), catalyst to feed ratio (W/F) and reactant/product partial pressure (p) constitute the independent variables. The dependent variables include, the reaction conversion (X), the equilibrium conversion (X_e), reaction rate ($-r$) and the activation energy (E_{act}). The different parameters have been estimated in the following sections

7.2.1 Independent Variables

This section details the calculations of the independent variables (T_m, *W/F*, *p*). The ratio *W/F* is the ratio of the weight of the catalyst to the molar flow rate of the MCH feed. The weight of the catalyst that was used for all the experiments was 0.1 g. The unit for *W/F* was g s mol^{-1}. The structured catalyst was tested at three different flowrates. The values for the different flowrates and their corresponding *W/F* values have been listed in Table 7.1.

MCH molar flowrate - F_{MCH} (mol h^{-1})	**W/F (g s mol^{-1})**
0.023	14690
0.035	9790
0.047	7345

Table 7.1 Molar flowrates (mol h^{-1}) and the corresponding W/F (g s mol^{-1}) values.

A detailed inspection of the independent variables T_m and *p* has been done in the following sections.

7.2.1.1 Mean bed temperature (T_m)

The mean bed temperature (T_m) was determined for each run by averaging the longitudinal reading of the catalytic zone (5 cm) with the reactor's wall temperature, which is approximated by averaging the temperature of the zone in the absence of a reaction. The calculation of the mean bed temperature is shown in Equation 7.1

$$T_m = \frac{T_{ave} + T_w}{2} \tag{7.1}$$

where T_{ave} is the average temperature of the catalytic zone, T_w is the wall temperature (in the absence of reaction) and T_m is the mean bed temperature. This has been schematically shown in Figure 7.1. The mean bed temperature (T_m), the wall temperature (T_w) and the reaction temperature (T_r) along the bed during dehydrogenation of MCH have been graphically described in Figure 7.2 and Figure 7.3.

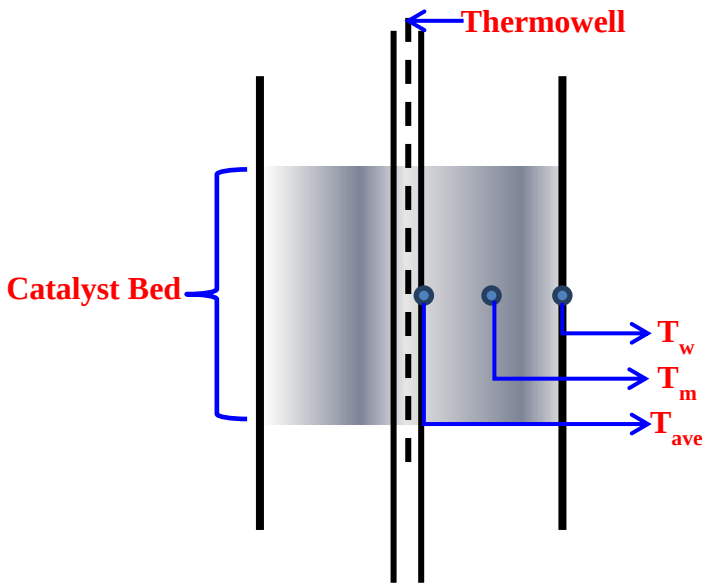

Figure 7.1 Schematic illustration of mean bed temperature (T_m).

The endothermic nature of the reaction is clearly evident from the profile (*Figure 7.2* and *Figure 7.3*); in addition the improved heat transfer characteristics of the Fecralloy can also be seen. The dehydrogenation of MCH over the pelleted catalysts results in a temperature drop of ~ 50 °C, whilst the reaction on the structured catalyst the temperature drop is ~ 15 °C. This difference in temperature profile could play a part in the difference in selectivity profiles between the structured catalysts and both the pelleted catalysts.

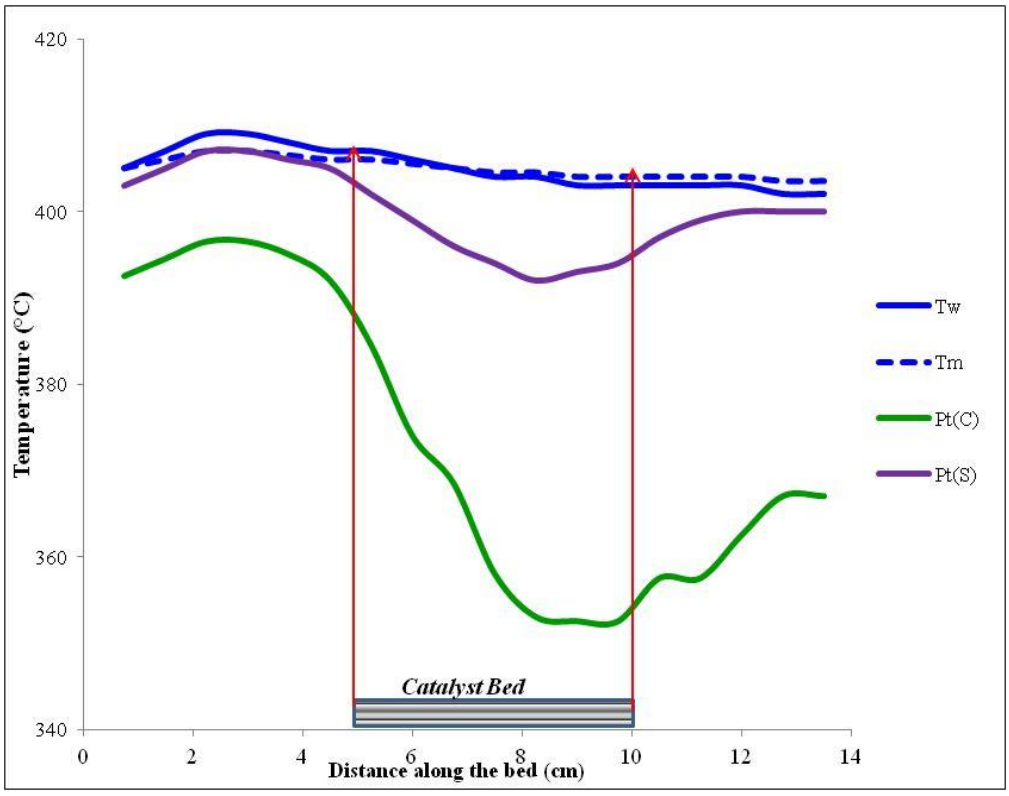

Figure 7.2 Comparison of reaction temperature (T_r) profile of structured catalyst and pelleted catalyst T_w = 400 °C, W/F = 14690 g s mol^{-1}, H_2/MCH = 9.

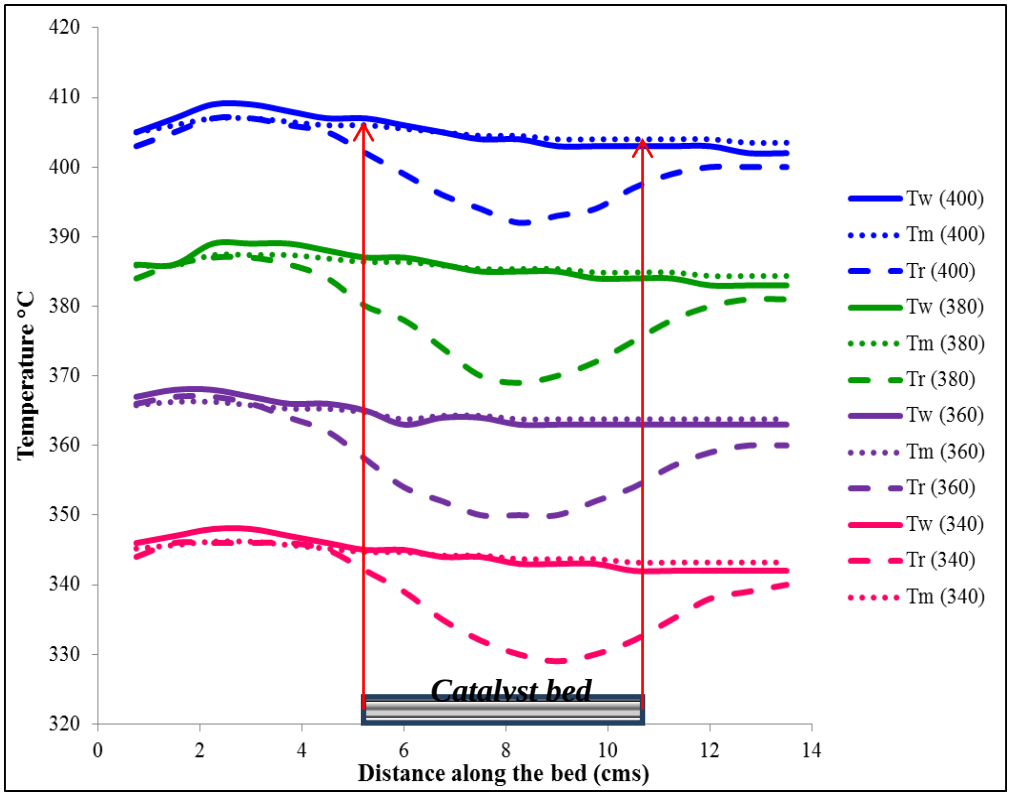

Figure 7.3 Reaction temperature (T_r) profile and mean bed temperature for Pt/Al_2O_3/Fecralloy catalyst at T_w = 340 °C - 400 °C, W/F = 14690g s mol^{-1}, H_2/MCH = 9.

7.2.1.2 Partial pressure of reactant/products (p)

The calculation of partial pressure required the molar flowrates (mol h^{-1}) of the feed going into the reactor. For the given set of data, there are two feeds MCH (F_{MCH}) and H_2 (F_{H2}). The total flowrate (F_T) is the summation of the molar flow rates of both the reactants as shown in Equation 7.2. The molar flowrates used for the dehydrogenation experiments are listed in Table 7.2.

$$F_T = F_{MCH} + F_{H2} \tag{7.2}$$

F_{MCH} (mol h^{-1})	F_{H2} (mol h^{-1})	F_T (mol h^{-1})
0.023	0.211	0.234
0.035	0.3176	0.3526
0.047	0.423	0.47
0.023	0.023527	0.046527
0.023	0	0.023

Table 7.2 Molar flowrates of MCH and H_2 used for experiments.

The initial partial pressure of each of the reactants, H_2 (p_{H2i}) and MCH (p_{MCHi}) is determined from Equations 7.3 and 7.4 respectively, where y_{MCHi} is the initial mole fraction of MCH and y_{H2i} is the initial mole fraction of H_2. P_T is the total pressure of the system in bar. For the dehydrogenation system used in this research the total pressure of the system is 1 bar. Therefore, the initial partial pressure of the system can be given by Equations 7.5 and 7.6, and the initial mole fraction of each reactant is obtained from Equations 7.7 and 7.8. The range of initial partial pressures has been tabulated in Table 7.3.

$$p_{H2i} = y_{H2i} \cdot P_T \tag{7.3}$$

$$p_{MCHi} = y_{MCHi} \cdot P_T \tag{7.4}$$

$$p_{H2i} = y_{H2i} \tag{7.5}$$

$$p_{MCHi} = y_{MCHi} \tag{7.6}$$

$$y_{H2i} = \frac{F_{H2i}}{F_T} \tag{7.7}$$

$$y_{MCHi} = \frac{F_{MCHi}}{F_T} \tag{7.8}$$

y_{MCHi}	p_{MCHi} (bar)	y_{H2i}	p_{H2i} (bar)
0.1	0.1	0.9	0.9
0.1	0.1	0.9	0.9
0.1	0.1	0.9	0.9
0.5	0.5	0.5	0.5
1	1	0	0

Table 7.3 Initial mole fractions and partial pressure of the reactants MCH and H_2.

The final partial pressures of the products are determined by Equations 7.9, 7.10 and 7.11, where y_{H2f}, $y_{MCHf,}$ *and* y_{TOLf} are the final mole fractions of the products H_2, MCH and TOL (toluene) respectively. The final mole fractions of H_2, MCH and TOL are given by Equations 7.12, 7.13 and 7.14 respectively. The parameters ε and θ are given by Equations 7.15 and 7.16 respectively. The experimental results obtained when the catalyst was tested at a temperature of 400 °C have been shown in Table 7.4.

$$p_{H2f} = y_{H2f} \tag{7.9}$$

$$p_{MCHf} = y_{MCHf} \tag{7.10}$$

$$p_{TOLf} = y_{TOLf} \tag{7.11}$$

$$y_{H2f} = \frac{y_{MCHi} \cdot (\theta + 3X)}{(1 + \varepsilon X)} \tag{7.12}$$

$$y_{MCHf} = \frac{y_{MCHi} \cdot (1 - X)}{(1 + \varepsilon X)} \tag{7.13}$$

$$y_{TOLf} = \frac{y_{MCHi} \cdot X}{(1 + \varepsilon X)} \tag{7.14}$$

$$\varepsilon = 3 \cdot y_{MCHi} \tag{7.15}$$

$$\theta = \frac{y_{H2i}}{y_{MCHi}} \tag{7.16}$$

y_{MCHf}	p_{MCHf} (bar)	y_{H2f}	p_{H2f} (bar)	y_{TOLf}	p_{TOLf} (bar)
0.003	0.003	0.923	0.923	0.074	0.074
0.014	0.014	0.920	0.920	0.066	0.066
0.017	0.017	0.919	0.919	0.063	0.063
0.057	0.057	0.767	0.767	0.176	0.176
0.077	0.077	0.692	0.692	0.231	0.231

Table 7.4 Final partial pressures and mole fractions of the products MCH, H_2 and TOL at T = 400 °C.

7.2.2 Dependent Variables

This sections focuses on the estimation of the dependent variables, conversion (X), equilibrium conversion (X_e), Activation Energy (E_{act}) and reaction rate ($-r$). The calculation of each of the variables has been briefly discussed.

7.2.2.1 Reaction Conversion (X)

The reaction conversion for every experimental run was obtained for a given W/F, mean bed reactant temperature and mole fractions of MCH and H_2 in the feed. The MCH feed that was used for all the experiments had a purity of 99.98%. Hence an accurate estimation of the reaction conversion could be done, by subtracting the % of MCH remaining in the final product stream from 100 %. Therefore, reaction conversion (X) can be given by Equation 7.17.

$$X = 100\ \% - \%\ MCH\ remaining\ in\ the\ product \tag{7.17}$$

The reaction conversion for all the experiments was obtained by gas chromatography analysis, all of which have been discussed in Chapter six.

7.2.2.2 Equilibrium Comversion (X_e)

For the given values of T_m and initial mole fractions of H_2 and MCH the equilibrium conversion (X_e) for a reaction can be calculated from (K_e) which is defined as:

$$K_e = \frac{(p_{TOLf} \cdot p_{H2}{}^3)}{p_{MCHf}} \tag{7.18}$$

Substituting Equations 7.9 - 7.14 in Equation 7.18 resulted in Equation 7.19. Equation 7.19 is solved iteratively to obtain the equilibrium conversion X_e. The value K_e is obtained from Equation 7.20 which is obtained from the correlation developed by Schildhauer et al (Schildhauer et al., 2001). The unit for K_e is bar^3.

$$\frac{X_e \cdot y_{MCHi}{}^3 \cdot (\theta + 3X_e)^3}{(1-X_e)\cdot(1+\varepsilon X_e)^3} \cdot P_T{}^3 - K_e = 0 \tag{7.19}$$

$$K_e = 3600\, exp\left[\left(\frac{217650}{8.314}\right)\cdot\left(\frac{1}{T(k)} - \frac{1}{650}\right)\right] \tag{7.20}$$

The equilibrium conversion was solved iteratively using Equation 7.19. The resulting values obtained at different operating temperatures have been shown in Table 7.5.

T(K)	K_e (bar^3)	X_e
613.15	319.96	0.9975
633.15	1232.56	0.9994
653.15	4371.78	0.9998
673.15	14382.50	0.9999

Table 7.5 Equilibrium Conversion for dehydrogenation of MCH at T = 340 °C - 400 °C.

To obtain the reaction rate at a given conversion we need to understand how the observed conversion reaches the equilibrium conversion. The graphical plotting of the MCH conversion versus space time over a narrow interval of T_m (380 °C - 400 °C) shows an exponential approach to the equilibrium conversion for all sets of experiments as illustrated in Figure 7.4. Using TableCurve 2D the best kinetic fit was obtained (Equation 8100 in

TableCurve 2D software). The kinetic expression obtained to describe the reaction is shown in Equation 7.21. In Equation 7.21, *k* is the apparent rate constant.

$$X_{obs} = X_e \left(1 - exp\left(-k\left(\frac{W}{F}\right)\right)\right) \quad (7.21)$$

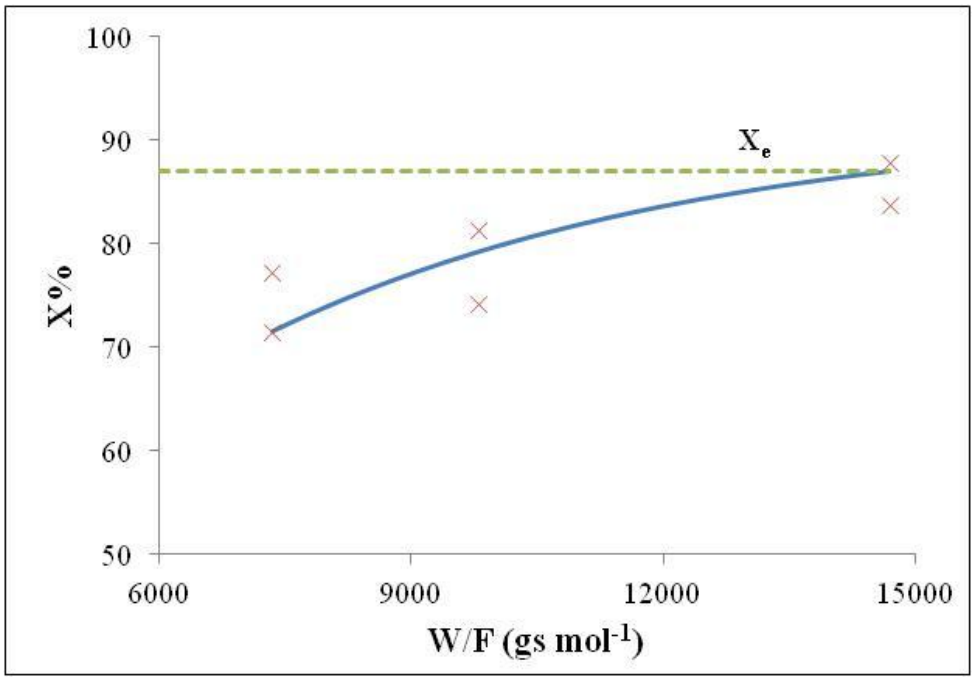

Figure 7.4 Observed conversion shows an exponential approach to equilibrium value.

7.2.2.3 Activation Energy (E_{act})

The reaction rate constant for the reaction taking place at the different operating temperatures, was obtained by plotting a graph of (Volume of the bed /total volumetric feed) versus Ln ($1-X/X_e$) for each temperature. The reaction rate constant was the slope of the graph and the calculated value was found to be 0.072 s^{-1}. The structured catalyst was tested at atmospheric pressure therefore it was assumed the reaction followed pseudo first order kinetics. Due to the endothermic nature of the reaction there was a temperature drop in the middle of the catalyst bed. The T_m and T_r values that were obtained along the reactor bed were fitted into a polynomial equation (TableCurve2D software Equation 7907).

From the parameters obtained it was possible to predict the conversion profile which changed with temperature across the reactor bed. A pseudo first order model was used to

predict the conversion across the reaction bed and the predicted conversion was fitted to the observed conversion as illustrated in Figure 7.5. At a reaction temperature of 340 °C and 400 °C the model showed deviation in values suggesting further parameterisation of values needed to be done. From the derived kinetic model, it was possible to obtain the activation energy for the developed structured catalyst which was found to be 52 kJ mol^{-1}.

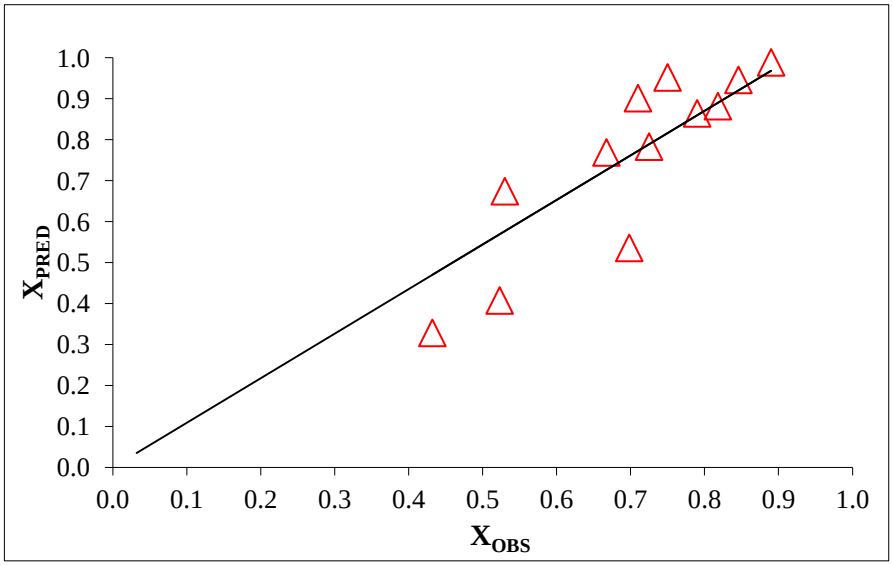

Figure 7.5 Pseudo first order kinetic model describing conversion across the bed for the structured catalyst.

This is very close to 51.9 kJ mol^{-1} value reported by Jothimurugesan et al when they investigated the methylcyclohexane dehydrogenation over 0.3 %Pt - 0.3 %Re/Al_2O_3, and in close vicinity of 58.6 kJ mol^{-1} value reported by Pacheco and Petersen for a similar 0.3 %Pt - 0.3 %Re/Al_2O_3 catalyst (Jothimurugesan et al.,1985,Pacheco and Petersen, 1984a).

7.2.2.4 Reaction rate (- r)

Differentiating the Equation 7.21, with respect to *W/F* it is possible to obtain the rate of reaction (- *r*) at the observed conversion which is given by Equation 7.22.

$$-r = k \cdot X_e \cdot exp(-k\left(\frac{W}{F}\right)) \qquad (7.22)$$

Re-arranging Equation 7.21 and substituting in Equation 7.22 gives,

$$- r = k \cdot Xe \cdot (1 - \frac{Xobs}{Xe}) \quad (7.23)$$

Using Equation 7.23 it was possible to estimate the rate of reaction for the dehydrogenation of MCH over the developed structured catalyst where $-r$ describes the rate of disappearance of MCH. Equation 7.23 shows that the maximum rate of reaction is when $X_{obs} = 0$. When $X_{obs} = X_e$ the reaction becomes zero i.e. equilibrium has been attained.

7.3 Catalyst Deactivation

To determine the long term performance of the Pt/Al_2O_3/Fecralloy catalyst life tests were carried out to test the activity of the catalyst over a period of 400 h. In this section it is attempted to do an empirical fit to the deactivation data (X vs TOS) using Table Curve 2D software. This approach helped determine the population of the active sites and the decay constants.

7.3.1 Empirical curve fit to reaction data

The deactivation data for the structured catalyst was plotted and the best empirical curve fit was achieved by using two exponential decay functions as described in Equation 7.24. In the equation X describes the observed conversion, t is the time on stream and a,b,c,d are the empirical correlation parameters.

$$X = f_1(t) + f_2(t) \quad (7.24)$$

$$f_1(t) = a \cdot exp(-b\,t) \quad (7.25)$$

$$f_2(t) = c \cdot exp(-d\,t) \quad (7.26)$$

The first term of the Equation 7.24 represents the initial fast phase of deactivation whilst the second term describes the slow steady second phase of deactivation. Both deactivation phases are described by the general equation $f(t) = i \cdot exp(-j\,t)$, where i represents the population of active sites with a decay constant of j. Therefore, in our study the empirical correlation parameters may signify:

a the population of highly active sites

b the decay constant of those highly active sites, h^{-1}

c the population of less active sites

d the decay of those less active sites, h^{-1}

Based on the two-phase exponential decay an empirical curve fit to the experimental deactivation data for the structured and commercial catalyst was done which is illustrated in Figure 7.6 and Figure 7.7 respectively. The empirical correlation parameters are listed in Table 7.6.

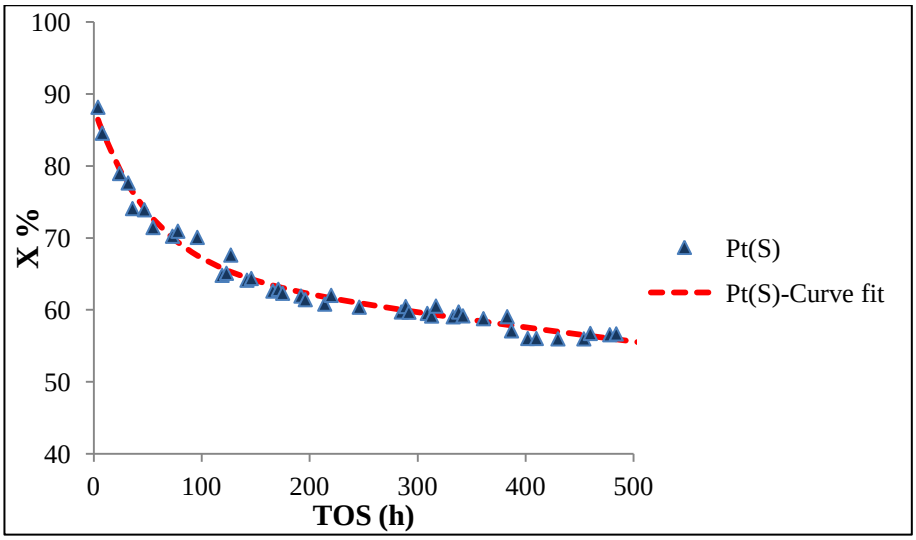

Figure 7.6 Empirical curve fit to deactivation data for structured catalyst at : T = 400 °C, P = 1 bar and W/F = 14690 g s mol^{-1}.

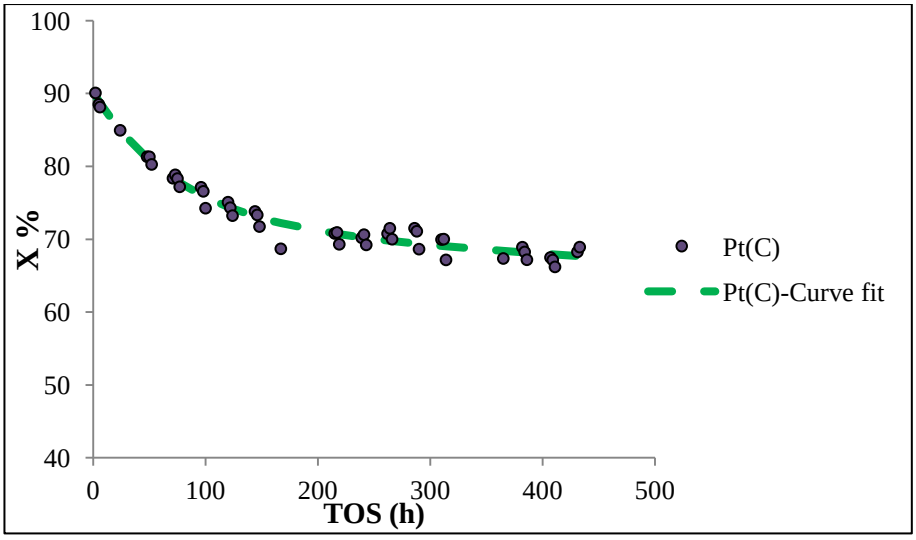

Figure 7.7 Empirical curve fit to deactivation data for commercial catalyst at : T = 400 °C, P = 1 bar and W/F = 14690 g s mol^{-1}.

Catalyst	Symbol	a	b	c	d	b/d
1 wt % Pt/Al_2O_3/Fecralloy	Pt(S)	22	0.019	66.17	0.000349	54
1 wt% Pt/Al_2O_3	Pt(C)	18.4	0.013	71.73	0.000137	95

Table 7.6 Results of fitting the deactivation curves by the sum of two independent exponential functions for structured and commercial catalyst.

The results for the empirical results detail the population of the different types of sites in the structured and commercial catalysts (*Table 7.6*). For the structured catalyst, the population of the highly active sites is around 25% of the total active sites, while the slowly deactivated site population is approximately 75 % of the total sites. The ratio of (b/d) for the structured catalyst suggests that the rapidly deactivating sites deactivate 54 times faster than the lesser active sites. For the commercial catalyst, the rapidly deactivating sites represent 20 % of the total population of sites whilst the slow deactivating sites are 80% of the total active sites. The ratio of (b/d) for the commercial catalyst suggests that the highly active sites deactivate 95 times faster than the lesser active sites.

These results suggest that for the commercial catalyst (*Figure 7.7*), the initial steep deactivation curve is caused by the rapid deactivation of the highly active metal sites, which further results in substantial loss of activity in the second phase of deactivation. However for the structured catalyst (*Figure 7.6*), the results from the empirical analysis suggests, that

highly active sites deactivate at a slower rate when compared to the commercial catalyst. This result therefore suggests that the initial phase of deactivation, taking place for the structured catalyst, could possibly be attributed to the deactivation of the metal sites and additionally to the deactivation of the acid sites of the catalyst as well.

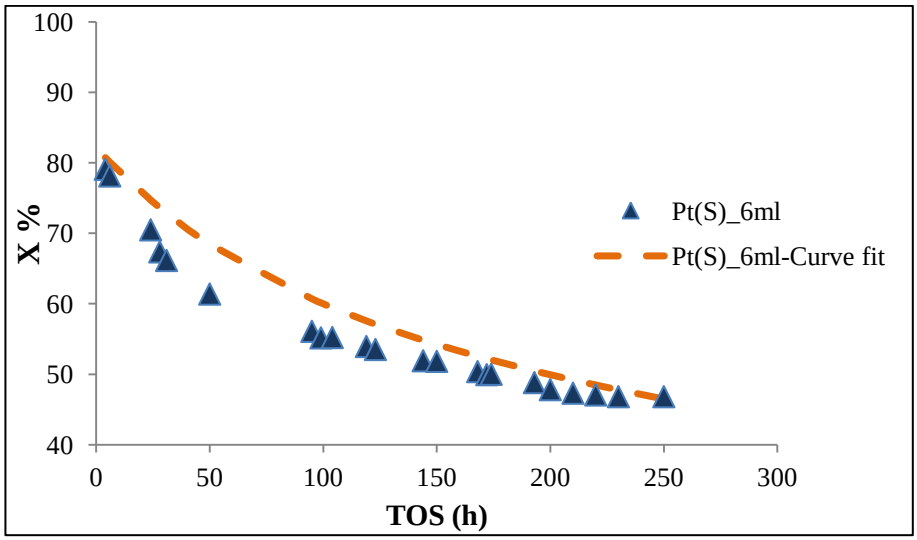

Figure 7.8 Empirical curve fit to deactivation data for structured catalyst at : T = 400 °C, P = 1 bar and W/F = 9790 g s mol^{-1}.

W/F (g s mol^{-1})	Symbol	a	b	c	d	b/d
14690	Pt(S)	22	0.019	66.17	0.000349	54
9790	Pt(S)_6ml	21.08	0.013	61.04	0.000662	21

Table 7.7 Comparison of Empirical parameters of structured catalysts at W/F = 14690 g s mol^{-1} and W/F = 9790 g s mol^{-1} at T = 400 °C and P= 1 bar.

A comparison of the deactivation profiles of the structured catalyst tested at two different reactor space times (*Figure 7.8* and *Figure 7.6*) suggest that at slower reactor space time the catalyst deactivates faster. An empirical analysis of the deactivation profile (at *W/F* = 9790 g s mol^{-1}), as described in Table 7.7, further indicates that the highly active sites deactivate 21 times fast than the lesser active sites. In addition the analysis describes a similar distribution of the highly active sites and lesser actives for the structured catalyst when tested at different reactor space times. Thus confirming validity of the model.

8 Research Summary, Conclusions and Future Work

8.1 Overview

In this chapter, the conclusions drawn from the experiments conducted during this research project have been summarised. As stated earlier, the aim of this project was to investigate the dehydrogenation reaction of methylcyclohexane over a structured catalyst, in order to improve reaction kinetics. This research had two primary objectives. The first one was to develop a suitable structured catalyst with an adherent washcoat. The second objective was to carry out a thorough catalyst evaluation study i.e the activity, selectivity and stability of the developed catalyst and compare the results with conventional pelleted catalysts. The catalysts used in study are detailed in Table 8.1.

Catalyst	Supplier
1 wt% Pt/Al_2O_3/Fecralloy	In-house
1 wt% Pt/Al_2O_3	In-house (pelleted)
1 wt% Pt/Al_2O_3	Commercial

Table 8.1 Catalysts tested in the research project.

8.2 Research Conclusions

This section details the main research outcomes. First, the main results from the catalyst preparation are detailed. Following this, the conclusions with regard to the catalytic performance are addressed for the various catalysts. The catalytic performance is evaluated based on three parameters: initial catalytic activity, long-term selectivity and the long term stability.

8.2.1 Preparation of Structured Catalyst

The primary objective of this research was to develop a suitable structured catalyst that would help overcome the thermodynamic limitations of the MCH dehydrogenation reaction. The structured catalyst consisted of three parts an alloy support, a catalytic washcoat and an active phase which was impregnated onto the alloy support. Each step of preparation involved detailed study of work by previous authors followed by optimisation study. The prepared catalyst was characterized by a range of analytical systems such as ESEM, EDX , XRD and STEM. The following are the main conclusions obtained from the preparation and characterization of the catalyst:

- The alloy support used as the support was Fecralloy supplied by Goodfellow. The geometry of the support was in the form of rods with d = 0.5mm. The alloy constituted Fe (77.8%), Cr (22 %), Al (5%), Y(0.1 %) and Si (0.1%). Prior to any preparation the alloy was pre-treated using sandpaper and then chemically cleaned.

- An oxidation study, with varying operating parameters of time and temperature was then carried out on the Fecralloy rods in a TGA which was utilized as a small scale oven. The study was carried out at T = 800 °C - 1200 °C and t = 0.5 h - 16 h. ESEM analysis of the surface morphology of the rods after oxidation at T > 1000 °C for time periods of 16 h resulted in spallation of the oxide layer. In addition, XRD and EDX line scan analysis confirmed a phase transformation to a lower surface area α - Al_2O_3. At T < 900 °C, SEM analysis revealed a surface morphology which appeared to be smooth. SEM, XRD and EDAX line scan analysis data suggested the temperature of oxidation was between 900 °C - 1000 °C.

  Oxidation at 1000 °C for time periods less than 4 h resulted in a morphology which described transient aluminas; however the growth did not appear to be dense. A study of the diffusion data, suggested the forward diffusion of Al to the surface had been initiated and the concentration of Al at the surface appeared to be increasing. Thermal oxidation at 1000 °C for 16 h resulted in a dense growth of platelets which given the increased time of exposure, appeared to be undergoing a phase transformation. Oxidation at 1000 °C for 8 h, resulted in a transient alumina layer, with a whisker like morphology formed densely across the surface of the rods. EDX

line scan analysis confirmed the increased concentration of Al present on the surface. XRD data suggested that alumina present on the surface was representative of high surface area transient aluminas. Following the time and temperature oxidation study, it was attempted to scale-up the oxidation. The optimum conditions of oxidation were found to be 950 °C for 10 h under flowing air.

- The oxidised Fecralloy rods were then washcoated with an alumina layer. This was done by the method of dip-coating in an alumina slurry. A two-step hybrid method was initially carried out, however due to the increased presence of cracks on the surface, the method was modified and a one-step hybrid method as suggested in a patent was optimised and used for the washcoating of the Fecralloy rods.

  The slurry was prepared by combining a binder sol (Boehmite powder dispersed in distilled water) with PURALOX and HNO_3 in a fixed molar ratio. This method of preparation of catalyst could possibly result in an increased acidity of the developed catalyst. The final coating load was found to be 1.3 %. The coating appeared to be adherent with a thickness of 6 µm with no cracks on the surface. The prepared catalyst was to be tested for the dehydrogenation of MCH, which is a very fast reaction; hence despite the thin layer of washcoat, the catalyst would still be active for dehydrogenation of MCH and would help reduce resistance to diffusion. However the thin layer could make the catalyst more susceptible to rapid catalyst deactivation.

- The washcoated Fecralloy rods were impregnated with an active phase by the technique of wet impregnation. STEM analysis of the platinum dispersion revealed that platinum was highly dispersed across the alumina washcoat. However the platinum was dispersed as fine particles (~ 1nm), clusters of atoms (4 - 5 nm) and larger clusters of atoms (~ 6 nm). Work by previous authors has suggested the difference in dispersion of size of the platinum could have an effect on the selectivity of the catalyst towards dehydrogenation of methylcyclohexane.

8.2.2 Performance of catalyst for dehydrogenation of MCH

The second objective of the research was to evaluate the performance of the prepared catalyst for the dehydrogenation of MCH and to ensure the catalyst had good dehydrogenation activity, high selectivity and increased long-term selectivity towards the formation of aromatics and low rates of deactivation. The catalyst was tested under a range of operating conditions to determine the catalyst activity and to obtain a better understanding on how the catalyst behaved at the different operating parameters. Long term, life time tests were additionally performed on the catalyst to study the deactivation rate and the stability of the catalyst when continuously tested for a time period > 400 h. The results obtained were compared with conventional commercial and in-house prepared Pt/Al_2O_3 catalysts. The alumina used to prepare the in-house catalyst was PURALOX, which was also used to prepare the alumina washcoat. A detailed evaluation of the performance of all the catalysts and the main conclusions with regards to the activity, selectivity and stability are summarized in the following sub-sections.

8.2.2.1 Catalyst Activity

The initial activities of the structured catalyst and the commercial catalyst were evaluated at a range of operating conditions. The most important observations with regard to initial activity are :

- With increasing W/F the catalyst activity increased for both the catalysts due to increase in contact time and hence increase in dehydrogenation activity. The activity of the structured catalyst and commercial catalyst were similar.

- As the temperature was increased the catalytic activity for both the catalysts increased. The activity of the structured catalyst was higher than the commercial catalyst. At a reaction T = 360 °C the catalytic activity of the structured catalyst was similar to the catalytic activity of the commercial catalyst at reaction T = 400 °C. The Fecralloy support is conductive in nature, and the temperature drop in the bed with the structured catalyst was 15 °C compared to the pelleted catalysts which resulted in a temperature drop of around 30 °C. Thus suggesting the reduced temperature drop in

the bed improves the catalytic activity and efficiency of the reaction. The improved efficiency of the structured catalyst could also be attributed to the thin washcoat layer providing very little resistance to diffusion when compared to the spherical pelleted conventional catalysts.

- The catalytic activity was studied at increasing H_2/MCH ratio. It was found that with increasing H_2/MCH ratio the catalytic activity was enhanced for both the catalysts.

8.2.2.2 Catalyst Selectivity

For both the pelleted catalysts, the toluene selectivity was maintained above 99%. However for the structured catalyst, the initial selectivity was around 99%, but with increasing TOS and as the catalyst deactivated the selectivity gradually decreased to around 95 %. The selectivity study was based on GC-MS analyses and mainly focused on three main aspects: identifying the main side reactions associated with MCH dehydrogenation, determining the effect of the operating parameters on by-products yields and determining the effect of catalyst deactivation on the long-term selectivity. The main findings of the selectivity study were:

- The yield of by-products for the structured catalyst was much higher when compared to the pelleted catalysts thus resulting in a lower selectivity.

- With increasing *W/F* there was an increase in formation of by-products derived from toluene, due to the increased conversion. Yield of substituted biphenyl, which is a possible coke precursor, increased with increasing contact time, suggesting faster deactivation as *W/F* increased.

- As the temperature of reaction increased toluene selectivity increased. However there was an increase in formation of substituted biphenyls and substituted cyclopentanes which are potential coke-precursors. For the structured catalyst, increasing reaction temperature resulted enhanced its isomerization activity.

- Benzene and xylene were formed in an equal molar ratio, suggesting both products were formed simultaneously through toluene disproportionation and the absence of

toluene demethylation. However in the absence of hydrogen or low H_2/MCH ratio, for the structured catalyst, there was an increased formation of benzene and the molar ratio of benzene to xylene increased to around 5 and 4 respectively. Thus suggesting increasing concentration of hydrogen suppressed the demethylation activity of the structured catalyst. Further, the commercial catalyst did not depict such a change in the molar ratio thus suggesting difference activity of the metallic function between both the catalysts.

- The isomerization ability of the structured catalyst was suppressed in the presence of excess hydrogen. In addition it was found, in the absence of hydrogen, the demethylation activity of the metallic function of the structured catalyst was enhanced.

- For the structured catalyst, with increasing TOS in the long term life tests the selectivity of the declined sharply. There was a steady increase in yield of formation of substituted cyclopentanes and benzene. In addition it was found the benzene to xylene molar ratio steadily increased with increasing TOS suggesting an increased presence of kink sites on the platinum that dispersed. Work by previous authors suggested, the demethylation reaction (resulting in a C-C bond breaking) activity was enhanced on the kink sites of the platinum.

- The difference in by-products for the structured catalyst could possibly be attributed to three main factors: uneven platinum size distribution across the alumina washcoat, increased acidity of the alumina washcoat and possible interference of the underlying alloy on the side reactions.

- The in-house prepared pelleted catalyst gave a higher yield of xylene and substituted biphenyls when compared to the commercial catalyst suggesting increased acidity of the PURALOX support.

8.2.2.3 Catalyst Stability

In order to gauge the stability of the catalyst long term deactivation or life time tests were performed on the structured catalyst for a time around 400 h. Long term life time tests were also performed on commercial and in-house prepared pelleted catalysts to compare the deactivation profiles. The main findings with regard to catalyst deactivation were:

- The long term deactivation study on the three catalysts described a similar deactivation profile. The initial phase of deactivation was characterized by a rapid rate of decay over a relatively short period of time. The second phase of decay had a much slower rate and lasted a much longer time.

- The long term deactivation was fitted by the sum of two exponential decay functions. The empirical parameters obtained described the distribution of the active sites and their respective decay constants. It has been suggested that the dehydrogenation of MCH takes place on two different groups of active sites, highly active sites which rapidly deactivated, and the lesser active sites which were more resistant to deactivation.

- Using the empirical model, it was found the commercial catalyst had an increased population of more active sites when compared to the structured catalyst. Thus the rapid deactivation for the structured catalyst can be attributed to two factors: the rapid deactivation of the active sites and increased coke formation on the acid sites of the catalyst resulting in rapid deactivation.

- A significant enhancement of the catalyst stability can be achieved by reducing the steepness of the initial phase of deactivation. This can be done by reducing the population of highly active sites and trying to achieve a thicker alumina washcoat on the Fecralloy support with decreased acidity.

8.3 Future Work and recommendations

The results obtained from this research are promising and encourage further research and development effort. This study is only a step forward in the use of structured catalysts in packed bed reactors in order to replace the conventional pelleted packed bed reactors. However the catalyst preparation would need further optimisation and require to be subjected to more rigorous catalytic testing such as testing the catalyst at increased pressure and studying the effect of this parameter on toluene selectivity.

In order to improve the selectivity of the catalyst further detailed study on the catalytic washcoating procedure needs to be done. It should be attempted to achieve higher coating load of increased thickness thus reducing the susceptibility of the structured catalyst to rapid deactivation. The addition of surfactants such as TRITON X or stabilizers such as La_2O_3 could be added to improve the coating load of the alumina washcoat. In addition to the range of characterization systems that were used during catalyst preparation, an acid site characterization using NH_3-TPD or pyridine adsorption using IR could also be done. This would provide an improved insight on the distribution and concentration of acid sites which would further help in optimising the preparation of the structured catalyst and subsequently improve its selectivity.

Testing the structured catalyst with the catalytic washcoat (without platinum) for the dehydrogenation of MCH could give a better understanding on the of the catalytic activity of the alumina washcoat and the influence of the underlying alloy oxides on the side reactions taking place during dehydrogenation of MCH. In addition further work can be carried out by adding Fe_2O_3 and Cr_2O_3 promoters to the washcoated Fecralloy to study how they would behave catalytically.

Additional kinetic modelling and studies on the reaction and diffusion data would help extend the data beyond the range of the experimental conditions and would give a better insight on the catalyst efficiency and activity. Further, a detailed study on the heat conduction across the bed could be done, this would allow for better kinetic modelling and an improved understanding on the conductive nature of the Fecralloy.

References

A. Moulijn, J. & Cybulski, A. 2005. The Present and the Future of Structured Catalysts. *Structured Catalysts and Reactors.* CRC Press.

Agrafiotis, C. & Tsetsekou, A. 2000. The effect of powder characteristics on washcoat quality. Part I: Alumina washcoats. *Journal of the European Ceramic Society,* 20**,** 815-824.

Airiskallio, E., Nurmi, E., Heinonen, M. H., Väyrynen, I. J., Kokko, K., Ropo, M., Punkkinen, M. P. J., Pitkänen, H., Alatalo, M., Kollár, J., Johansson, B. & Vitos, L. 2010. Third element effect in the surface zone of Fe-Cr-Al alloys. *Physical Review B,* 81**,** 105-109.

Al Humaidan, F. 2008. Hydrogen storage in liquid organic hydride: producing hydrogen catalytically from methylcyclohexane. *PhD,* University of Manchester.

Alhumaidan, F., Cresswell, D. & Garforth, A. 2010. Long-term deactivation of supported Pt catalysts in the dehydrogenation of methylcyclohexane to toluene. *Industrial and Engineering Chemistry Research,* 49**,** 9764-9770.

Ali, L. I., Ali, A.-G. A., Aboul-Fotouh, S. M. & Aboul-Gheit, A. K. 1999. Dehydrogenation of cyclohexane on catalysts containing noble metals and their combinations with platinum on alumina support. *Applied Catalysis A: General,* 177**,** 99-110.

Arai, H., Seiyama, T., Tominaga, H. & Harakawa, M. 1980. The Influence of Platinum Particle Size on the Activity and Selectivity of Reforming Reaction. *In:* Delmon, B. & Froment, G. F. (eds.) *Studies in Surface Science and Catalysis.* Elsevier.

Asteman, H. & Spiegel, M. 2008. A comparison of the oxidation behaviours of Al_2O_3 formers and Cr_2O_3 formers at 700 °C - Oxide solid solutions acting as a template for nucleation. *Corrosion Science,* 50**,** 1734-1743.

Attard, G. & Barnes, C. 1998. *Surfaces,* Oxford University Press.

Avila, P., Montes, M. & Miró, E. E. 2005. Monolithic reactors for environmental applications: A review on preparation technologies. *Chemical Engineering Journal,* 109**,** 11-36.

Badini, C. & Laurella, F. 2001. Oxidation of FeCrAl alloy: influence of temperature and atmosphere on scale growth rate and mechanism. *Surface and Coatings Technology,* 135**,** 291-298.

Baker, R. T. K., Prestridge, E. B. & Garten, R. L. 1979. Electron microscopy of supported metal particles: I. Behavior of Pt on titanium oxide, aluminum oxide, silicon oxide, and carbon. *Journal of Catalysis,* 56**,** 390-406.

Baron, K., Blakely, D. W. & Somorjai, G. A. 1974. Low energy electron diffraction studies of the surface structures of adsorbed hydrocarbons (n-heptane, toluene, benzene, ethylene, and cyclohexane) on stepped (high miller index) platinum surfaces. *Surface Science,* 41**,** 45-66.

Bartholomew, C. H. & Farrauto, R. J. 2006. *Fundamentals of Industrial Catalytic Processes, Second Edition,* New Jersey, John Wiley & Sons.

Berthome, G., N'dah, E., Wouters, Y. & Galerie, A. 2005. Temperature dependence of metastable alumina formation during thermal oxidation of FeCrAl foils. *Materials and Corrosion,* 56**,** 389-392.

Blachère, J. R., Schumann, E., Meier, G. H. & Pettit, F. S. 2003. Textures of alumina scales on FeCrAl alloys. *Scripta Materialia,* 49**,** 909-912.

Blakely, D. W. & Somorjai, G. A. 1976. The dehydrogenation and hydrogenolysis of cyclohexane and cyclohexene on stepped (high miller index) platinum surfaces. *Journal of Catalysis,* 42**,** 181-196.

Blakely, D. W. & Somorjai, G. A. 1977. The stability and structure of high miller index platinum crystal surfaces in vacuum and in the presence of adsorbed carbon and oxygen. *Surface Science,* 65**,** 419-442.

Buscail, H., Heinze, S., Dufour, P. & Larpin, J. P. 1997. Water-vapor-effect on the oxidation of Fe-21.5 wt.%Cr-5.6 wt.%Al at 1000°C. *Oxidation of metals,* 47**,** 445-464.

Chai, M.-R. & Kawakami, K. 1991. Kinetic model and simulation for catalyst deactivation during dehydrogenation of methylcyclohexane over commercial Pt-, PtRe- and presulfided PtRe-Al_2O_3 catalysts. *Journal of Chemical Technology & Biotechnology,* 51**,** 335-345.

Chapman, L. R. & Watton, J. F. 1981. *Application of an alumina coating to oxide whisker covered surface on Al-containing Stainless steel foil*. US4279782 A.

Clemendot, F., Gras, J. M., Van Duysen, J. C. & Zachariey, G. 1993. Influence of yttrium and method of fabrication on the oxidation behaviour of FeCrAl alloys at high temperature in air. *Corrosion Science,* 35**,** 901-905, 907-908.

Coughlin, R. W., Kawakami, K. & Hasan, A. 1984. Activity, yield patterns, and coking behavior of Pt and PtRe catalysts during dehydrogenation of methylcyclohexane: I. In the absence of sulfur. *Journal of Catalysis,* 88**,** 150-162.

Cristiani, C., Finocchio, E., Latorrata, S., Visconti, C. G., Bianchi, E., Tronconi, E., Groppi, G. & Pollesel, P. 2012. Activation of metallic open-cell foams via washcoat deposition of Ni/$MgAl_2O_4$ catalysts for steam reforming reaction. *Catalysis Today,* 197**,** 256-264.

Cusumano, J. A., Dembinski, G. W. & Sinfelt, J. H. 1966. Chemisorption and catalytic properties of supported platinum. *Journal of Catalysis,* 5**,** 471-475.

Davis, S. M., Zaera, F. & Somorjai, G. A. 1984. Surface structure and temperature dependence of n-hexane skeletal rearrangement reactions catalyzed over platinum single crystal surfaces: Marked structure sensitivity of aromatization. *Journal of Catalysis,* 85**,** 206-223.

De Deugd, R. M., Chougule, R. B., Kreutzer, M. T., Meeuse, F. M., Grievink, J., Kapteijn, F. & Moulijn, J. A. 2003. Is a monolithic loop reactor a viable option for Fischer–Tropsch synthesis? *Chemical Engineering Science,* 58**,** 583-591.

De La Banda, J. F. G. & Melo, A. C. Y. F. V. 1986. Dehydrogenation of methylcyclohexene on a PtNaY catalyst. Study of kinetics and deactivation. *Applied Catalysis,* 26**,** 103-121.

Desai, P. H. & Richardson, J. T. 1986. Crystallite size effects in nickel catalysts: Cyclohexane dehydrogenation and hydrogenolysis. *Journal of Catalysis,* 98**,** 392-400.

Doolittle, W. J., Skoularikis, N. D. & Coughlin, R. W. 1987. Reactions of methylcyclohexane and n-heptane over supported Pt and PtRe catalysts. *Journal of Catalysis,* 107**,** 490-502.

Edwards, P. P., Kuznetsov, V. L., David, W. I. F. & Brandon, N. P. 2008. Hydrogen and fuel cells: Towards a sustainable energy future. *Energy Policy,* 36**,** 4356-4362.

El Kadiri, H., Molins, R., Bienvenu, Y. & Horstemeyer, M. F. 2005. Abnormal high growth rates of metastable aluminas on FeCrAl alloys. *Oxidation of metals,* 64**,** 63-97.

Gräf, I., Rühl, A.-K. & Kraushaar-Czarnetzki, B. 2014. Experimental study of heat transport in catalytic sponge packings by monitoring spatial temperature profiles in a cooled-wall reactor. *Chemical Engineering Journal,* 244**,** 234-242.

Groppi, G. & Tronconi, E. 1996. Continuous vs. Discrete Models of Nonadiabatic Monolith Catalysts. *AIChE Journal,* 42**,** 2382-2387.

Groppi, G. & Tronconi, E. 2005. Honeycomb supports with high thermal conductivity for gas/solid chemical processes. *Catalysis Today,* 105**,** 297-304.

Grünenfelder, N. F. & Schucan, T. H. 1989. Seasonal storage of hydrogen in liquid organic hydrides: description of the second prototype vehicle. *International Journal of Hydrogen Energy,* 14**,** 579-586.

Heck, R. M., Gulati, S. & Farrauto, R. J. 2001. The application of monoliths for gas phase catalytic reactions. *Chemical Engineering Journal,* 82**,** 149-156.

Henn, F. C., Dalton, P. J. & Campbell, C. T. 1989. Probing ensemble effects in surface reactions. 4. Cyclopentene adsorption on clean and bismuth-covered platinum(111). *The Journal of Physical Chemistry,* 93**,** 836-846.

Herz, R. K., Gillespie, W. D., Petersen, E. E. & Somorjai, G. A. 1981. The structure sensitivity of cyclohexane dehydrogenation and hydrogenolysis catalyzed by platinum single crystals at atmospheric pressure. *Journal of Catalysis,* 67**,** 371-386.

Holmen, A., Venvik, H. J., Myrstad, R., Zhu, J. & Chen, D. 2013. Monolithic, microchannel and carbon nanofibers/carbon felt reactors for syngas conversion by Fischer-Tropsch synthesis. *Catalysis Today,* 216**,** 150-157.

Jedliński, J., Smoła, G., Kowalski, K., Bernasik, A., Nocuń, M., Camra, J. & Bonarski, J. 2009. The mechanism of early oxidation stages of Fe20Cr5Al-type alloys at 1123 K. *Materials at High Temperatures,* 26**,** 259-272.

Jia, L., Shen, M. & Wang, J. 2007. Preparation and characterization of dip-coated γ-alumina based ceramic materials on FeCrAl foils. *Surface and Coatings Technology,* 201**,** 7159-7165.

Jodłowski, P. J., Kryca, J., Iwaniszyn, M., Jędrzejczyk, R., Thomas, J., Kołodziej, A. & Łojewska, J. 2013. Methane combustion modelling of wire gauze reactor coated with Co_3O_4–CeO_2, Co_3O_4–PdO catalysts. *Catalysis Today,* 216**,** 276-282.

Jossens, L. W. & Petersen, E. E. 1982. Fouling of a platinum reforming catalyst accompanying the dehydrogenation of methyl cyclohexane. *Journal of Catalysis,* 73**,** 377-386.

Jothimurugesan, K., Bhatia, S. & Srivastava, R. D. 1985. Kinetics of dehydrogenation of methylcyclohexane over a platinum-rhenium-alumina catalyst in the presence of added hydrogen. *Industrial & Engineering Chemistry Fundamentals,* 24**,** 433-438.

Kadiri, H. E., Molins, R., Bienvenu, Y. & Horstemeyer, M. F. 2005. Abnormal High Growth Rates of Metastable Aluminas on FeCrAl Alloys. *Oxidation of Metals,* 64**,** 63-97.

Kariya, N., Fukuoka, A. & Ichikawa, M. 2002. Efficient evolution of hydrogen from liquid cycloalkanes over Pt-containing catalysts supported on active carbons under "wet–dry multiphase conditions". *Applied Catalysis A: General,* 233**,** 91-102.

Land, D. P., Pettiette-Hall, C. L., Mciver, R. T. & Hemminger, J. C. 1989. Detection of reaction intermediates in the conversion of cyclohexane to benzene on platinum(111). *Journal of the American Chemical Society,* 111**,** 5970-5972.

Lee, K. S., Oh, K. H., Park, W. W. & Ra, H. Y. 1998. Growth of [alpha]-alumina oxide film in high temperature oxidation of Fe-20Cr-5Al alloy thin strip. *Scripta Materialia,* 39**,** 1151-1155.

Lefevere, J., Gysen, M., Mullens, S., Meynen, V. & Van Noyen, J. 2013. The benefit of design of support architectures for zeolite coated structured catalysts for methanol-to-olefin conversion. *Catalysis Today,* 216**,** 18-23.

Liang, J. J. & Weng, H. S. 1993. Rearrangement and Disproportionation of Toluene over La1-x$Sr_x$$NiO_3$ Catalysts. *Journal of Catalysis,* 140**,** 302-310.

Liu, D.-J., Winstead, D. R. & Van Den Bussche, N. 2003. *Method of preparing a catalyst layer over a metallic surface of a recuperator*. US 6,540,843.

Liu, F., Götlind, H., Svensson, J.-E., Johansson, L.-G. & Halvarsson, M. 2008. Early stages of the oxidation of a FeCrAlRE alloy (Kanthal AF) at 900 °C: A detailed microstructural investigation. *Corrosion Science,* 50**,** 2272-2281.

Löfberg, A., Essakhi, A., Paul, S., Swesi, Y., Zanota, M. L., Meille, V., Pitault, I., Supiot, P., Mutel, B., Le Courtois, V. & Bordes-Richard, E. 2011. Use of catalytic oxidation and dehydrogenation of hydrocarbons reactions to highlight improvement of heat transfer in catalytic metallic foams. *Chemical Engineering Journal,* 176–177**,** 49-56.

Maatman, R. 1959. How to Make a More Effective Platinum-Alumina Catalyst. *Industrial & Engineering Chemistry,* 51**,** 913-914.

Martínez T, L. M., Sanz, O., Centeno, M. A. & Odriozola, J. A. 2010. AISI 304 austenitic stainless steel monoliths: Modification of the oxidation layer and catalytic coatings after deposition and its catalytic implications. *Chemical Engineering Journal,* 162**,** 1082-1090.

Meille, V. 2006. Review on methods to deposit catalysts on structured surfaces. *Applied Catalysis A: General,* 315**,** 1-17.

Meille, V., Pallier, S., Santa Cruz Bustamante, G. V., Roumanie, M. & Reymond, J.-P. 2005. Deposition of γ-Al_2O_3 layers on structured supports for the design of new catalytic reactors. *Applied Catalysis A: General,* 286**,** 232-238.

Mennicke, C., Schumann, E., Al-Badairy, H., Tatlock, G. J., Göbel, M., Borchardt, G. & Le Coze, J. 1998. High Temperature Oxidation of UHP-Based Fe20Cr5Al Alloys. *physica status solidi (a),* 167**,** 419-426.

Ngomo, H. M. & Susu, A. A. 2001. Investigation of Prolonged deactivation-regeneration regimes on the dehydrogenation activity of platinum/alumina catalyst. *Petroleum Science and Technology,* 19**,** 283-298.

Nijhuis, T. A., Beers, A. E. W., Vergunst, T., Hoek, I., Kapteijn, F. & Moulijn, J. A. 2001. Preparation of monolithic catalysts. *Catalysis Reviews,* 43**,** 345-380.

Nychka, J. A. 2005. Quantification of aluminum outward diffusion during oxidation of FeCrAl alloys. *Oxidation of metals,* 63**,** 325-334.

Okada, Y., Sasaki, E., Watanabe, E., Hyodo, S. & Nishijima, H. 2006. Development of dehydrogenation catalyst for hydrogen generation in organic chemical hydride method. *International Journal of Hydrogen Energy,* 31**,** 1348-1356.

Pacheco, M. A. & Petersen, E. E. 1984a. On a general correlation for catalyst fouling. *Journal of Catalysis,* 86**,** 75-83.

Pacheco, M. A. & Petersen, E. E. 1984b. On the development of a catalyst fouling model. *Journal of Catalysis,* 88**,** 400-408.

Parera, J. M. & Beltramini, J. N. 1988. Stability of bimetallic reforming catalysts. *Journal of Catalysis,* 112**,** 357-365.

Pérez, O.-L., Romeu, D. & Yacamán, M. J. 1983. The relation between dispersion and particle size on supported catalysts. *Journal of Catalysis,* 79**,** 240-241.

Pinna, F. 1998. Supported metal catalysts preparation. *Catalysis Today,* 41**,** 129-137.

Rebhan, D. M. & Haensel, V. 1988. A kinetic and mechanistic study of cyclohexene disproportionation: An example of irreversible hydrogen transfer. *Journal of Catalysis,* 111**,** 397-408.

Richardson, J. T. 1989. *Principles of Catalyst Development,* New York, Plenum Press.

Rioux, R. M., Song, H., Yang, P. & Somorjai, G. A. 2008. Chapter 7 - Platinum Nanoclusters' Size and Surface Structure Sensitivity of Catalytic Reactions. *Metal Nanoclusters in Catalysis and Materials Science,* 1**,** 149-166.

Rochefort, A., Le Peltier, F. & Boitiaux, J. P. 1992. Particle size effect in supported platinum: Methylcyclohexane dehydrogenation. *Journal of Catalysis,* 138**,** 482-490.

Samad, J. E., Nychka, J. A. & Semagina, N. V. 2011. Structured catalysts via multiple stage thermal oxidation synthesis of FeCrAl alloy sintered microfibers. *Chemical Engineering Journal,* 168**,** 470-476.

Satyapal, S., Petrovic, J., Read, C., Thomas, G. & Ordaz, G. 2007. The U.S. Department of Energy's National Hydrogen Storage Project: Progress towards meeting hydrogen-powered vehicle requirements. *Catalysis Today,* 120**,** 246-256.

Schildhauer, T., Newson, E. & Müller, S. 2001. The Equilibrium Constant for the Methylcyclohexane–Toluene System. *Journal of Catalysis,* 198**,** 355-358.

Schwarz, J. A. & Heise, M. S. 1990. Preparation of metal distributions within catalyst supports: IV. Multicomponent effects. *Journal of Colloid and Interface Science,* 135**,** 461-467.

Sinfelt, J. H. 1964. Bifunctional Catalysis. *Advances in Chemical Engineering,* 5**,**37-54

Sinfelt, J. H. 2000. The turnover frequency of methylcyclohexane dehydrogenation to toluene on a Pt reforming catalyst. *Journal of Molecular Catalysis A: Chemical,* 163**,** 123-128.

Sinfelt, J. H., Hurwitz, H. & Shulman, R. A. 1960. Kinetics of methylcyclohexane dehydrogenation over Pt-Al_2O_3. *Journal of Physical Chemistry,* 64**,** 1559-1562.

Sirijaruphan, A., Goodwin Jr, J. G., Rice, R. W., Wei, D., Butcher, K. R., Roberts, G. W. & Spivey, J. J. 2005. Effect of metal foam supports on the selective oxidation of CO on Fe-promoted Pt/γ-Al_2O_3. *Applied Catalysis A: General,* 281**,** 11-18.

Smorygo, O., Mikutski, V., Marukovich, A., Vialiuha, Y., Ilyushchanka, A., Mezentseva, N., Alikina, G., Vostrikov, Z., Fedorova, Y., Pelipenko, V., Bunina, R. & Sadykov, V. 2009. Structured catalyst supports and catalysts for the methane indirect internal steam reforming in the intermediate temperature SOFC. *International Journal of Hydrogen Energy,* 34**,** 9505-9514.

Somorajai, G. A. 1994. *Introduction to Surface Chemistry and Catalysis*, John Wiley & Sons.

Somorjai, G. A. 1977. Active Sites in Heterogeneous Catalysis. *Advances in Catalysi,* 26**,** 2-66.

Somorjai, G. A. & Blakely, D. W. 1975. Mechanism of catalysis of hydrocarbon reactions by platinum surfaces. *Nature,* 258**,** 580-583.

Somorjai, G. A. & Zaera, F. 1982. Heterogeneous catalysis on the molecular scale. *The Journal of Physical Chemistry,* 86**,** 3070-3078.

Tanabe, K. 1970. Chapter 5 - Correlation between Acid-Base Properties and Catalytic Activity and Selectivity. *Solid Acids and Bases,* 1**,** 5-38.

Taube, M., Rippin, D., Knecht, W., Hakimifard, D., Milisavljevic, B. & Gruenenfelder, N. 1985. A prototype truck powered by hydrogen from organic liquid hydrides. *International Journal of Hydrogen Energy,* 10**,** 595-599.

Taube, M., Rippin, D. W. T., Cresswell, D. L. & Knecht, W. 1983. A system of hydrogen-powered vehicles with liquid organic hydrides. *International Journal of Hydrogen Energy,* 8**,** 213-225.

Tsakiris, D. 2007. Catalytic production of hydrogen from liquid organic hydrides.n*PhD*, University of Manchester.

Tschudin, S., Shido, T., Prins, R. & Wokaun, A. 1999. Characterisation of Catalysts Used in Wall Reactors for the Catalytic Dehydrogenation of Methylcyclohexane. *Journal of Catalysis,* 181**,** 113-123.

Valentini, M., Groppi, G., Cristiani, C., Levi, M., Tronconi, E. & Forzatti, P. 2001. The deposition of γ-Al_2O_3 layers on ceramic and metallic supports for the preparation of structured catalysts. *Catalysis Today,* 69**,** 307-314.

Van Trimpont, P. A., Marin, G. B. & Froment, G. F. 1986. Kinetics of methylcyclohexane dehydrogenation on sulfided commercial platinum/alumina and platinum-rhenium/alumina catalysts. *Industrial & Engineering Chemistry Fundamentals,* 25**,** 544-553.

Wolf, E. E. & Petersen, E. E. 1977. Kinetics of deactivation of a reforming catalyst during methylcyclohexane dehydrogenation in a diffusion reactor. *Journal of Catalysis,* 46**,** 190-203.

Wu, X., Weng, D., Xu, L. & Li, H. 2001. Structure and performance of γ-Al_2O_3 washcoat deposited by plasma spraying. *Surface and Coatings Technology,* 145**,** 226-232.

Yacamán, M. & Gómez, A. 1984. On the geometrical model of catalytic activity. *Applications of Surface Science,* 19**,** 348-359.

Yu, H., Chen, H., Pan, M., Tang, Y., Zeng, K., Peng, F. & Wang, H. 2007. Effect of the metal foam materials on the performance of methanol steam micro-reformer for fuel cells. *Applied Catalysis A: General,* 327**,** 106-113.

Zaera, F., Gellman, A. J. & Somorjai, G. A. 1986. Surface science studies of catalysis: classification of reactions. *Accounts of Chemical Research,* 19**,** 24-31.

Zhang, D., Zhang, L., Liang, B. & Li, Y. 2009. Effect of Acid Treatment on the High-Temperature Surface Oxidation Behavior of FeCrAlloy Foil Used for Methane Combustion Catalyst Support. *Industrial & Engineering Chemistry Research,* 48**,** 5117-5122.

Zhao, S., Zhang, J., Weng, D. & Wu, X. 2003. A method to form well-adhered γ-Al_2O_3 layers on FeCrAl metallic supports. *Surface and Coatings Technology,* 167**,** 97-105.

Appendix 1

A1.1 Bill of materials

Part specification for the gas supply module

Part	Specification	Model No	Quantity
1/8” Stainless Steel Tube	Outer Diamter = 1/8” Max.Pressure = 2500 psig	Swagelok (SS316-200)	5 meters
Needle Valve	Body Material : 316SS KEL-F Stem 1/4” Swagelok Colour Code : Green	Whitey-Sawgelok (SS-1KS4)	2
Check Valve	Body Material : 316SS 1/4” Swagelok Working pressure = 206 bar Back pressure = 70 bar Cracking pressure = 0.7 bar	Nupro-Sawgelok (SS-4C-10)	3
Pressure Gauges	Body Material : 316SS Pressure range = 1- 10 bar ¼” NPT connector Filled with glycerin	Wika (232.05-X)	2
Mass Flow Controller	Fluid : H2/N2/Air Flow = 50 – 500 ml/min Max.Operating Pressure = 100 bar Operating Temp = ambient I/O signal = 0 -5 VDC	Brooks 5850 TR	2
Read out & Control unit	I/O signal = 0-5 VDC Supply output : 15 V 4 channels	Brooks Instruments (Read out & Control device 0154)	1

Part specification for the MCH feed module

Part	Specification	Model No	Quantity
Feed Tank	Body Material : Glass Capacity : 1 L	Fisher Scientific	1
Weighing Scale	Max Range = 25 kg Readbility = 0.001 g	Fisher Brand	1
HPLC pump	Range = 0.05 – 2 ml/min Max.Pressure = 200 bar	Jasco PU 980	1
Low flow Metering Valve	Body Material : 316-SS 1/16” Swagelok Max.Pressure = 2000 psig	B-SS1A Swagelok	
1/16” Stainless steel tube	Outer Diamter = 1/16” Max.Pressure = 2500 psig	Swagelok (SS316)	1 meter

Part specification for reactor module

Part	Specification	Model No	Quantity
Reactor	Body material : Pyrex	Fabricated	1
Furnace	3 zone Max operating Temp : 1300 °C	Carbolite TZF 12/38/400	1
Multi-trend Temperature Indicator	6 independent readings 85-250 Vac 50-60 Hz 50 VA	Penny & Giles Instrument Ltd	1
Bed thermocouples	Type: K type Diameter : 0.5 mm Grounded	RS 443 7929	1

Part specification for separation module

Part	Specification	Model No	Quantity
Single Walled Condenser	Body Material : Pyrex End joints : 14/23	Fabricated	1
Double Walled Condenser	Body Material : Pyrex End joints : 17/26	Fabricated	1
PTFE sleeves	14/23 and 17/26 sleeves for ground	Fisher Scientific	4

	glass joints		
Digital Stirrer		Eurostar digital IKA labortechnik	1
Cooling Bath		Camlab Freyka	1

A1.2 Properties of MCH

Property	Value
Molecular weight (MW)	98.2 $gmol^{-1}$
Melting Point(T_m)	-127 °C
Boiling Point (T_b)	101 °C
Density (ρ)	0.7702 g/cc
Specific Gravity(SG)	0.7748
Vapour Density (air=1)	3.4
Vapour Pressure at 20°C (P_v)	0.1106 bar
Critical Temperature (T_c)	229.04 °C
Critical Pressure (P_c)	34.71 bar
Critical Volume (V_c)	367.79 cc/mol
Critical Compressibility factor (Zc)	0.2684
Acentric factor (W)	0.2350
API	51.1
Watson K	11.31
Viscosity @ 37.7°C	0.7640 cst
Viscosity @ 99°C	0.4757
Auto-ignition Temperature	258 °C
Explosive Limit (vol% in air)	1.2 - 6.7 %

A1.3 Properties of BOC gases

Specifications	H_2	Air
Molecular Weight	2.02	28.97
Boiling Point	-252 ^oC	-
Specific Volume	12.00 m^3/kg	0.833 m^3/kg
T_c.	-239.9 ^oC	-140.6 ^oC
P_c	1294 kPa	3774 kPa
Flammable limits	4.0 – 75 % in Air CAS	Supports combustion
Toxicity	Simple asphyxiant	Simple asphyxiant
Compatibility	Noncorrosive	Noncorrosive
Minimum Purity	99.995 %	-
Maximum impurity	50 ppm	-

A1.4 Mass Flow Controller calibration

Hydrogen: Calibrated using bubble flow meter

MFC set point %	Flowrate ml/min
8.0	50
12.0	69
13.5	79
14.0	81
16.0	92
24	158.59

Appendix 2

A2.1 Preparation of in-house prepared catalyst

- 0.01g of γ-Al_2O_3 was loaded with 1% wt Pt. Therefore, the required amount of Pt is:

Pt(wt) = $\frac{1}{100}$ x 0.01 = 0.0001 g

Hexachloroplatinic acid ($H_2PtCl_6.6H_2O$) (MW: 517.92 g/mol) used as Pt precursor; therefore,

$$moles\ of\ H_2PtCl_6{\cdot}6H_2O\ required = \frac{0.01\ g\ of\ Pt}{195.078\ g\ of\ Pt\ per\ mol\ of\ H_2PtCl_6.6H_2O}$$

$$moles\ of\ H_2PtCl_6{\cdot}6H_2O\ required = 5.126\ x\ 10^{-6}$$

- The volume of hexachloroplatinic acid ($H_2PtCl_6.6H_2O$) solution 0.0001M required to deliver 5.126x10^{-6} moles is calculated by:

$$V = \frac{number\ of\ moles}{Concentration\ of\ solution} = \frac{5.126\ x\ 10^{-6}\ mols}{0.0001\ M}$$

V = 51.26 ml

The loading of platinum on the catalyst was confirmed using EDX analysis. Multiple spot analysis on the sample confirmed a loading of 1% platinum with an accuracy $\pm$ 0.01%.

Appendix 3

A3.1 GC-MS Calibration Plots

Standards of the main by-products of different concentrations of 0.01 %v/v - 0.1% v/v were made in dicholoromethane. The samples were run in a GC-MS twice to check repeatability of the results. The results were found to be reproducible with an accuracy of ± 2%.

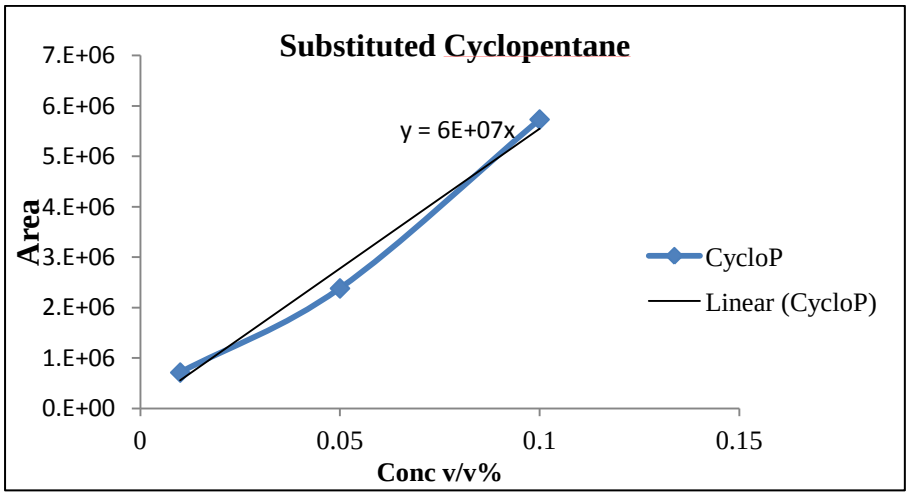

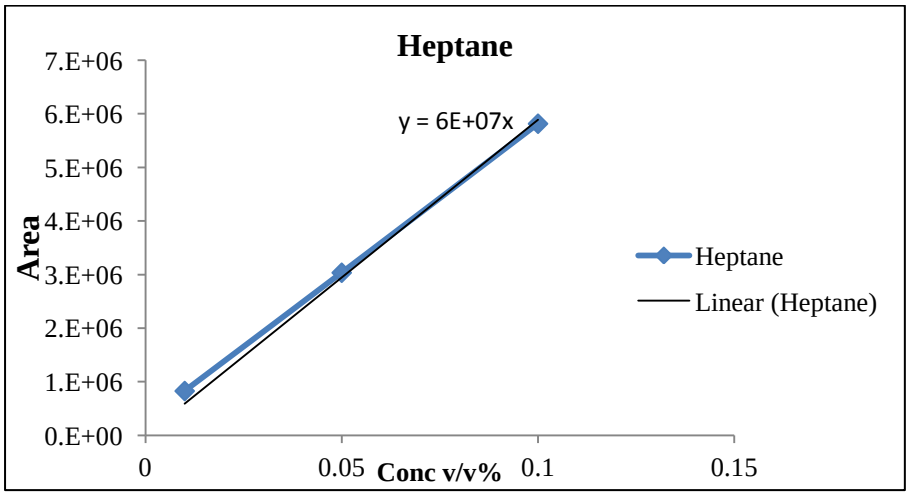

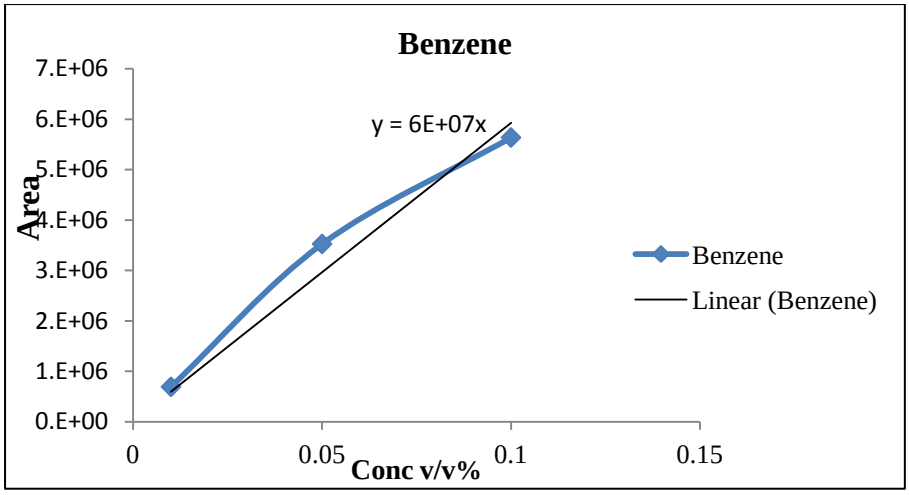
Benzene
7.E+06
6.E+06
5.E+06
4.E+06
3.E+06
2.E+06
1.E+06
0.E+00
Area
y = 6E+07x
0
0.05
0.1
0.15
Conc v/v%
Benzene
Linear (Benzene)

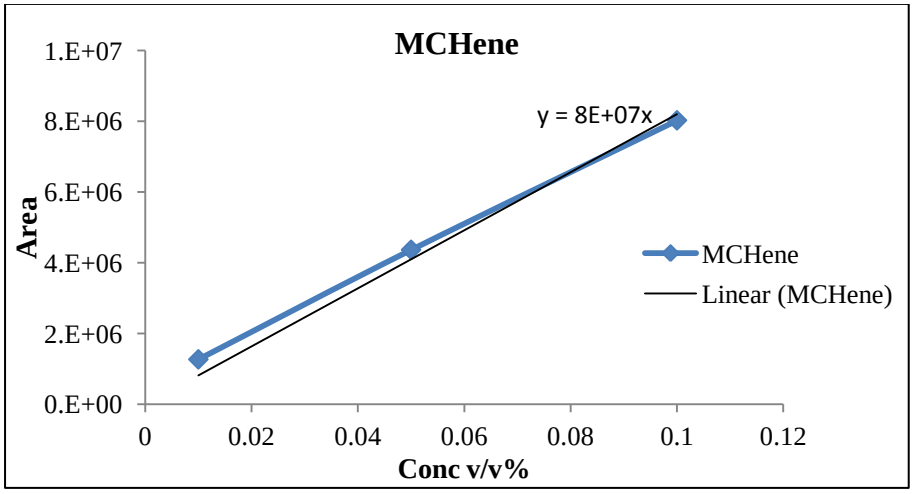
MCHene
1.E+07
8.E+06
6.E+06
4.E+06
2.E+06
0.E+00
Area
y = 8E+07x
0
0.02
0.04
0.06
0.08
0.1
0.12
Conc v/v%
MCHene
Linear (MCHene)

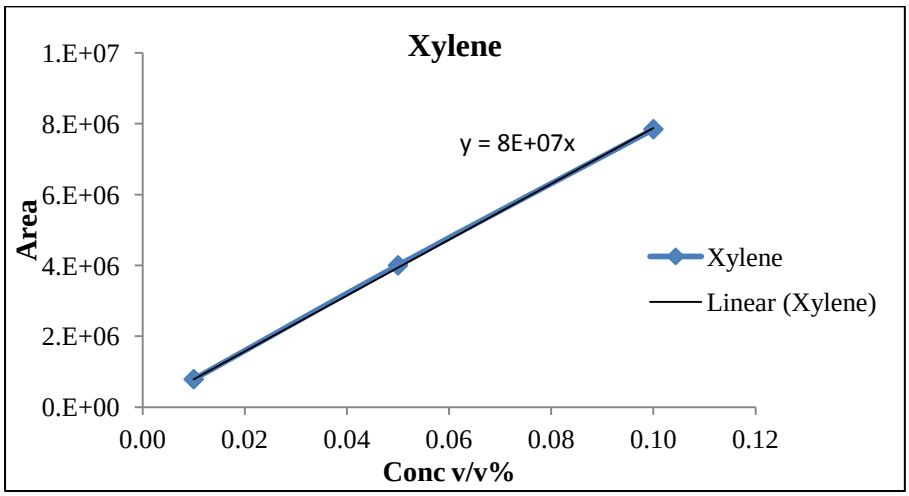
Xylene
1.E+07
8.E+06
6.E+06
4.E+06
2.E+06
0.E+00
Area
y = 8E+07x
0.00
0.02
0.04
0.06
0.08
0.10
0.12
Conc v/v%
Xylene
Linear (Xylene)

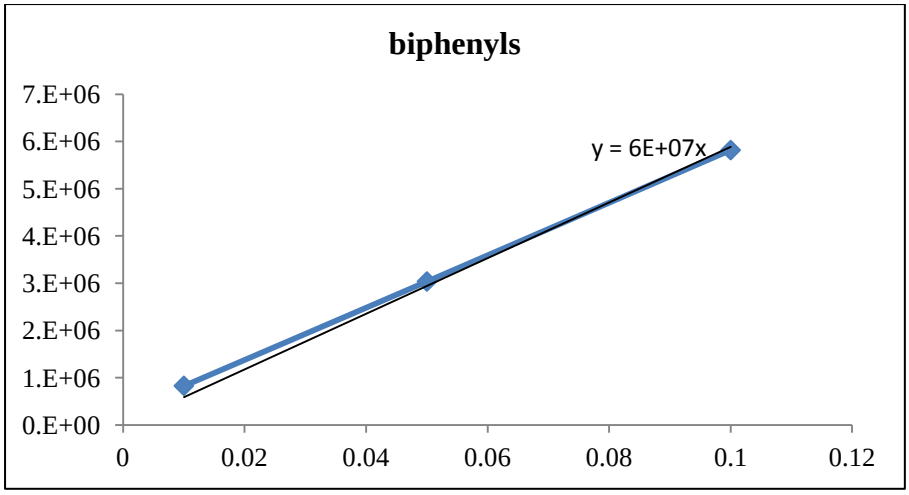
biphenyls
7.E+06
6.E+06
5.E+06
4.E+06
3.E+06
2.E+06
1.E+06
0.E+00
0
0.02
0.04
0.06
0.08
0.1
0.12
y = 6E+07x

A3.2 Concentration of by-products yield for commercial catalyst

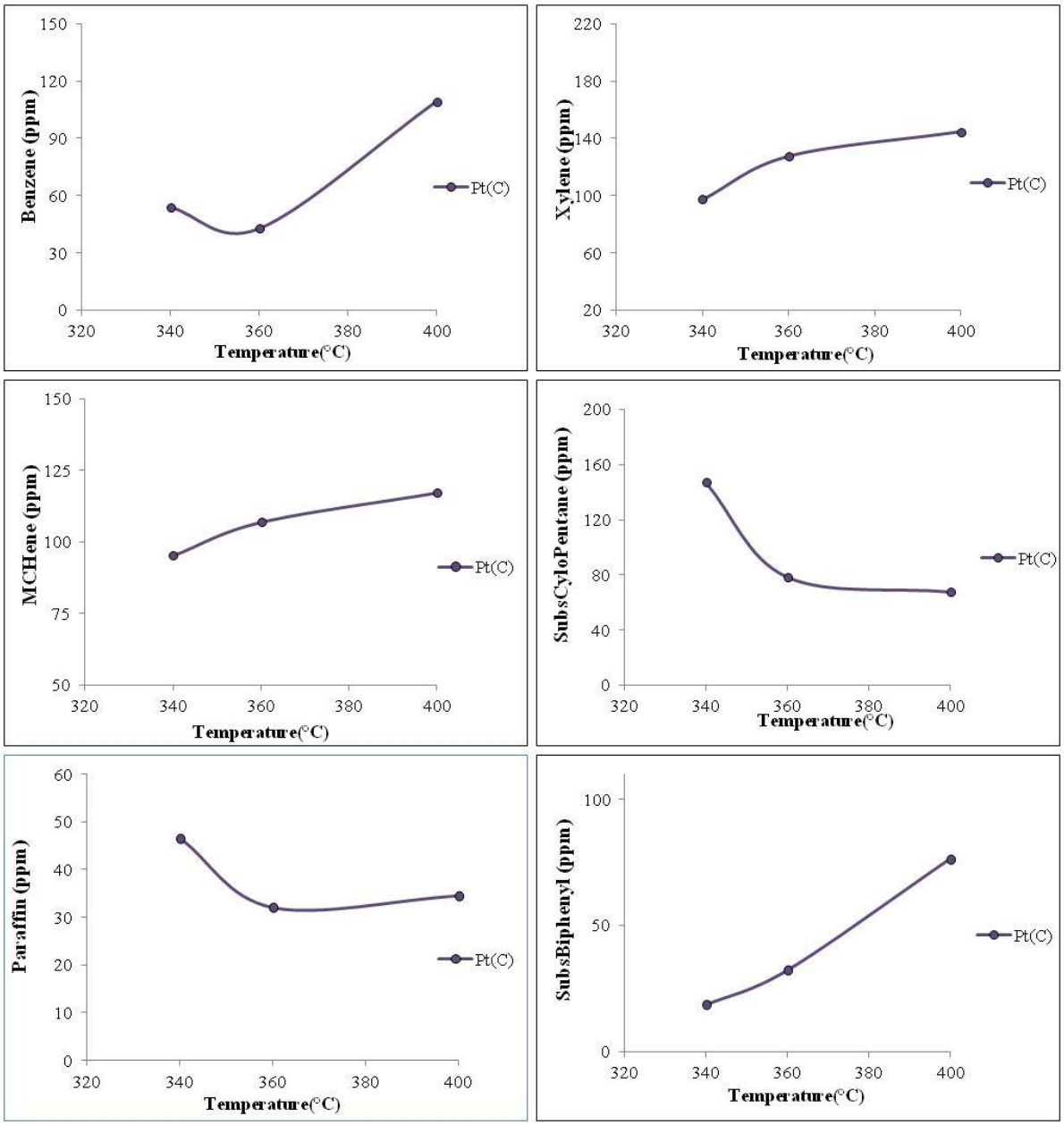

Change in the by-product concentration for the commercial catalyst at T = 340 °C - 400 °C, W/F = 14690 g s mol^{-1}. P = 1bar and H_2/ MCH = 9

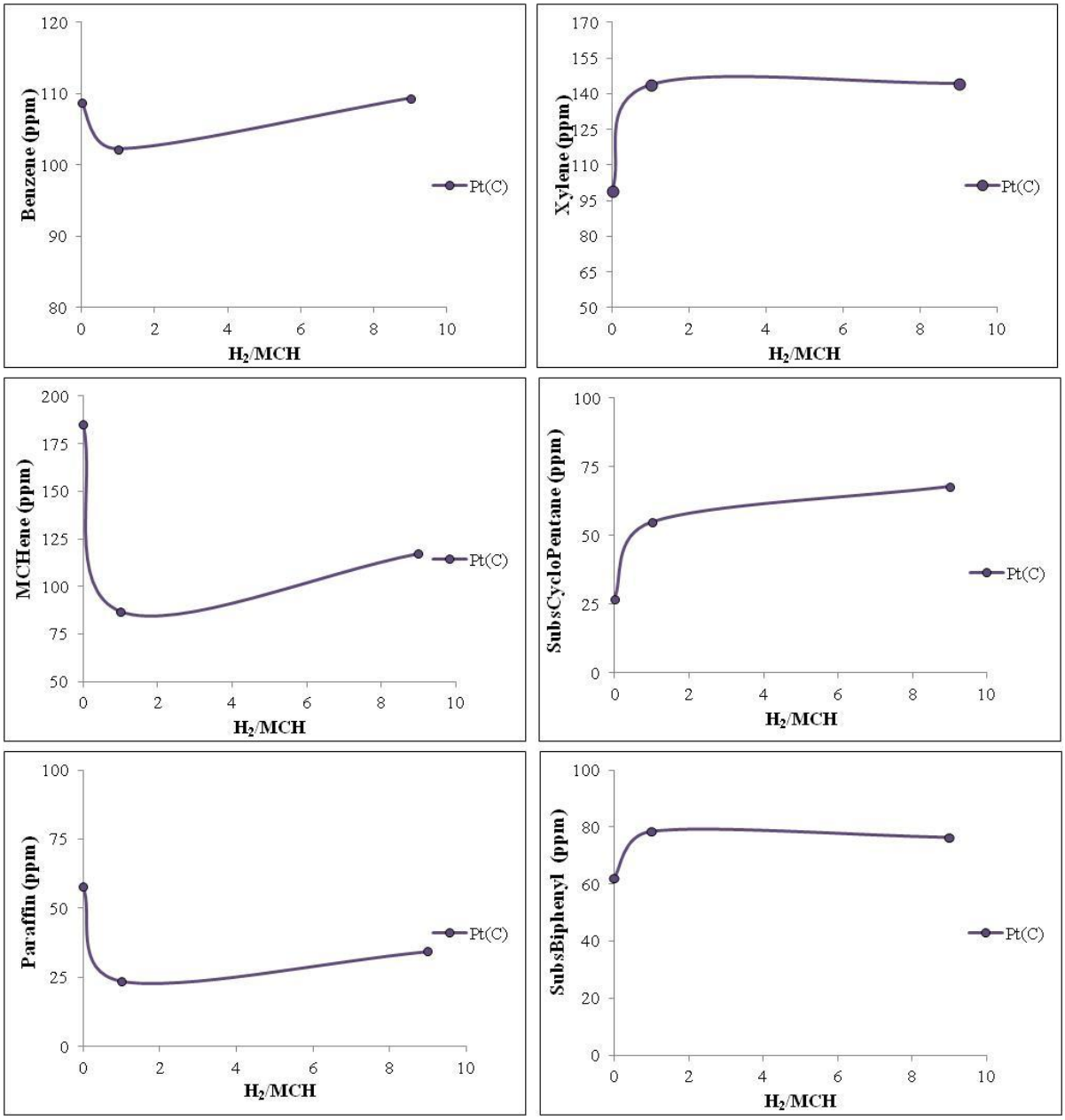

Change in the by-product concentration for the commercial catalyst at T = 400 °C, W/F = 14690 g s mol^{-1}. P = 1bar and H_2/ MCH = 0 - 9

Appendix 4

A4.1 List of Publications

The author has published two articles. The citations of the published articles are given below.

Rallan,C.,Akah,A., Hill,P., & Garforth,A. 1985. Growth of Hierarchically Structured High-Surface Area Alumina on FeCrAl Alloy Wires. *Indian Journal of Materials Science*, 2013**,** 495-502.

Rallan,C. & Garforth,A. 2014. Growth of Hierarchically Structured High-Surface Area Alumina on FeCAlloy® rods. Chinese *Journal of Chemical Engineering***,** In Press, Accepted Manuscript.

Development and Testing of Novel Structured Catalysts

Chandni Rallan and Arthur Garforth

School of Chemical Engineering and Analytical Science,
University of Manchester,
Manchester,M13 9PL, UK
chandni.rallan@postgrad.manchester.ac.uk

Structured metallic supports are currently found in catalytic converters for vehicles and similar, with a trend being towards the use of these in packed bed reactors to replace the pelleted catalyst structure [1]. Whilst the metal support offers exceptional heat transfer, the use of the system is currently limited due to surface adhesion issues. However, optimization of the wash-coat approach presents a possible solution to the issue, ensuring greater surface adhesion through the use of a platelet substructure formed by thermally oxidising FeCralloy rods [2 - 4].

In this work, 0.5mm diameter FeCralloy® rods were calcined at 950°C for 10 hours, forming a γ-Al_2O_3 surface with high porosity and surface area. This structured layer acted as an anchor to bind additional coatings of alumina via wash-coat techniques, thereby improving the layer thickness and increasing adhesion of the catalytic surface. Optimisation of the layer thickness and catalytic properties were then conducted, using a range of analytical systems, finally the modified FeCralloy® rods were tested in a fixed bed reactor rig to assess the impact on yield for the dehydrogenation of methylcyclohexane.

The metal support alloy had a composition of 72.8% Fe, 22% Cr, 5% Al, 0.1% Y and 0.1% Si, was calcined at 950˚C for 10h and prior to further loading with multiple alumina washcoats by dipcoating. The alumina slurry used was a dispersion of γ-Al_2O_3 (d=5µm, PURALOX®, *supplied by Sasol*) in HNO_3. Coated samples were calcined in a furnace at 650˚C for 2h, following which SEM and EDX were utilized to determine the surface morphology and composition. Further characterization of the alumina phase by XRD was conducted, and finally Platinum was loaded onto the

prepared support by wet impregnation, with the catalyst tested under a range of operating conditions in the dehydrogenation rig – as shown in table 1.

Table 8: Range of Operating Conditions

Operating Variable	Unit	Value Range
Temperature	˚C	300-400
Pressure	bar	1-9
MCH flowrate	$cm^{-3}hr^{-1}$	3-6
H_2 flowrate	$cm^{-3}min^{-1}$	70-200
H_2/MCH ratio		0-9
WHSV	hr^{-1}	0.2-0.5

The SEM analysis revealed platelet-like morphologies on the surface of the FeCralloy rods indicating the formation of the desired γ-Al_2O_3 subsurface following thermal oxidation, with the alumina coated samples (post calcination) possessing a uniform adherent coating with a thickness of ~6µm, which coating remained intact following catalytic testing. This was clarified by SEM analysis post catalytic testing.

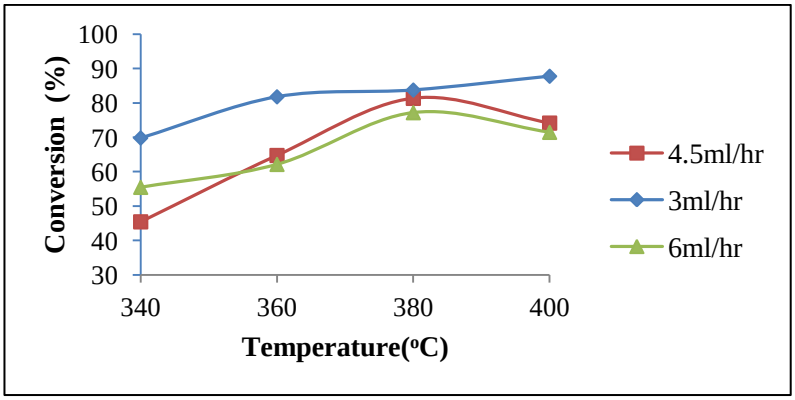

Figure 1: Conversion of 1%Pt/γ Al_2O_3/FeCralloy® Versus Temperature at $V_{(MCH)}$=3-6 $cm^{-3}hr^{-1}$ P=1bar WHSV=0.24-0.49hr^{-1}

High conversion (fig 1) of MCH during dehydrogenation testing was achieved using the FeCralloy rods, with the reaction showing increased selectivity(>99%) towards the formation of toluene and significantly improved conversions at higher temperatures and reduced temperature drop across the reaction bed. Experimental rate data has been analyzed and by the method of regression fitted onto different kinetic models. Long term life tests have been performed to gauge the stability of the

prepared catalyst and to build deactivation into the kinetic model for the system.The developed supported catalyst proves to be highly beneficial where improved heat transfer across the catalytic bed is required, to avoiding the formation of hot or cold spots and thus improving the conversion and kinetic interpretation.

References

1. Meille, V., Pallier, S., et al., *Deposition of γ-Al_2O_3 layers on structured supports for the design of new catalytic reactors.* Applied Catalysis A: General, **2005**. 286(2): p. 232-238.
2. Avila, P., M. Montes, and E.E. Miró, *Monolithic reactors for environmental applications: A review on preparation technologies.* Chemical Engineering Journal, **2005**. 109(1-3): p. 11-36.
3. Williams, J.L., *Monolith structures, materials, properties and uses.* Catalysis Today, **2001**. 69(1-4): p. 3-9.
4. Heck, R.M., S. Gulati, and R.J. Farrauto, *The application of monoliths for gas phase catalytic reactions.* Chemical Engineering Journal, **2001**. 82(1-3): p. 149-156.

Development and Testing of Novel Structured Catalysts

Chandni Rallan[a] and Arthur Garforth[b]*

[a] School of Chemical Engineering and Analytical Science, University of Manchester, Manchester,M13 9PL, UK

[b] School of Chemical Engineering and Analytical Science, University of Manchester, Manchester, M139PL,UK
arthur.garforth@manchester.ac.uk *

Keywords: FeCralloy®, gamma alumina, catalytic supports, packed bed reactors, dehydrogentation, kinetic modelling
Topics: Preparation and Characterization of Structured catalysts; Structured catalysts and reactors for innovative environmental, automotive and energy applications

ABSTRACT

Structured metallic supports are currently found in catalytic converters for vehicles and similar, with a trend being towards the use of these in packed bed reactors to replace the pelleted catalyst structure [1]. Whilst the metal support offers exceptional heat transfer, the use of the system is currently limited due to surface adhesion issues. However, optimization of the wash-coat approach presents a possible solution to the issue, ensuring greater surface adhesion through the use of a platelet substructure formed by thermally oxidising FeCralloy rods [2 - 4].

In this work, 0.5mm diameter FeCralloy® rods were calcined at 950°C for 10 hours, forming a γ-Al_2O_3 surface with high porosity and surface area. This structured layer acted as an anchor to bind additional coatings of alumina via wash-coat techniques, thereby improving the layer thickness and increasing adhesion of the catalytic surface. Optimisation of the layer thickness and catalytic properties were then conducted, using a range of analytical systems, finally the modified FeCralloy® rods were tested in a fixed bed reactor rig to assess the impact on yield for the dehydrogenation of methylcyclohexane.

The metal support alloy had a composition of 72.8% Fe, 22% Cr, 5% Al, 0.1% Y and 0.1% Si, and was calcined at 950˚C for 10h and prior to further loading with alumina washcoats by dipcoating. The alumina slurry used for dipcoating was a dispersion of γ-Al_2O_3 (d=5µm, PURALOX®, *supplied by Sasol*) in HNO_3, in the ratio 2.16mmol/g. The slurry was stirred under controlled conditions of time, temperature and pH. Coated samples were further calcined in a furnace at 650˚C for 2h, following which SEM and EDX were utilized to determine the surface morphology and composition. Further characterization of the alumina phase by XRD was conducted, and finally Platinum was loaded onto the prepared support by wet impregnation, with the catalyst tested under a range of operating conditions in the dehydrogenation rig – as shown in table 1.

Table 9: Range of Operating Conditions

Operating Variable	Unit	Value Range
Temperature	˚C	300-400
Pressure	bar	1-9
MCH flowrate	ml/hr	3-6
H_2 flowrate	ml/min	70-200
H_2/MCH ratio		0-9
WHSV	hr^{-1}	0.2-0.5

The SEM analysis revealed platelet-like morphologies on the surface of the FeCralloy rods indicating the formation of the desired γ-Al_2O_3 subsurface following thermal oxidation, with the alumina coated samples (post calcination) possessing a uniform adherent coating with a thickness of ~6µm, which coating remained intact following catalytic testing. This was clarified by SEM analysis post catalytic testing.

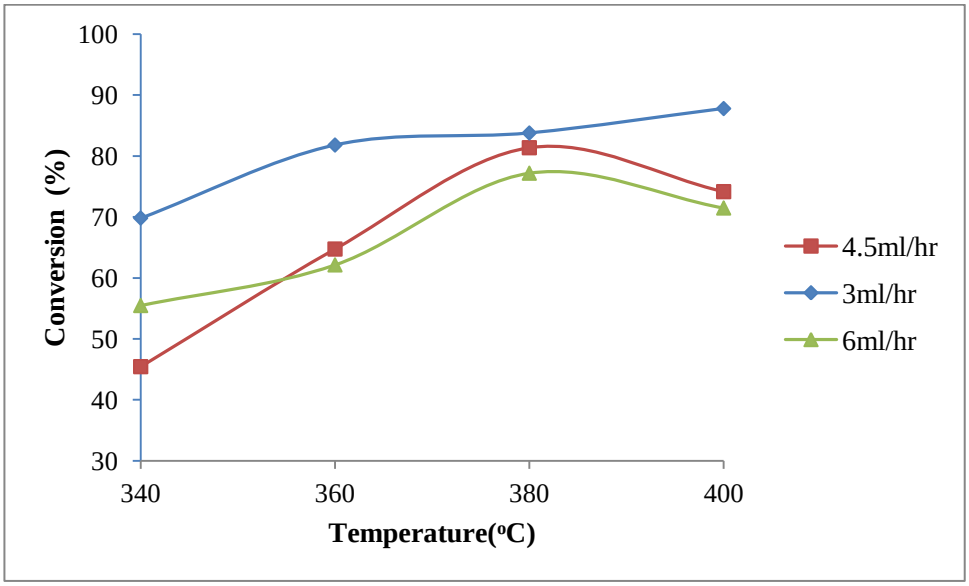

Figure 1: Conversion of 1%Pt/γ Al_2O_3/FeCralloy® Versus Temperature at $V_{(MCH)}$=3-6 ml/hr P=1bar WHSV=0.24-0.49hr^{-1}

High conversion (fig 1) of MCH during dehydrogenation testing was achieved using the FeCralloy rods, with the reaction showing increased selectivity(>99%) towards the formation of toluene and significantly improved conversions at higher temperatures and reduced temperature drop across the reaction bed. Experimental rate data has been analyzed and by the method of regression fitted onto different kinetic models. Long term life tests have been performed to gauge the stability of the prepared catalyst and to build the deactivation into the kinetic model for the system.

The developed supported catalyst proves to be highly beneficial where improved heat transfer across the catalytic bed is required, to avoiding the formation of hot or cold spots and thus improving the conversion and kinetic interpretation.

References

1. Meille, V., Pallier, S., et al., *Deposition of γ-Al_2O_3 layers on structured supports for the design of new catalytic reactors.* Applied Catalysis A: General, 2005. 286(2): p. 232-238.
2. Avila, P., M. Montes, and E.E. Miró, *Monolithic reactors for environmental applications: A review on preparation technologies.* Chemical Engineering Journal, 2005. 109(1-3): p. 11-36.
3. Williams, J.L., *Monolith structures, materials, properties and uses.* Catalysis Today, 2001. 69(1-4): p. 3-9.
4. Heck, R.M., S. Gulati, and R.J. Farrauto, *The application of monoliths for gas phase catalytic reactions.* Chemical Engineering Journal, 2001. 82(1-3): p. 149-156.

Structured metallic supports are currently found in catalytic converters for vehicles and similar, with a trend being towards the use of these in packed bed reactors to replace the pelted catalyst structure [1]. Whilst the metal support offers exceptional heat transfer, the use of the system is currently limited due to surface adhesion issues. However, optimization of the wash-coat approach presents a possible solution to this surface adhesion process, ensuring greater surface adhesion through the use of a platelet substructure formed by thermally oxidising FeCralloy rods [2 - 4].

In this work, 0.5mm diameter FeCralloy rods were calcined at 950°C for 10 hours, forming a γ-Al_2O_3 surface with high porosity and surface area. This structured layer acted as an anchor to bind additional coatings of alumina via wash-coat techniques, thereby improving the layer thickness and increasing adhesion of the catalytic surface. Optimisation of the layer thickness and catalytic properties were then conducted, using a range of analytical systems, finally the modified FeCralloy rods were tested in a fixed bed reactor rig, under a range of operating conditions to assess the impact on yield for the dehydrogenation of methylcyclohexane.

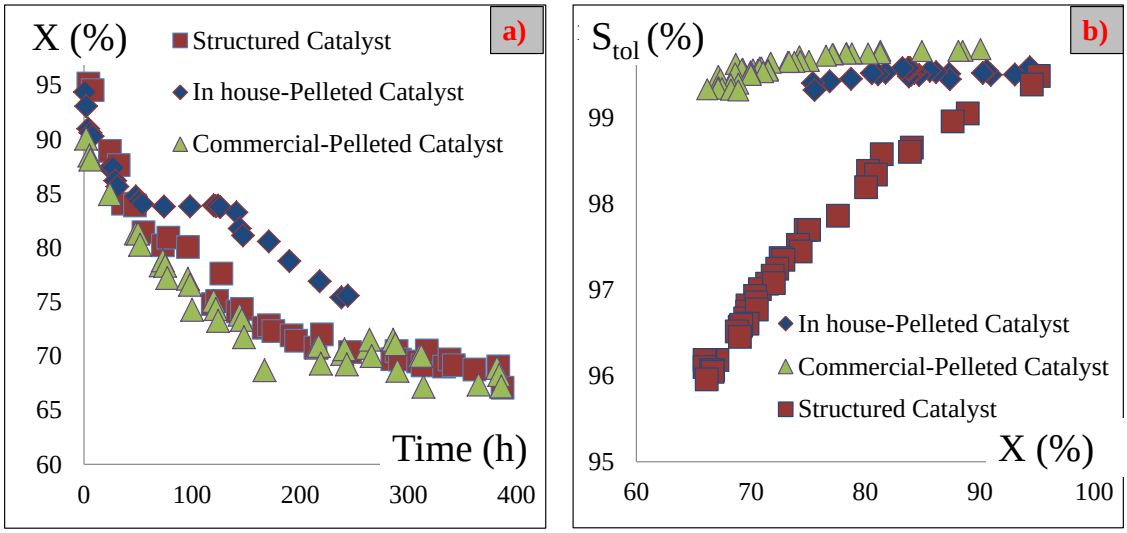

Figure 1: Long term life tests at T=400°C and LHSV=0.24hr^{-1} describing (a)Comparison of deactivation pattern of developed catalyst with pelleted catalyst (b) Toluene selectivity of different catalysts

Experimental rate data has been analyzed and by the method of regression fitted onto different kinetic models. Long term life tests have been performed to gauge the stability of the prepared catalyst and to build the deactivation into the kinetic model for the system. Figure 1a illustrates a similar deactivation pattern for all the catalysts tested.The structured catalyst has a slightly lower selectivity in comparison to the pelleted catalyst (fig 1b), which has been further investigated.

The developed supported catalyst proves to be highly beneficial where improved heat transfer across the catalytic bed is required, to avoiding the formation of hot or cold spots and thus improving the conversion and kinetic interpretation.

References

1. Meille, V., Pallier, S., et al., *Deposition of γ-Al_2O_3 layers on structured supports for the design of new catalytic reactors.* Applied Catalysis A: General, 2005. 286(2): p. 232-238.
2. Avila, P., M. Montes, and E.E. Miró, *Monolithic reactors for environmental applications: A review on preparation technologies.* Chemical Engineering Journal, 2005. 109(1-3): p. 11-36.
3. Williams, J.L., *Monolith structures, materials, properties and uses.* Catalysis Today, 2001. 69(1-4): p. 3-9.
4. Heck, R.M., S. Gulati, and R.J. Farrauto, *The application of monoliths for gas phase catalytic reactions.* Chemical Engineering Journal, 2001. 82(1-3): p. 149-156.